

A Microfluidic Platform Enables Large-Scale Single-Cell Screening to Identify Genes Involved in Bacterial Persistence

THÈSE N° 7641 (2017)

PRÉSENTÉE LE 31 MARS 2017

À LA FACULTÉ DES SCIENCES DE LA VIE

UNITÉ DU PROF. MCKINNEY

PROGRAMME DOCTORAL EN BIOTECHNOLOGIE ET GÉNIE BIOLOGIQUE

ÉCOLE POLYTECHNIQUE FÉDÉRALE DE LAUSANNE

POUR L'OBTENTION DU GRADE DE DOCTEUR ÈS SCIENCES

PAR

AMANDA VERPOORTE

acceptée sur proposition du jury:

Prof. A. Radenovic, présidente du jury
Prof. J. McKinney, Prof. S. Maerkl, directeurs de thèse
Prof. D. Bumann, rapporteur
Prof. J. Michiels, rapporteur
Prof. M. Gijs, rapporteur



ÉCOLE POLYTECHNIQUE
FÉDÉRALE DE LAUSANNE

Suisse
2017

Contents

List of figures	7
List of tables	11
Acknowledgements	13
Résumé	15
Abstract	17
1 Introduction	19
1.1 <i>High content screening</i>	19
1.1.1 Background	19
1.1.2 High content screening: challenges and limitations	20
1.2 <i>The rise of microfluidics</i>	22
1.2.1 Introduction to microfluidics	22
1.2.2 Microfluidic platforms for single-cell imaging of prokaryotes	24
1.3 <i>Microfluidic screening platforms</i>	27
1.3.1 Two-phase system: droplet microfluidics	27
1.3.2 Single-phase system: flow microfluidics	28
1.3.3 Conclusion	29
1.4 <i>Bacterial persistence phenomenon during antibiotic exposure</i>	29
1.4.1 A historical perspective	30

1.4.2	Clinical relevance of persistence	31
1.4.3	The discovery of a high persistence mutant enabled in depth study of the phenomenon	32
1.4.4	Tackling persistence with microfluidics and time-lapse microscopy	32
1.4.5	Mechanisms of bacterial persistence	35
1.5	<i>Aim and motivation</i>	38
2	The high-throughput microfluidic screening platform for prokaryotes	41
2.1	<i>Design of the microfluidic screening platform</i>	41
2.2	<i>Mold and PDMS device fabrication</i>	43
2.3	<i>Double layers microfluidic device</i>	44
2.4	<i>Characterization of the microfluidic screening platform</i>	45
2.5	<i>Spotting procedure and optimization of live cell array</i>	47
2.6	<i>Proof of concept screenings</i>	49
2.6.1	<i>Mycobacterium smegmatis</i> as a model organism	49
2.6.2	Single-cell imaging on chip and subcellular proof of concept screen	49
2.6.3	Proof of concept screen to identify phenotypes emerging in fluctuating environment: bacterial persistence	52
2.7	<i>Conclusion and outlook</i>	57
3	The microfluidic platform enables large-scale screening to identify genes involved in bacterial persistence	59
3.1	<i>Screening a cytosolic DsRed-expressing M. smegmatis mutant library</i>	59
3.1.1	The DsRed-expressing <i>M. smegmatis</i> mutant library	59
3.1.2	Experimental procedure of the genetic persistence screen	60
3.1.3	Primary screen – DsRed-expressing <i>M. smegmatis</i> mutant library	61
3.1.4	Secondary screen – DsRed-expressing <i>M. smegmatis</i> mutant library	64
3.1.5	Batch culture analysis and candidate mutant validation	68
3.2	<i>Screening the mCherry-DnaN Wag31-GFP expressing M. smegmatis mutant library</i>	71
3.2.1	The mCherry-DnaN Wag31-GFP <i>M. smegmatis</i> mutant library	72
3.2.2	Experimental procedure of the genetic persistence screen	72
3.2.3	Primary screen – mCherry-DnaN Wag-GFP-expressing <i>M. smegmatis</i> mutant library	73

3.2.4	Secondary screen – mCherry-DnaN Wag-GFP-expressing <i>M. smegmatis</i> mutant library	74
3.3	<i>Discussion and outlook</i>	76
4	Quantitative single-cell analysis of <i>Mycobacterium smegmatis</i> mutants with altered rates of persistence during antibiotic exposure	83
4.1	<i>Microfluidic platform modifications for single cell studies</i>	83
4.2	<i>Scoring cell lysis</i>	84
4.3	<i>Influence of the size of the microcolony on division and killing during antibiotic exposure</i>	86
4.4	<i>Dynamics of cell division and cell death in <i>M. smegmatis</i> mutants displaying altered rates of persistence during and after antibiotic exposure</i>	87
4.4.1	Experimental procedure for single-cell experiments	87
4.4.2	Selection of mutants with altered rate of persistence	89
4.4.3	Dynamics of cell division and cell death during INH exposure	90
4.4.4	Analysis of persister cells occurrence	93
4.5	<i>Discussion and outlook</i>	96
5	Perspectives and outlook	99
5.1	<i>Results overview</i>	99
5.2	<i>Limitations</i>	101
5.3	<i>Outlook</i>	103
6	Materials and Methods	105
6.1	<i>Bacterial strains and culture conditions</i>	105
6.2	<i>Kill curves in batch culture</i>	106
6.3	<i>Minimum inhibitory concentration assays</i>	106
6.4	<i>Mutagenesis and generation of a <i>M. smegmatis</i> mutant library</i>	106
6.5	<i>Microfluidic device and fabrication</i>	107
6.6	<i>Cell preparation and spotting procedure</i>	111
6.7	<i>Chip priming and medium switch</i>	112
6.8	<i>Time-lapse movies acquisition – persistence screen</i>	112
6.9	<i><i>M. smegmatis</i> mutant candidates selection</i>	113
6.10	<i>Identification of fMycoMarT7 transposon insertion sites</i>	113

6.11	<i>Electrocompetent cells preparation and electroporation</i>	114
6.12	<i>Flowing bacterial cells in the microfluidic screening platform for time-lapse microscopy</i>	114
7	Appendices	117
8	Bibliography	121
9	Curriculum vitae	129

List of figures

Figure 1.1: Microfluidic platform for single-cell screening of bacteria.	25
Figure 1.2 Tackling persistence with microfluidics and time-lapse microscopy.	34
Figure 2.1: Schematic of the microfluidic screening platform.	42
Figure 2.2: Photograph of the micro-fabricated PDMS microfluidic screening platform.	44
Figure 2.3: Schematic of micromechanical valve functioning.	45
Figure 2.4: Characterization of the HCS/HTS microfluidic screening platform.	46
Figure 2.5: Live cell array spotting procedure.	47
Figure 2.6: Cross-contamination between microchambers during spotting process.	48
Figure 2.7: Proof-of-concept screen for mutations affecting morphological and subcellular markers.	51
Figure 2.8: Mechanism of action of isoniazid.	53
Figure 2.9: Proof-of-concept screen for bacterial persistence mutants.	55

Figure 2.10: Outcome of the proof-of-concept screen for bacterial persistence mutants.	57
Figure 3.1: The screening process and representative mutants with altered persistence rates.	62
Figure 3.2: Ds-Red-expressing <i>M. smegmatis</i> mutant library primary screen coverage and selection criteria for mutants with altered rates of persistence.	64
Figure 3.3: Secondary screen coverage and outcome.	65
Figure 3.4: Schematic of two distinct dynamics for enhanced survival to antibiotic exposure.	67
Figure 3.5: Kill curves of mutants with altered persistence..	69
Figure 3.6: Primary screen coverage of mCherry-DnaN Wag31-GFP-expressing <i>M. smegmatis</i> mutant library and selection criteria for mutants with altered persistence rates.	74
Figure 3.7: Secondary screen coverage and outcome.	75
Figure 3.8: MIC versus FSR diagram.	78
Figure 4.1: Influence of SYTOX® Green on wild-type <i>M. smegmatis</i> expressing DsRed.	85
Figure 4.2: Representative time-lapse movie of single-cell analysis of cell divisions and cell deaths during antibiotic exposure.	85
Figure 4.3: Division and death events in microcolonies of different sizes.	87
Figure 4.4: The microfluidic screening platform and its three independent subsets.	88
Figure 4.5: Kill curves for of mutants with altered persistence.	89

Figure 4.6: Quantitative single-cell analysis of cell division and killing during antibiotic exposure.	92
Figure 4.7: Independent lineage of persisters cells.	94
Figure 4.8: Fractions of physically intact cells upon antibiotic removal as indicated by SYTOX® Green negative.	96
Figure 7.1: Growth of DsRed-expressing <i>M. smegmatis</i> mutants with altered rates of persistence.	117

List of tables

Table 1.1: Comparison between different microfluidic platforms for single cell imaging of prokaryotes.	26
Table 3.1: DsRed-expressing mutants displaying increased persistence phenotype.	66
Table 3.2: DsRed-expressing mutants displaying decreased persistence phenotype.	66
Table 3.3: Mutants with increased persistence exhibiting distinctive dynamics leading to enhance survival during antibiotic exposure.	67
Table 3.4: Fractional survival ratios (FSR) and minimum inhibitory concentrations (MIC).	71
Table 3.5: mCherry-DnaN Wag-GFP-expressing mutants displaying increased and decreased persistence phenotype.	76
Table 4.1: Fractional survival ratio and minimum inhibitory concentration of selected mutants for single cell analysis.	90
Table 4.2: Slopes of death rates slopes.	93

Table 4.3: Quantitative measurements of independent single-cell experiments.	93
Table 4.4: Summary of persistence frequency.	95
Table 6.1. Summary of flow layer mold fabrication with microchambers of height 1.4 μ m	109
Table 6.2. Summary of fabrication of microchambers of height 0.8 μ m.	110
Table 6.3. Summary of control layer mold fabrication	110
Table 7.1: Transposon insertion sites in DsRed-expressing <i>M. smegmatis</i> mutants with altered rates of persistence.	118
Table 7.2: Transposon insertion sites in DnaN-mCherry- and Wag-GFP-expressing <i>M. smegmatis</i> mutants with altered rates of persistence.	119

Acknowledgements

The present thesis would not have been possible without the help of many contributors.

First of all, I would like express my gratitude to my supervisors, Prof. John McKinney and Prof. Sebastian Maerkl, for giving me the opportunity to carry out this project in their labs and for mentoring me throughout my PhD. I had a wonderful time, and I learned from both on very distinct subjects (from mycobacteria to microfluidics!).

I would like also to thank all my colleagues, who made my journey fantastic. A special thank to Neeraj Dhar, who is always ready to help and has a solution to any problem, to Jean-Baptiste Bureau, Meltem Elitas and Nicolas Dénervaud for helping me to start with the project. Through my PhD, lab members became more friends than colleagues, especially Matt & Kat with our crazy moments at Sat after long days in the lab (KatMatSat was always an option, even though I tried AmMattKat, I couldn't compete). But also Zela – first time that I met someone louder than me, Thomas – the victim of Zela's loudness (I might have contributed to that), Vivek, Chiara, Joëlle, François, Alex, Paul, Suzanne, Cécile, all of you contributed to make the McKinney lab a amazing place to work. I would like to thank also all the LBNC lab members for their help and support (and patience!): Francesca, Zoe, Ekaterina, Ivan, Nadanai, Barbora, Gregoire, Henrike, and Matthew.

Above all, I would like to thank my family, especially my sister Virginia (my second mom) and parents, for their UNLIMITED and ETERNAL support; I could always count on them at ANY time. I wouldn't stand where I am now without them.

And last but not least, Francesco, la force tranquille, always ready to help me out in any possible ways, always by my side, often trying to put me back on (what other would call) "normal" tracks, which is definitely not an easy task!

Résumé

Les cellules persistantes représentent une fraction minime de la population bactérienne réfractaire au traitement antibiotique. La persistance est décrite comme un état phénotypique transitoire dont les mécanismes restent largement inconnus. Plusieurs hypothèses ont été avancées, parfois contradictoires, qui s'accordent toutefois sur un point: l'hétérogénéité phénotypique est à l'origine de la persistance. De nouvelles approches sont nécessaires afin d'élucider les facteurs permettant la survie de certaines bactéries face aux antibiotiques. L'imagerie cellulaire à haut débit utilise la microscopie comme instrument de criblage et permet de visualiser des phénotypes au niveau de la cellule. De ce fait, cette méthode est particulièrement adaptée pour étudier la persistance des bactéries. Traditionnellement effectuée avec des cellules eucaryotes dans des microplaques, l'imagerie cellulaire à haut débit pour des cellules procaryotes nécessite le développement de nouvelles stratégies de criblage en raison de la petite taille des ces cellules.

La microfluidique est une boîte à outils exceptionnelle pour l'étude des bactéries. Associée à la microscopie automatisée, elle permet l'analyse de processus dynamiques. En outre, cette technique permet un contrôle précis de l'environnement tout en facilitant l'imagerie au niveau de la cellule. De nombreuses plates-formes dédiées aux procaryotes ont été développées, cependant ces technologies de pointe ne permettent pas l'imagerie en parallèle de milliers de génotypes, indispensable au criblage à haut-débit.

La présente thèse porte sur le développement d'une plate-forme microfluidique de criblage cellulaire à haut-débit spécialement conçue pour les procaryotes. La plate-forme permet l'imagerie de 1152 souches bactériennes en parallèle aux niveaux cellulaire et intracellulaire. Dans un premier temps, nous démontrons la capacité de la plate-forme à non seulement, cribler des phénotypes présentant une division cellulaire anormale, mais également le criblage de phénotypes n'apparaissant que lors de profils complexes du milieu de croissance, tel que la persistance. Dans un second temps, nous utilisons la plate-forme afin de réaliser un criblage cellulaire génétique d'une librairie mutante de *Mycobacterium smegmatis* traitée à l'antibiotique isoniazide (INH). Ce criblage a permis l'identification de 31 mutants présentant un taux de persistance altéré comparé à la souche sauvage lors du traitement antibiotique, dont 8 présentaient un taux de persistance diminué et 23 présentaient un taux de persistance accru. Finalement, certains mutants ont été sélectionnés pour des études approfondies, réalisées avec la même plate-forme, afin d'identifier la dynamique de division et mortalité cellulaire sous-jacente à la persistance. L'étude révèle une dynamique surprenante où le mutant présentant un taux de persistance diminué, paradoxalement, présente également un taux de mortalité réduit comparé à la souche sauvage.

La plate-forme microfluidique de criblage cellulaire à haut-débit est particulièrement versatile et peut être exploitée pour de nombreuses études bactériennes, puisqu'elle permet notamment l'imagerie d'objets intracellulaires. Cette nouvelle technologie ouvre de nouvelles portes aux microbiologistes.

Mot clefs

Microfluidique, plate-forme de criblage, imagerie cellulaire à haut débit, microscopie automatisée, persistance bactérienne, isoniazide, hétérogénéité phénotypique, *Mycobacterium smegmatis*.

Abstract

Persistent cells, representing a small fraction of a bacterial population, are refractory to antibiotic therapy. It is a phenotypic transient state. The underlying mechanisms of persistence remain largely unknown, but even divergent hypotheses agree on a fundamental component: persistence arises from phenotypic heterogeneity. Novel approaches are needed to elucidate which factors allow some bacteria to persist but not others. High-content screening (HCS), which uses microscopy as a screening tool, enables the visualization of single-cell phenotypes and is thus particularly suited for studying bacterial persistence. Traditionally performed with eukaryotic cells in micro-well plate format, executing HCS with prokaryotic cells required the development of a screening novel strategy due to their much smaller size.

Microfluidics has proved to be a remarkable toolbox for bacterial studies. In combination with time-lapse microscopy, it permits the study of dynamic processes with single-cell resolution in a tightly controlled microenvironment. Though numerous microfluidic platforms for prokaryotes imaging have been developed, the current state of the art does not allow the imaging of thousands of genotypes in parallel, as is required for high-content screening.

The focus of this thesis is to develop a high-throughput microfluidic screening platform enabling high-content imaging of prokaryotic cells. This platform allows 1152 bacterial strains to be imaged in parallel on both the single-cell and sub-

cellular level with precise control over the growth environment. First, we demonstrate the ability of the platform to effectively screen for both altered cell division phenotypes through subcellular markers imaging in a static environment and for phenotypes emerging in complex medium profiles, such as bacterial persistence. Second, we employed our platform in a genetic screen, exposing a mutant library of *Mycobacterium smegmatis* to the antibiotic isoniazid (INH), and identified a total of 31 mutants with altered persistence rates during antibiotic exposure as compared to the wild-type. Eight of these mutants had decreased persistence rates while 23 mutants displayed increased persistence. Third, using the same platform we performed in depth analysis of mutants with altered rates of persistence in order to identify the cell division and cell death dynamics underlying persistence. This single-cell analysis revealed unexpected dynamics where a mutant with decreased persistence displayed a lower killing rate compared to the wild-type.

This high-throughput microfluidic screening platform is highly versatile and can be used in a wide range of bacterial studies, as it is capable of imaging not only single cells, but also subcellular markers, such as those based on the cell cycle or bacterial septa. This novel technology thus opens new doors for microbiologists.

Key words

Microfluidics, screening platform, high-content screening, time-lapse microscopy, bacterial persistence, isoniazid, phenotypic heterogeneity, *Mycobacterium smegmatis*, single-cell analysis.

1 Introduction

Biological systems and organisms are extremely complex and often require global approach to understand the underlying properties. The constant improvement and development of novel technologies in biology as well as engineering is allowing us to tackle clinically important and intractable problems such as bacterial persistence against antibiotics, which is the focus of this thesis. Approaches such as time-lapse microscopy and high content screening are new tools that can be used to address this biological challenge.

1.1 High content screening

1.1.1 Background

High-content screening (HCS) has emerged as a biological tool to address diverse biological questions, ranging from protein localization changes ([Chong *et al.*, 2015](#)) to cell differentiation ([Chia *et al.*, 2010](#)). This technique uses microscopy as a screening tool to investigate the effects of perturbation agents such as small molecules, RNAi, or chemicals on cellular phenotypes. Characterized by its ability to process thousands of samples simultaneously, HCS has become a fundamental analytical tool. HCS was initially developed and used by pharmaceutical industries

for drug discovery; however, it has recently become more accessible for fundamental scientific applications (Mattiuzzi *et al.*, 2016).

Major technological advances during the last two decades have facilitated the visualization of phenotypes in cells and small organisms (*C. elegans*) for HCS (Sönnichsen *et al.*, 2005). These developments include microscope automation, faster autofocus, improved automated fluid handling, development of new fluorescent probes, and improvement of image analysis methodologies, including the ability to extract quantitative data from images (Boutros *et al.*, 2015). With these improvements, HCS has been used to gain insight into many different biological processes, revolutionizing cell biology. For instance, using this approach Chia *et al.* identified genes involved in self-renewal and pluripotency properties in human embryonic stem cells (hESCs) by perturbing a GFP-hESC cell line using a genome-wide short interference RNA (siRNA) assay (Chia *et al.*, 2010). Similarly, Nieland *et al.* investigated synaptogenesis in mouse primary cortical neurons exposed to a lentiviral RNAi library and uncovered novel gene regulators in synapse formation (Nieland *et al.*, 2014). Thus, HCS is a very promising approach that is continuously expanding and evolving; nonetheless, application of HCS to fundamental biological problems still presents numerous challenges, as highlighted in the next section.

1.1.2 High content screening: challenges and limitations

HCS offers great perspectives regarding the interrogation of cell libraries, yet several aspects require improvements to broaden its systematic application. Challenges are mainly bound to the experimental procedure, as most of the HCS assays involve end-point measurements, typically performed in micro-well plates with fixed eukaryotic cells, which entails several limitations:

- Limited control over cell environment,
- Lack of temporal resolution,
- Use restricted to eukaryotic cells, *i.e.*, mammalian cells and yeast.

First, using classic micro-well plates limits control over the growth environment and prohibits experiments requiring complex environmental perturbations. Cells are confined in wells where depletion of nutrients and accumulation of metabolic wastes limits long-term experimentation. In addition, the accurate addition of compounds between wells or the removal of compounds from the medium remains a difficult task in conventional micro-well plates.

Second, HCS typically records end-point measurements only, which precludes the study of dynamic processes, as temporal information is disregarded, potentially leading to misinterpreted results. Temporal resolution is essential for monitoring dynamic processes in live cells. One of the most suitable and powerful tools available for monitoring cells over time is time-lapse microscopy (Zanella *et al.*, 2010). Using this approach, Honarnejad *et al.* investigated in live cells the mechanisms involved in disruption of calcium homeostasis in extra-short time-lapse movies (less than 30 seconds) (Honarnejad *et al.*, 2013). Another remarkable study reported several novel genes involved in mitosis based on live monitoring (over 48 hours) of a HeLa cell line expressing a histone tagged with green fluorescent protein (GFP) (Neumann *et al.*, 2010).

Third, the aforementioned studies were all performed on eukaryotic cells – more specifically, on mammalian cells – which are easier to image due to their large size, the wide availability of cell lines, and their relatively slow growth rate. However, HCS has also been applied to microbes, and more precisely to yeasts; for example, using an integrated HCS-synthetic genetic array method, the spindle morphogenesis in live and fixed budding *Saccharomyces cerevisiae* expressing a GFP-tagged tubulin was explored (Vizeacoumar *et al.*, 2010). Using a similar technique, protein localization in *S. cerevisiae* was assessed under chemical and genetic stimuli (Chong *et al.*, 2015), and in the budding yeast open reading frame (ORF)-GFP collection (Huh *et al.*, 2003), in a systematic and quantitative fashion.

To our knowledge, no high-content screenings with single-cell resolution and quantitative measurements have yet been performed using prokaryotes. The use of micro-well plates is not well suited for prokaryotes, as they are dispersed in the medium; thus, single-cell imaging is not feasible in micro-well plates and screenings

are limited to population-averaged measurements. For example, Campen *et al.* screened a mycobacterial mutant library by measuring fluorescence intensity in a 96-well plate to investigate the mechanism of action of the anti-tuberculosis drug isoniazid (INH) (Campen *et al.*, 2015). However, this screen was unable to measure single-cell phenotypes or cell-cell interactions within microcolonies. Other screens involving prokaryotes used micro-well plates for HCS. For instance, Christophe *et al.* quantified intracellular colonization of murine cells by a strain of *Mycobacterium tuberculosis* that constitutively expressed enhanced GFP (eGFP), using intracellular eGFP spots as a proxy for counting the number of bacilli within the host cells (Christophe *et al.*, 2010). HCS has also been used to screen for inhibitors of biofilm formation in *Pseudomonas aeruginosa* by measuring biofilm coverage coupled to cellular metabolic activity (Navarro *et al.* 2014). However, these experiments were performed in micro-well plates and did not allow any single-cell measurements of bacterial phenotypes but, rather, measurements averaged across the entire population. In contrast to screening methods based on micro-well cultures, microfluidics could potentially provide a powerful toolbox for HCS of bacteria, as it facilitates the management, imaging, and long-term culturing of small bacterial cells. Thanks to both miniaturization and precise control over the environmental conditions and the stimuli applied to cells (Cheong *et al.*, 2010), microfluidic technologies are particularly well suited for HCS, as discussed in the following sections.

1.2 The rise of microfluidics

1.2.1 Introduction to microfluidics

Microfluidics is a microengineering science that involves manipulation of small volumes of liquids, typically nanoliters or smaller. It is similar to miniaturized plumbing where fluids are constrained within microchannels ranging typically from 1 to 500 μm (Whitesides, 2006). This technology offers many advantages due to its "micro" properties; for example, microfluidics-based assays typically require very

small volumes of reagents, thus reducing experimental costs while simultaneously allowing parallelization of thousands of individual assays. The designs of microfluidic devices, while diverse, are often adapted for specific purposes. A typical microfluidic device may be based on a single channel – as in the case of devices used for capillary electrophoresis, for instance – or may involve more complicated designs comprising thousands of microchannels controlled by micro-mechanical valves, such as in microfluidic large-scale integration (mLSI) devices ([Araci *et al.*, 2012](#); [Melin *et al.*, 2007](#)).

Inherently, microfluidics deals with the peculiarities of fluid mechanics at microscale, which are very different than those of the "macro-world". At the microscale, viscous forces dominate fluid flow, contrasting with the macroscale where inertial forces are dominant. Consequently, fluid flow within microchannels is typically laminar (non-turbulent), allowing highly precise temporal and spatial control of solute concentrations ([Squires and Quake, 2005](#)). Microfluidic platforms are also highly versatile in that, with the use of micromechanical valves, dynamic switches can be made between different medium sources. Further, microfluidic devices are often made of polydimethylsiloxane (PDMS), an elastomeric material that is easily manipulated using soft lithographic techniques; PDMS is ideal for optical measurements due to its transparency, biocompatibility, and gas permeability. Given these advantages, microfluidics has found its place in numerous applications across fields, including cell biology ([Velve-Casquillas *et al.*, 2009](#)), drug discovery ([Kang *et al.*, 2008](#); [Miller *et al.*, 2011](#)), diagnostics ([Piraino *et al.*, 2016](#)), gene network expression and synthetic biology ([Niederholtmeyer *et al.*, 2015](#)), chemical synthesis ([Elvira *et al.*, 2013](#)), and molecular biology ([Ahrberg *et al.*, 2016](#)). The following sections will review microfluidic platforms developed for microbes (specifically prokaryotes), and microfluidic screening platforms suitable for high-throughput high-content screening.

1.2.2 Microfluidic platforms for single-cell imaging of prokaryotes

The small scale of microfluidic platforms particularly facilitates imaging small cells, such as bacteria. A plethora of devices has been developed for studies coupling precise control over the culture environment with single-cell observation of bacteria by time-lapse microscopy (Bennett *et al.*, 2009; Groisman *et al.*, 2004; Long *et al.*, 2013; Okumus *et al.*, 2016; Yawata *et al.*, 2016). This precise control over the environment, combined with single-cell imaging by time-lapse microscopy, offers great opportunities for studying bacterial growth, division, and death. For instance, Wang *et al.* developed a platform, the so-called “mother machine”, that allows for single-cell imaging of *Escherichia coli* over hundreds of generations to investigate long-term growth and division patterns. The device consists of hundreds of narrow “growth channels” connected perpendicularly to a “feeding channel” for both medium renewal in the growth channel and removal of emerging cells (Figure 1.1a). The “mother cell” rests at the bottom of the channel and is imaged by timelapse microscopy (Wang *et al.*, 2010). In another approach, chip-integrated micromechanical valves and a peristaltic pump were used to perform circulation and washing cycles in a bacterial growth chamber loop (or microchemostat), thus preventing biofilm formation of planktonic *E. coli*. Continuous removal of a fraction of the bacterial population while adding fresh nutrients enabled constant environmental conditions in the 16-nL bioreactors, and, hence, long-term imaging of bacteria (Figure 1.1b). These bacteria carried a synthetic circuit that autonomously regulated cell density through a negative-feedback mechanism based on quorum sensing. Programmed cell density oscillations, monitored at single-cell resolution, proved to be more accurate and stable in the microchemostat compared to macroscale batch cultures (Balagaddé *et al.*, 2005). Yet, the height of the bioreactors used in this study (10 μm) is still large compared to the dimensions of an *E. coli* cell (diameter of approximately 1 μm) and therefore isn’t optimized for single-cell imaging. Danino *et al.* developed a microfluidic device with low-ceiling chambers of 100 x 100 μm^2 in order to investigate a gene circuit generating synchronized oscillations of a reporter gene in *E. coli* (Figure 1.1c). This global intercellular coupling revealed a mechanism of emergent coordinated behavior at the colony level (Danino *et al.*, 2010).

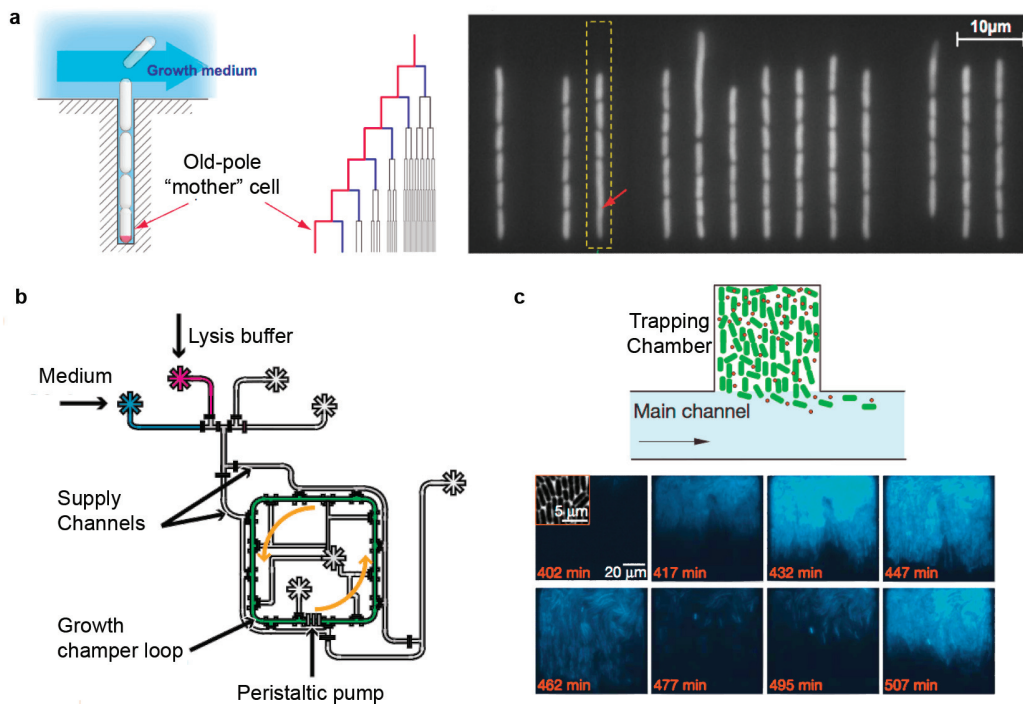


Figure 1.1: Microfluidic platform for single-cell screening of bacteria. (a) Schematic illustration and fluorescence images of the microfluidic “mother machine”. The mother cell is trapped at the bottom of the channel. Images adapted from Wang *et al.* 2010. (b) Schematic illustration of the microchemostat. The green loop is the growing chamber divided into several addressable segments for maintaining constant environmental conditions. Images adapted from Balagadé *et al.* 2005. (c) Microfluidic device used for maintaining *E. coli* at a constant density. The main channel supplies growth medium to cells in the low-ceiling trapping chamber. Fluorescence images of a representative experimental run demonstrate synchronization of oscillations in a population of *E. coli* residing in the microfluidic device. Image adapted from Danino *et al.*, 2010.

These microfluidic devices were nevertheless limited to the use of a single bacterial strain and thus are low-throughput in terms of the number of different genotypes that can be analyzed in parallel. Taniguchi and coworkers made some progress in this respect. They designed a microfluidic device with a slightly increased throughput: the platform enabled the simultaneous imaging of 96 different strains of *E. coli* immobilized on a poly-L-lysine coated coverslip (Taniguchi *et al.*, 2010).

However, their platform lacked dynamic control over the environment and, most importantly, the cells had to be loaded manually from 96 independent inlets. Further, this design was not meant for long-term time-lapse experiments but rather for a single time-point observation. Table 1.1 lists the different characteristics of each platform described in this section, such as spatial resolution required for single-cell imaging, the number of conditions tested, and throughput in terms of the number of different bacterial strains (genotypes) that could be imaged in a single experiment.

	Spatial resolution	Throughput in terms of:	
		Genotypic	Conditions tested
Wang <i>et al.</i> , 2010	++++	1	1
Balagaddé <i>et al.</i> , 2005	++	1	1
Danino <i>et al.</i> , 2010	++++	1	1
Taniguchi <i>et al.</i> , 2010	+++	96	1

Table 1.1: Comparison between different microfluidic platforms for single cell imaging of prokaryotes. A high spatial resolution is required for imaging of single cells or fluorescently tagged subcellular objects; these platforms enable single-cell imaging with different resolution. Throughputs are indicated in terms of the number of bacterial strains (genotypes) and the number of conditions that can be tested in a single experiment.

These different microfluidic platforms were developed to study microbes with single-cell resolution at the small scale of bacterial cells. These approaches allow quantitative measurements not only of the physiological parameters of single cells, but also of their behavior. Although the single-cell studies detailed in this section have provided novel microbiological insights, these methods are not amenable for the study of large numbers of different bacterial strains (genotypes). Thus, there is still a strong need to develop high-throughput microfluidic platforms enabling the study of large numbers of bacterial strains in parallel.

1.3 Microfluidic screening platforms

Microfluidics is particularly suited for high-throughput screening (HTS) due to its economy of scale (decreased consumption of reagents) and its miniaturization, facilitating parallelization of thousands of experiments on a small footprint ([Maerkl, 2009](#)). In the following sections, I will emphasize the strengths and limitations for screening purposes of different microfluidics systems, e.g. single-phase and two-phase systems.

1.3.1 Two-phase system: droplet microfluidics

Droplet microfluidics is an exceptional tool for screening: it allows ultra high-throughput (>10,000 Hz) while reducing volumes of reagent and providing single-cell measurements in a controlled chemical environment ([Guo *et al.*, 2012](#); [Kaminski *et al.*, 2016](#)). It uses two immiscible phases to generate micro-droplets, i.e. water droplets in an immiscible oil carrier. Individual cells are encapsulated in these droplets via stochastic, Poisson-distributed confinement; upon encapsulation, droplets are easily manipulated (e.g., split, sorted, merged, etc.) and are independently controlled and monitored. Each droplet becomes an independent bioreactor capable of hosting a unique biochemical reaction in an ultra-small volume. Brouzes *et al.* developed a high-throughput droplet-based microfluidic screening platform for the analysis of mammalian cells exposed to different optically-encoded drug concentrations ([Brouzes *et al.*, 2009](#)). Similarly, Shim *et al.* encapsulated individual bacterial cells in picoliter droplets to measure the expression of specific enzyme (alkaline phosphatase) coupled to red fluorescent protein (RFP). The platform was applied to quantify enzymatic activity differences between two mutants for the targeted enzyme ([Shim *et al.*, 2009](#)).

Despite its promise as an ultra high-throughput screening technique, droplet microfluidics suffers from several limitations. First, with a few exceptions ([Jiang *et al.*, 2016](#); [Jakiela *et al.*, 2013](#)), the detection of fluorescence in droplets is limited to single time-point measurements, with no temporal tracking of the same individual

cells over time, as in flow cytometry. Second, droplet microfluidics doesn't provide the high spatial resolution required for single-cell imaging or subcellular imaging, because the cells are "free-floating" within droplets (Maerkl, 2009). Finally, this technique does not facilitate complex medium profiles, such as switching between different medium sources or applying spatial or temporal gradients (Kaminski *et al.*, 2016).

1.3.2 Single-phase system: flow microfluidics

Single-phase systems offer some advantages over their two-phase counterparts: first, individual cell phenotypes can easily be monitored over time; second, the microenvironment can be precisely tuned, including complex medium perturbation, as, for instance, repeated switches between different medium sources. However, this increase in precision and the amount of information gained comes at the cost of reduced throughput.

Many microfluidic screening platforms were designed for drug screening, where one strain (i.e. one genotype) of cells is exposed to different drugs or different drug concentrations (Du *et al.*, 2015). As an example, Wang *et al.* developed a microfluidic platform for HCS of tumor cells that allows multi-parameter measurements. Cells were exposed to a spatial gradient of anti-tumor drug concentrations, and measurements of plasma membrane permeability, nuclear size, mitochondrial transmembrane potential, and intracellular redox state were simultaneously recorded (Ye *et al.*, 2007).

In another approach, PDMS traps were used for single-cell analysis of aging eukaryotic cells. The trapping device captures up to 8,000 individual yeast cells in cup-shaped PDMS structures and can retain them through time, with fresh medium continuously flowing and removing daughter cells, which can then be trapped in downstream structures. Although this platform allows numerous cells to be monitored in parallel, it is still restricted to the analysis of just one strain per experiment (Jo *et al.*, 2015).

A major improvement in throughput – in terms of the number of strains (genotypes) that can be imaged simultaneously – is the screening platform developed by Dénervaud *et al.* for *S. cerevisiae*. This platform allows the imaging of 1,152 different yeast strains in parallel at single-cell resolution. This study addressed protein localization and abundance in *S. cerevisiae* using a GFP fusion library, including the dynamics of single-cell gene expression under stressful conditions (Dénervaud *et al.*, 2013).

In conclusion, of the few devices that are appropriate for HTS at the single-cell level, all were developed for eukaryotic cells, whose cellular volume is hundreds or thousands of times that of a typical bacterium. Furthermore, most of these platforms are limited to the screening of a single strain (genotype). Although the platform introduced by Dénervaud *et al.* did enable HCS of multiple strains in parallel, it was developed for yeast and thus is unsuitable for application to prokaryotes.

1.3.3 Conclusion

Most of the HCS/HTS methods developed to date are suitable only for application to eukaryotic cells. There have been some attempts to develop two-phase microfluidic platforms for prokaryotes; however, as described previously, droplet microfluidics does not allow single-cell imaging and is therefore not suitable for HCS. Regarding single-phase microfluidic systems, no microfluidic screening platform has been developed for HCS of prokaryotes enabling imaging of numerous strains (genotypes) in parallel.

1.4 Bacterial persistence phenomenon during antibiotic exposure

Since their discovery by Antoni van Leeuwenhoek in the 17th century, bacteria have been studied intensively. Yet, many biological questions regarding prokaryotes still

puzzle microbiologists. A fascinating example with great clinical relevance is bacterial persistence during antibiotic treatment. Persistence is a classical “unsolved problem” where phenotypic heterogeneity has been implicated (Dhar *et al.*, 2007). This phenotypic heterogeneity within a clonal population motivated the use of single-cell tools such as HCS in order to tackle persistence.

1.4.1 A historical perspective

Persistent cells are cells that survive antibiotic exposure, usually constituting a small fraction of a bacterial population. Bacterial persistence during drug treatment has dramatic clinical consequences, as it is the root of latency in infectious diseases, such as tuberculosis (Dutta *et al.*, 2014; Gomez *et al.*, 2004), and in recurring infections, such as urinary tract infections (Anderson *et al.*, 2003; Hannan *et al.*, 2012). Antibiotic persistence is a transient (non-heritable) phenotype that differs from antibiotic resistance, the latter being attributed to genetic mutation.

Fractional survival of a bacterial population during prolonged drug exposure was first observed by Hobby *et al.* in 1942 (Hobby *et al.*, 1942), who reported that 99% of a *Streptococcus* population was killed by exposure to penicillin, although the remaining 1% seemed able to survive. Later, Bigger attempted to sterilize cultures of *Staphylococcus pyogenes* using bactericidal doses of penicillin (Bigger, 1944), but failed to completely eliminate all drug-sensitive staphylococcal cells, even under prolonged antibiotic exposure. At these high penicillin concentrations, a small fraction of the population, approximately one per million, was able to survive, though this feature was not passed on to their progeny after antibiotic withdrawal and regrowth. Consequently, Bigger named these cells *persisters*, thereby differentiating them from *resisters*, which had acquired a stable (heritable) genetic mutation. He noticed that persister cells could arise either by being carried over in the inoculum or during antibiotic treatment through contact with their new environment; as an example, he found that incubating bacteria in cold medium increased the percentage of persisters. Bigger hypothesized that, because penicillin actively targets dividing cells, the persister cells might be in a transient,

physiologically dormant state. Although this hypothesis was not proven at that time, it was supported by several experiments. Specifically, the frequency of persister cells increased when cell division was inhibited by various methods, e.g. by culturing cells in minimal media or low (suboptimal) temperatures, or by exposing them to bacteriostatic agents. These observations gave rise to a dogma that has persisted up to the present day, viz. that persisters are dormant (non-dividing) or slowly dividing cells.

1.4.2 Clinical relevance of persistence

Several infectious diseases are particularly difficult to cure due to the recalcitrance of genetically sensitive microorganisms to sterilization by antibiotic treatment. Pathogens that are notoriously difficult to cure with antibiotics include *inter alia* *Mycobacterium tuberculosis*, *Pseudomonas aeruginosa*, *Candida albicans*, and uropathogenic *Escherichia coli* (Gomez *et al.*, 2004; Fauvart *et al.*, 2011). Latent bacterial infections and relapses following chemotherapy are thought to be clinical manifestations of persistence. It was recently shown that patients with chronic *Candida albicans* infections displayed high numbers of persister cells (Lafleur *et al.*, 2010). Using a mathematical model, Levin *et al.* demonstrated the importance of persistence in lengthening treatment regimens, increasing the risk of treatment failure, and promoting the emergence of mutations causing resistance (Levin *et al.*, 2006). Acquired resistance could arise through horizontal gene transfer (Lewis *et al.*, 2007) but also through stochastic mutations occurring during bacterial replication. In this context, targeting persister cells with new antimicrobial therapies becomes of even greater clinical interest. More specifically, it has been postulated that the development of drugs that can effectively kill persister cells might significantly reduce the length of treatment regimens of chronic infections and increase the therapeutic success rate (Fauvart *et al.*, 2011).

1.4.3 The discovery of a high persistence mutant enabled in depth study of the phenomenon

Following the pioneering studies by Hobby and Bigger, the study of persistence mechanisms was delayed for decades due to its challenging nature. After all, these cells only occur as a transient phenotypic state and they comprise a very small fraction of a bacterial population (typically less than 1%). Population-averaged measurements are thus inappropriate for analyzing persistence; this complication, combined with a general lack of suitable single-cell technologies, has hindered the in-depth analysis of the persistence phenomenon for decades.

A major breakthrough regarding persistence was the discovery of a highly persistent mutant by Moyed *et al.* (Moyed *et al.*, 1983). An *E. coli* mutant library was repeatedly exposed to ampicillin and mutants displaying increased persistence but normal growth rates were selected. More specifically, mutations at the *hipA* locus led to a 10,000-fold increase in the frequency of persister cells compared to the wild-type parental strain, i.e. reaching up to 1% persistence of the bulk population of *hipA* mutant cells versus 1 per 1,000,000 in the wild-type population. This mutant strain greatly facilitated further experiments on persistence, which were previously very arduous.

1.4.4 Tackling persistence with microfluidics and time-lapse microscopy

Time-lapse microscopy is a powerful tool for observing the dynamics of cellular behavior at the single-cell level. Single-cell time-lapse imaging is one of the few techniques that are suitable for studying rare phenotypic variations such as persistence, which typically represent < 1% of bacterial cells in a population. Indeed, in conventional population-averaged measurements, the behavior of the population majority will mask that of minor subpopulations such as persisters. Only a few experimental tools are currently available to study persistence; of these, time-lapse microscopy is the most powerful, as individual cells can also be tracked over time. Time-lapse microscopy combined with microfluidics enables temporal

tracking of cells in a tightly controlled microenvironment and facilitates mimicking the complex medium profile required to study persistence, that is, switching repeatedly between plain medium and medium containing antibiotics. Using this approach, Balaban *et al.* investigated the persistence of the high persister *hipA* strain of *E. coli* at the single-cell level. The bacteria were cultured in a microfluidic platform where they were confined in micro-channels in order to force the cells to grow as linear chains. The cells were exposed to lethal concentrations of ampicillin and cell deaths and divisions were monitored before, during, and after treatment. A small number of survivors resumed growth after antibiotic removal; these survivors (the persisters) exhibited strongly reduced growth rates prior to and during antibiotic exposure (Figure 1.2a). These observations were taken as evidence that persisters constituted a pre-existing population of non-growing or slowly growing cells. The authors concluded that two types of persisters exist, exhibiting different growth dynamics. Type I persisters are non-growing cells exiting the stationary phase; the size of this fraction thus depends on the size of the initial inoculum. Type II persisters are normal cells that have switched to a persistent state with a reduced growth rate, about an order of magnitude slower than normal (Balaban *et al.*, 2004). These experiments provided the first direct evidence to support Bigger *et al.*'s longstanding hypothesis about the nature of persisters (i.e. that persisters may be pre-existing, non-growing cells), but also suggested an alternative mode of persistence in slowly growing cells.

However, reduced growth rate doesn't seem to be the only explanation for persistence; indeed, fluoroquinolones, for instance, are able to kill non-growing cells but are not able to eliminate persisters (Dhar *et al.*, 2007). The universality of Bigger's postulate has recently been challenged by demonstrating that mycobacterial persisters actively divide in the presence of antibiotic (Wakamoto *et al.*, 2013). In this microfluidic setup, cells were seeded onto a coverslip and a semi-permeable membrane allowed diffusion of fresh nutrients from the microfluidic device clamped on top. Time-lapse microscopy revealed that the apparently stable number of persistent cells during prolonged drug exposure masks a highly dynamic state in which the rates of division and killing are balanced (Figure 1.2b). Furthermore, the single-cell growth rates of mycobacterial cells treated with the

anti-tuberculosis drug isoniazid (INH) was not correlated with survival or death; instead, survival was negatively correlated with the expression of bacterial catalase-peroxidase (KatG), which activates INH, at the single-cell level.

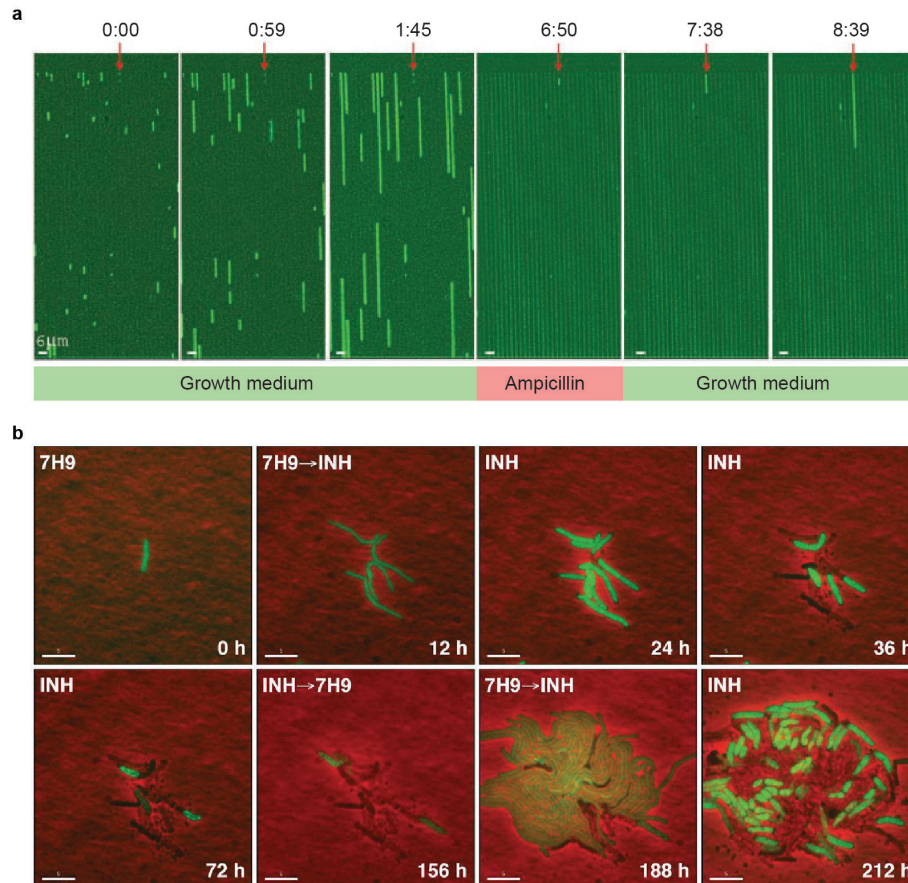


Figure 1.2 Tackling persistence with microfluidics and time-lapse microscopy. (a) Time-lapse microscopy of *hipA7 E. coli* expressing a yellow fluorescent protein (YFP). The bacteria grew and established linear microcolonies prior to exposure to ampicillin for 5 hours. Arrows indicate non-growing cells that resumed growth upon antibiotic removal. Time is represented as h:mm. Images adapted from Balaban *et al.*, 2004. **(b)** Time-lapse of *Mycobacterium smegmatis* growing in regular medium (7H9) for 12 hours then exposed to isoniazid (INH) for 6 days (at 12-156 hours) before resuming growth upon antibiotic removal (at 156 hours). A second antibiotic exposure (at 188-212 hours) demonstrated that the rare surviving cells remained antibiotic-sensitive and hence survival could not be attributed to acquired (heritable) resistance. Images adapted from Wakamoto *et al.*, 2013.

To conclude, the two aforementioned studies combining microfluidics with time-lapse microscopy – the first focused on a *hipA* strain of *E. coli* (Balaban *et al.*, 2004), the second on mycobacteria (Wakamoto *et al.*, 2013) – provided important insights into the link (or lack thereof) between single-cell growth rates and persistence. The first study supported Bigger’s postulate that persisters are non-growing cells; the second study challenged this idea. It is important to note that, for technical reasons, the first study was focused on a high-persistence *hipA* mutant strain of *E. coli*; thus, it is possible that the behavior of this mutant strain might not be representative of wild-type cells. On the other hand, mycobacterial KatG is not required for activation of drugs other than INH, so cell-to-cell variation of KatG expression cannot explain persistence in the context of other anti-tuberculosis drugs. It seems that the phenomenon (persistence) is more complex than originally postulated by Bigger and multiple mechanisms may account for persistence during antibiotic exposure, including some that have yet to be identified.

1.4.5 Mechanisms of bacterial persistence

Despite decades of research since the discovery of persistence in the 1940s, little is known about the factors determining whether a bacterial cell is able to persist during antibiotic exposure. Investigating mechanisms of persistence is challenging not only due to the transient nature of the phenomenon, but also to the low frequency of these cells in the main population (Dhar *et al.*, 2007). Despite this, several hypotheses have been put forward. These hypotheses, which will be described in the present section, are exhaustively covered by several reviews (Dhar *et al.*, 2007; Gefen *et al.*, 2009; Gerdes *et al.*, 2012; Amato *et al.*, 2014; Maisonneuve *et al.*, 2014; Harms *et al.*, 2016; Van den Bergh *et al.*, 2016).

Persistence is thought to arise from phenotypic heterogeneity generated by epigenetic mechanisms such as gene expression noise and variations in protein levels (Elowitz *et al.*, 2002), cell-cell interactions (quorum sensing), or cell cycle stage (Dhar *et al.*, 2007; Ackermann, 2015). Biological processes are inherently noisy and the low copy numbers of molecules in small bacterial cells unavoidably

limits the precision of gene expression, which contributes significantly to cell-cell phenotypic heterogeneity (Elowitz *et al.*, 2002; Koern *et al.*, 2005). The inherently stochastic nature of gene expression processes results in fluctuations in both transcription and translation, despite constant genetic and environmental conditions. Thus, the molecular composition of cells can be highly variable between individuals; as a consequence, each individual of an isogenic population exposed to the same environment will display different phenotypes and thus respond uniquely to environmental impacts. For instance, Wakamoto *et al.* demonstrated that KatG expression levels within an isogenic microcolony were highly variable and fluctuated over time, and that KatG levels correlated with isoniazid-mediated killing (Wakamoto *et al.*, 2013).

As mentioned already, single-cell growth rates may also play a critical role in bacterial tolerance to antibiotics. Bigger postulated more than 70 years ago that non-growing dormant cells are not targeted by antibiotics (Bigger, 1944). The hypothesis that persister cells switch to a physiologically dormant state was recently supported by Balaban *et al.*'s work (Balaban *et al.*, 2004), but has been challenged by Wakamoto *et al.* as discussed in the previous section (Wakamoto *et al.*, 2013). Furthermore, it has been demonstrated by flow cytometry that dormancy is neither necessary nor sufficient for persistence in mycobacteria (Orman *et al.*, 2013). Besides the overall growth rate, the growth stage has been shown to impact persistence levels: bacteria in the stationary phase of the growth cycle are refractory to many antibiotics. Keren and colleagues demonstrated the dependence between persistence of *E. coli* treated with ampicillin and growth stage; they showed that the number of persisters in the early exponential phase is stable, but increases during the exponential phase until reaching a plateau during stationary phase, where cells become almost completely tolerant to ampicillin. Furthermore, the authors showed that continuous subculture of early exponential-phase cultures dramatically reduced the number of persisters. They concluded that the production of persisters is dependent on the growth stage of the population, with formation of persisters being particularly favored during entry into stationary phase (Keren *et al.*, 2004).

Another hypothesis regarding the “molecular mechanisms” of persistence is that toxin-antitoxin (TA) modules are responsible for generating slow or non-growing persister cells. TA modules are operons composed of two genes: a stable toxin and an unstable antitoxin. The expression of a stable toxin typically reduces the growth rate by inhibiting a major cellular function, such as translation; the unstable antitoxin, which eventually gets degraded, suppresses the activity of the toxin by forming a non-functional heterodimer. To function, sufficient amount of toxin and an unbalanced level of toxin/antitoxin in favor of the toxin are both required (Harms *et al.*, 2016). In addition, it has been reported that the alarmone (p)ppGpp, a master regulator enabling bacterial survival during starvation, triggers persistence by activation of Lon protease, which in turns activates TA modules. More specifically, unusually high levels of (p)ppGpp in a small subpopulation of cells induces slow growth through TA activation – and thereby persistence (Maisonneuve *et al.*, 2011). Numerous TA modules were found to be upregulated in persister cells, as for instance the *hipA* “high persistence” toxin gene discovered by Moyed *et al.* (Moyed *et al.* 1983; Germain *et al.*, 2013). Similarly, overexpression of RelE, another toxin, in *E. coli* led to up to a 10,000-fold increase of persisters (Keren *et al.*, 2004). While these findings are promising, they do not provide a universal explanation for persistence, because some species displaying strong persistence do not encode any known TA modules in their genomes; a good example is *Mycobacterium leprae*, which is notoriously difficult to eliminate with antibiotics.

The DNA damage or “SOS” response might also play a critical role in bacterial tolerance to antibiotic exposure. The SOS response mediates DNA-damage repair and inhibits cell division. Dörr *et al.* exposed *E. coli* to sublethal concentrations of ciprofloxacin, which generates DNA double strand breaks, in order to activate the SOS response; a subsequent exposure to lethal concentrations of ciprofloxacin showed a highly increased persistence rate that was dependent on activation of the SOS gene network (Dörr *et al.*, 2009).

Cell-to-cell variation in the expression of drug efflux pumps may also play a role in persister formation: in a recent study, it was shown that in *E. coli* treated with β -

lactam antibiotics, the rare persister cells showed less cytoplasmic drug accumulation due to enhanced efflux activity ([Pu et al., 2016](#)).

Thus, many hypotheses – some of them apparently contradictory, and none of them explaining all of the observations in the literature – have been put forth to explain the mechanisms underlying persistence. However, all of the existing hypotheses do agree on one fundamental component: persistence arises from phenotypic heterogeneity rather than genetic mutations. This diversity may be beneficial for the population, as it provides flexibility for some individuals to survive sudden changes in the environment, such as antibiotic exposure ([Ackermann, 2015](#)). The ultimate nature of persister cells nonetheless remains elusive, as does the molecular basis of antibiotic tolerance.

1.5 Aim and motivation

This thesis focuses on three different aims, which will be sequentially described in the following paragraphs and are summarized here:

- I. Development of a high-throughput microfluidic screening platform for prokaryotic cells
- II. Microscopy-based genetic screen to identify genes involved in mycobacterial persistence
- III. Cellular dynamics underlying mycobacterial persistence in mutants with altered rates of persistence

The first aim is to engineer a high-throughput microfluidic screening platform for live-cell imaging of prokaryotic cells that enables the imaging of 1,152 different strains (genotypes) in parallel by time-lapse microscopy at single-cell and even subcellular resolution with precise control over the microenvironment.

As mentioned previously, conventional cell-based screening methods measure a signal averaged over large numbers of cells and provide little or no insight into phenotypic heterogeneity between individual cells. HCS, which uses microscopy as a

screening tool, enabled the observation of phenotypes at single-cell resolution. Yet, HCS are mostly restricted to fixed (dead) eukaryotic cells and the investigation of dynamic processes is not achievable. In addition, conventional cell-based HCS assays are usually performed in classical micro-well plates (Neumann *et al.*, 2010), which carry major disadvantages: first, limited and non-precise control over the microenvironment (in bulk live-cell assays, wastes accumulate and nutrients are consumed over time); second, the inability to observe single-cell phenotypes of prokaryotic cells, which are typically much smaller than eukaryotic cells.

The application of microfluidics has the capability to address these limitations. Furthermore, its combination with time-lapse microscopy permits the observation of dynamic processes with a precise control over the microenvironment. Despite the recent development of several microfluidic devices for single-cell observation of bacteria by time-lapse microscopy (Bennett *et al.*, 2009; Balagaddé *et al.*, 2005; Groisman *et al.*, 2005; Wang *et al.* 2010; Leng *et al.*, 2013; Okumus *et al.*, 2016; Yawata *et al.*, 2016; Balaban *et al.*, 2004; Danino *et al.*, 2010), these microfluidic devices remained of low genotypic throughput. Furthermore, microfluidic devices that have been developed for high-throughput screening at the single-cell level are tailored to accommodate eukaryotic cells and they are unsuitable for applications involving prokaryotic cells (Déneraud *et al.*, 2013).

To summarize, there is a lack of HCS/HTS tools available for bacterial imaging. The focus of the thesis is to bridge this gap by developing a highly versatile high-throughput microfluidic platform for microscopy-based screening of prokaryotic cells, which requires several features:

- I. Single-cell and subcellular resolution for prokaryotic cells
- II. Precise control over the microenvironment
 - a. Continuous medium renewal for long term imaging
 - b. Ability to generate complex environmental perturbations
- III. High genotypic throughput (parallel processing of many strains)

After designing, constructing, validating, and characterizing the new microfluidic device, I focused on my second aim, which was to investigate genes involved in

mycobacterial persistence during antibiotic treatment. Bacterial persistence is responsible for prolonged and recurrent infections, which often result in antibiotic treatment failure. Understanding the genetic and molecular basis of bacterial persistence will be critical to identify new targets for drug development, and for revising treatment regimens to increase their efficiency. Although recent studies have shed light on potential molecular mechanisms such as efflux pumps (Pu *et al.*, 2016), genetic noise (Elowitz *et al.*, 2002; Dhar *et al.*, 2007), TA modules (Maisonneuve *et al.*, 2011), enzyme fluctuations (Wakamoto *et al.*, 2013), etc., there are still more questions than answers and despite decades of research the underlying mechanisms responsible for persistence remain mostly unknown.

In this thesis, I seek to identify the genes involved in mechanisms of persistence in the model organism *Mycobacterium smegmatis*. Although persistence is not due to stable genetic changes (mutations) between individuals, we reason that this phenotype must nonetheless have a genetic basis and it should therefore be possible to identify mutants with altered rates of persistence. Furthermore, the available evidence – such as, for instance, the high persister *hipA* mutant in *E. coli* (Moyed *et al.*, 1983) – suggests that mechanisms causing persistence are genetically encoded, even though stable mutations are not involved (Harms *et al.*, 2016). Therefore, I applied the new microfluidic screening platform to a time-lapse microscopy-based genetic screen of a library of *M. smegmatis* mutants exposed to isoniazid (INH), a frontline anti-tuberculosis drug, to identify genes involved in persistence.

The last aim of the present work was to gain insight about the cellular dynamics (growth, division, death) underlying bacterial persistence. For that purpose, cell divisions and cell deaths were quantitatively investigated at the single-cell level using the same HTS microfluidic platform. As a “test case”, the dynamics of a mutant with decreased persistence (smaller fraction of survivors) was contrasted to the dynamics of a mutant displaying increased persistence (larger fraction of survivors), in order to determine which parameters might be linked to differential survival during antibiotic treatment.

2 The high-throughput microfluidic screening platform for prokaryotes

2.1 Design of the microfluidic screening platform

I developed a versatile microfluidic screening platform for time-lapse microscopy-based screening, allowing single-cell screening based on cellular phenotypes (e.g. morphology, growth, division, death) and subcellular phenotypes (e.g. expression of fluorescently tagged proteins). The new platform had to meet several criteria in order to carry out HCS/HTS with bacterial cells, the most important of which were:

- I. Single cell resolution of prokaryotic cells,
- II. Precise control over the growth environment,
- III. Imaging of thousands of mutant strains in parallel,

The microfluidic screening platform was adapted from a HCS/HTS microfluidic device designed for analyzing thousands of *S. cerevisiae* strains in parallel and on the single-cell level in a single experiment with precise control over the growth environment (Dénervaud *et al.*, 2013). However the volume of a *S. cerevisiae* cell being hundreds of times larger than the volume of a bacterium, the platform had to be re-engineered to achieve single-cell resolution at the prokaryotic size scale. The platform engineered here was designed for the high-throughput, single-cell analysis

of prokaryotes, and permits 1,152 bacterial strains or clones to be screened in a single experiment (Figure 2.1a).

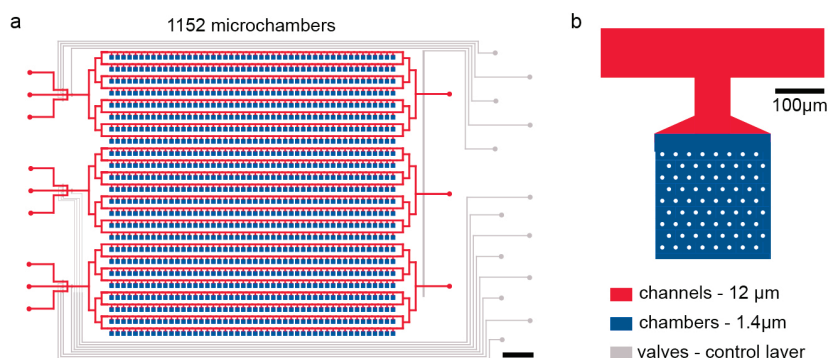


Figure 2.1: Schematic of the microfluidic screening platform. (a) The PDMS chip is divided into three independent sections and has a total of 1,152 chambers arranged in a 24 x 48 array. (b) A microchamber (blue) with dimensions 260 x 260 x 1.4 μm with 72 pillars (white) arranged in hexagons to prevent collapse.

S. cerevisiae cells, which the original device was designed to accommodate, are spherically shaped eukaryotic cells (width, 4-10 μm) that are much larger than rod-shaped bacteria such as *E. coli* or *M. smegmatis* (width, 1.0 or 0.5 μm , respectively). Therefore, the original HCS/HTS microfluidic platform required several important modifications before single-cell imaging of bacterial cells was possible. First, the microchamber ceiling height was lowered from 5 μm to 1.4 μm and the microchambers were restructured to prevent collapsing due to the very high aspect ratio of 260 : 1.4 (width : height). Indeed, this high aspect ratio proved highly problematic and required iterative design of the geometry of the microchambers. Polydimethylsiloxane (PDMS), a highly elastic material, generally requires a lower aspect ratio to prevent collapse. Therefore, a total of 72 pillars of diameter 10 μm organized hexagonally (to ensure equal distance between each pillar) were added to support the structure and prevent microchamber collapse (Figure 2.1b). In addition, the new microchambers were designed to allow unilateral perfusion via diffusion from the flow channel. The dimensions of the T-junctions connecting the microchambers to the flow channels were reduced to prevent delamination: lengths were reduced from 300 μm to 150 μm and widths were reduced from 150 μm to 70

μm . The final platform features 1,152 microchambers divided into three independent subsets arranged in 24 rows and 48 columns (Figure 2.1a) on a footprint of $1.8 \times 1.8 \text{ cm}^2$. Medium supply can be switched between two different medium sources using integrated elastomeric valves, ensuring precise control over the growth environment.

2.2 Mold and PDMS device fabrication

The platform, designed in L-edit, is composed of two functional layers: a flow layer and a control layer. The upper control layer consists of channels and microvalves of height $12 \mu\text{m}$ that control flow inputs and outputs. The lower flow layer consists of two structures: $12 \mu\text{m}$ high flow channels and $1.4 \mu\text{m}$ high microchambers. Due to PDMS shrinkage during curing, control and flow layer molds were scaled up to 100.5% and 101.5%, respectively, to fit the spotting pitch of the array.

The high-throughput microfluidic screening device was fabricated using standard techniques of soft lithography (Thorsen, 2002). A total of three masks were produced: one for the valves, one for the microchambers, and one for the flow channels. The chrome masks coated with AZ1518 were written on a DWL200 laser writer (Heidelberg Instruments Mikrotechnik) with a 10 mm head. Masks were developed with AZ351, etched, and finally stripped to remove residual resist. These masks were then used to pattern photoresist-coated wafers. Both a flow layer wafer and a control layer wafer were produced. The flow layer mold was fabricated as follows: first, to pattern microchambers, AZ nLof photoresist was spin-coated at $1.4 \mu\text{m}$ thickness on the silicon wafer. The resist was then exposed, developed, and hard-baked. Second, $12 \mu\text{m}$ high AZ9260 resist was spin-coated on top of the microchambers. The microchannels were made of AZ9260, since they required rounded cross sections to ensure hermetic valve closure. The resist was exposed and developed in two successive baths of AZ400K (dilution in deionized water 1:3; see Materials & Methods for details). To anneal the AZ9260 photoresist, the microchannels were baked a final time at high temperature. The control layer mold

was made of a single 12 μm high layer of SU8 GM1070. The resist was exposed and developed using standard photolithography methods (Xia *et al.*, 1998).

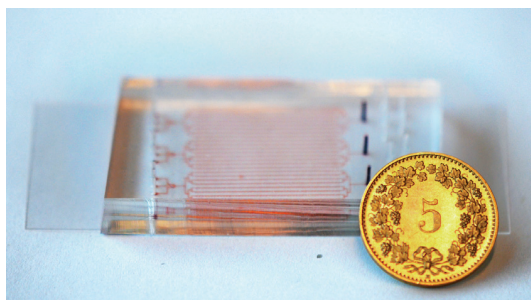


Figure 2.2: Photograph of the micro-fabricated PDMS microfluidic screening platform. A red food dye was injected for better visualization of the microfluidic channels and a Swiss 5-cent coin was placed for reference scale.

The microfluidic device consisted of two layers of PDMS: the flow layer and the control layer. PDMS was mixed with elastomer: curing agent ratios of 20:1 and 5:1 for the flow and control layers, respectively. The 20:1 mixture was poured on the flow layer wafer and spun at 1,750 rpm for 35 seconds. The 5:1 PDMS was poured on the control layer wafer and degassed for 10 minutes in a vacuum dessicator. Both molds were baked at 80°C for 30 minutes. Holes for the valves were punched on the control layer with a manual hole-puncher, then the control layer was manually aligned on the flow layer using a stereoscopic dissecting microscope. The layers were bonded together at 80°C for 90 minutes. Finally, each device was cut and peeled off the mold and inlet and outlet holes were punched in the flow layer (Figure 2.2).

2.3 Double layers microfluidic device

The microfluidic screening platform was fabricated by multilayer soft lithography (Thorsen *et al.*, 2002). It is an active device comprising two layers of elastomer, a flow layer and a control layer (Figure 2.3a), cast on two separate molds. These distinct layers are required for implementation of push-down micromechanical

valves actuated by pressure variations (Unger *et al.*, 2000). Elastomeric mechanical valves are fabricated by placing two layers of PDMS with perpendicular channels on top of each other. A thin membrane of PDMS separates the layers, and deflects downwards when pressure is increased in the upper channel (control layer) and collapses the channel beneath (flow layer) (Figure 2.3b). This is a reversible, highly responsive process, such that the flow channel can be opened and closed within milliseconds. These on-chip micromechanical valves allow rapid, precise, and, most importantly, dynamic medium changes within the screening platform.

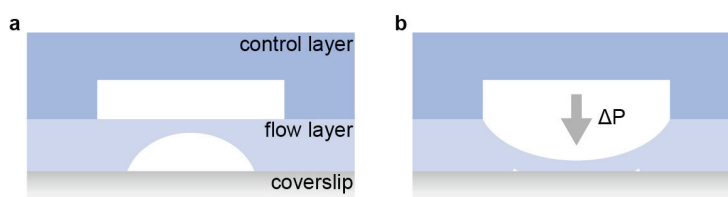


Figure 2.3: Schematic of micromechanical valve functioning. (a) Schematic representation of two layers of the PDMS microfluidic device, the upper control layer and the lower flow layer, bonded to a glass coverslip. (b) When pressure is applied in the control layer channel, the PDMS membrane is deflected downwards and closes the bottom flow channel.

2.4 Characterization of the microfluidic screening platform

As detailed above, the platform integrates mechanical valves that allow switching between different medium sources. Pump-driven convective flow in the horizontal flow channels permits rapid medium exchange throughout the device (Figure 2.1a). The microfluidic screening platform was also designed to prevent convective flow within microchambers, which could wash bacterial cells away. Therefore, medium exchange of a microchamber occurs exclusively through diffusion from the main horizontal flow channel.

The time required for medium renewal within microchambers after switching between different media was measured using the fluorescent dye sulforhodamine (Sigma Aldrich) as a fluid-phase tracer. The platform was connected to two medium

sources: 7H9 medium only, and 7H9 medium supplemented with sulforhodamine. The platform was initially primed with 7H9. At time 0 the medium was switched from 7H9 alone to 7H9 supplemented with sulforhodamine. Fluorescence was measured at the bottom of the microchambers in a square area ($200 \times 200 \mu\text{m}^2$) covering over 70% of the microchambers' total area (Figure 2.4 a, b). The time to reach 95% concentration of sulforhodamine after a switch was ~ 14 minutes; about the same time was required to reduce the concentration from 100% to 5% after a switch (Figure 2.4 c, d). I also verified that there was no significant time delay in medium exchange between microchambers located near the inlet area versus microchambers located near the outlet area. Finally, the time for the new medium to traverse a whole flow channel after switching was measured; the time delay between the first and last chambers was less than 25 seconds, which is negligible compared to the time to reach equilibrium (approximately 15 minutes).

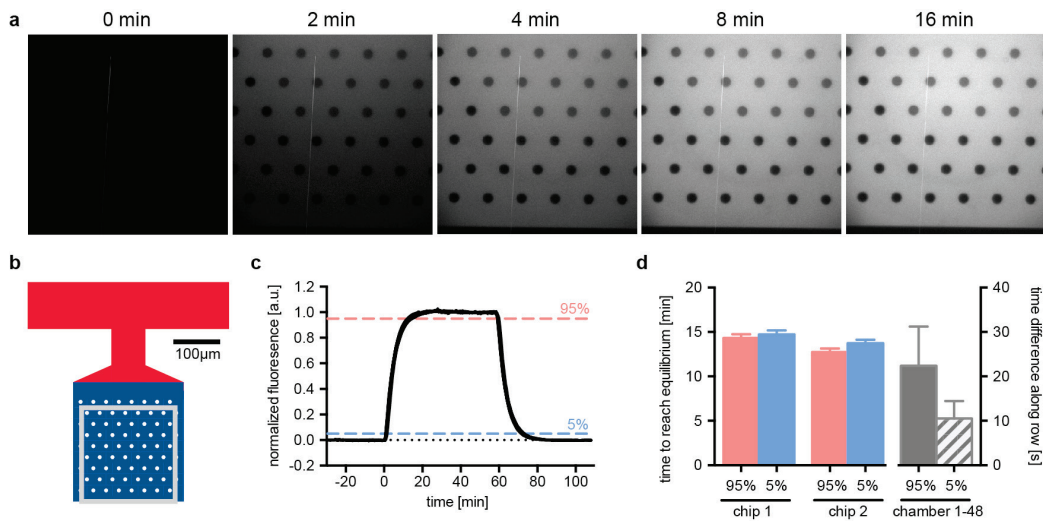


Figure 2.4: Characterization of the HCS/HTS microfluidic screening platform. (a) Representative time-series images of the diffusion into microchambers of a fluorescent dye, sulforhodamine, after switching of the medium sources. (b) A microchamber $260 \times 260 \mu\text{m}$ (blue); the gray square represents the area within which the average fluorescence was measured. (c) Normalized fluorescence values for 27 microchambers following a medium switch to medium with or without sulforhodamine, $n=2$ independent experiments, total of 27 microchambers analyzed. (d) Time to reach 95% or 5% equilibrium after a medium switch from different subsets and chips. Data represents means, $n=3$ independent experiments, 5 consecutive medium switches). Error bars correspond to the standard deviation of the means.

2.5 Spotting procedure and optimization of live cell array

Each bacterial mutant was assigned individually to a microchamber using a DNA microarrayer robot. Cells were spotted onto an epoxy-coated glass slide, and the high-throughput microfluidic screening device was immediately aligned to the spotted coverslip such that each individual *M. smegmatis* spot was enclosed by its corresponding microchamber (Figure 2.5). The assembled device was bonded at 37°C for 30 minutes before being primed with growth medium to prevent delamination.

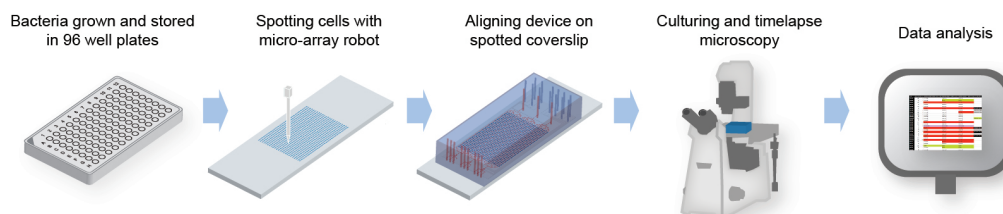


Figure 2.5: Live cell array spotting procedure. Bacterial cells were spotted onto an epoxy-coated coverslip using a microarrayer robot. The microfluidic screening platform was manually aligned on the spotted coverslip assigning each bacterial strain to a specific microchamber, followed by on-chip culturing and time-lapse imaging using an automated microscope, and finally analysis of time-lapse movies.

Various spotting conditions were tested to improve both cell survival and imaging quality. Notably, polyethylene glycol (PEG) and glycerol were added to prevent desiccation of the spotted cells during the spotting process in the microarrayer; cleaning of the metallic pins during the spotting process was improved; and spot size was increased to facilitate alignment between the spotted array and the microfluidic chip. However, due to the low heights of the microchambers, the wet spots induced microchamber collapse via capillary forces. The volume deposited was also greater than the volume of the microchambers ($260 \times 260 \times 1.4 \mu\text{m}^3$), leading to flooding and cross-contamination during alignment. In response, I tried spotting *M. smegmatis* in 7H9, their regular growth medium, and increasing

humidity in the spotting chamber to 60% to reduce evaporation and enhance cell survival. Without PEG or glycerol in the medium, mycobacteria tended to stick onto the metallic pins, resulting in cross-contamination between spots and thus washing pins required optimization to curtail contamination between microchambers. To assess the amount of cross-contamination in our microchambers, *M. smegmatis* strains expressing DsRed or GFP were alternatively spotted. Washing the pins for 2 seconds with 70% ethanol followed by 2 seconds with water between each inking reduced cross-contamination such that only 85 of 864 microchambers (9.8%) showed a mix of the two strains (Figure 2.6a). Most importantly, regrowth of the contaminating strain did not occur in most of these chambers, with only 7 chambers showing regrowth, or 0.81% of the total spotted microchambers (Figure 2.6b). Lastly, the size of the spots and thereby the number of cells deposited depended on the type of metallic pins; therefore, I decided to use pin size MP2 and SN3.

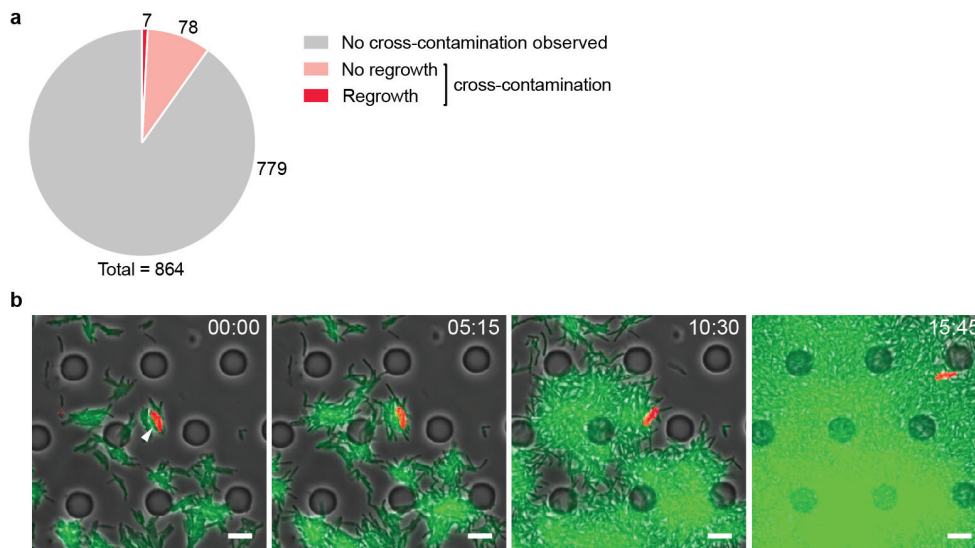


Figure 2.6: Cross-contamination between microchambers during spotting process. (a) A total of 864 microchambers were spotted in alternation with either *M. smegmatis* expressing GFP or DsRed; 85 microchambers showed cross-contamination, of which 78 did not regrow and 7 did regrow ($n = 3$ independent experiments). **(b)** Representative fluorescence and phase-contrast images of a microchamber spotted with a GFP-expressing *M. smegmatis* strain; white arrows indicate cross-contamination with DsRed-expressing cells that do not grow (presumably killed by the ethanol wash). Time is indicated as hh:mm and scale bars represent 5 μm.

2.6 Proof of concept screenings

2.6.1 *Mycobacterium smegmatis* as a model organism

The model organism that I used for the persistence screening is *Mycobacterium smegmatis*, a fast-growing strain of mycobacteria; its generation time in batch or microfluidic cultures is about three hours and it is non-pathogenic (biosafety level 1). *M. smegmatis* is often used as a non-pathogenic model organism for *Mycobacterium tuberculosis*. Despite significant genomic divergence between *M. tuberculosis* and *M. smegmatis*, this model organism offers great possibilities for comparative biology. However, studying persistence in *M. tuberculosis* goes beyond the scope of this work.

2.6.2 Single-cell imaging on chip and subcellular proof of concept screen

The platform was designed to achieve single-cell imaging of prokaryotes and possibly even subcellular imaging of fluorescently tagged objects, which would yield many more potential applications of the screening platform. In order to test the versatility of the platform, several strains of *M. smegmatis* expressing subcellular markers were cultured in the platform and imaged.

The first strain cultured in the platform was a *M. smegmatis* strain expressing two cell cycle markers: mCherry-DnaN and Wag31-GFP. DnaN is a marker of the replisome; it is the beta-clamp that tethers the polymerase to the DNA. At the initiation of chromosome replication, DnaN assembles at the origin of replication and it remains associated with the translocating DNA polymerase complex throughout the period of chromosome replication (C period). Wag31 is a marker of the cell division septum. It localizes around midcell at the time of cytokinesis and remains physically associated with the newly formed pole after cell separation; thus, the fusion protein Wag31-GFP can be used to determine precisely when and where

M. smegmatis daughter cells are compartmentalized ([Santi et al, 2013](#)). Both cell cycle markers were imaged successfully in the microfluidic screening platform, which is particularly encouraging given that both markers require a highly precise focus in order to be imaged. Bright mCherry-DnaN foci appeared during chromosome replication and disappeared upon replisome disassembly, and Wag-GFP foci indicated the time and place of cytokinesis (Figure 2.7a).

In order to determine whether errors in chromosome replication and cell division could be identified using the new HCS/HTS microfluidic platform, I conducted a mock screen using mutants defective in *parA*. The ParABS chromosome segregation system is required for the faithful partitioning of the chromosomes into daughter cells. It is composed of three elements: *parS* cis-regulatory sequences and ParA and ParB proteins. ParB oligomerizes and binds to *parS* sequences to form a partition complex, which is guided to the correct position by ParA. Deletion of either *parA* or *parB* results in severe chromosomal segregation defects and accumulation of small anucleate cells ([Santi et al, 2015](#)).

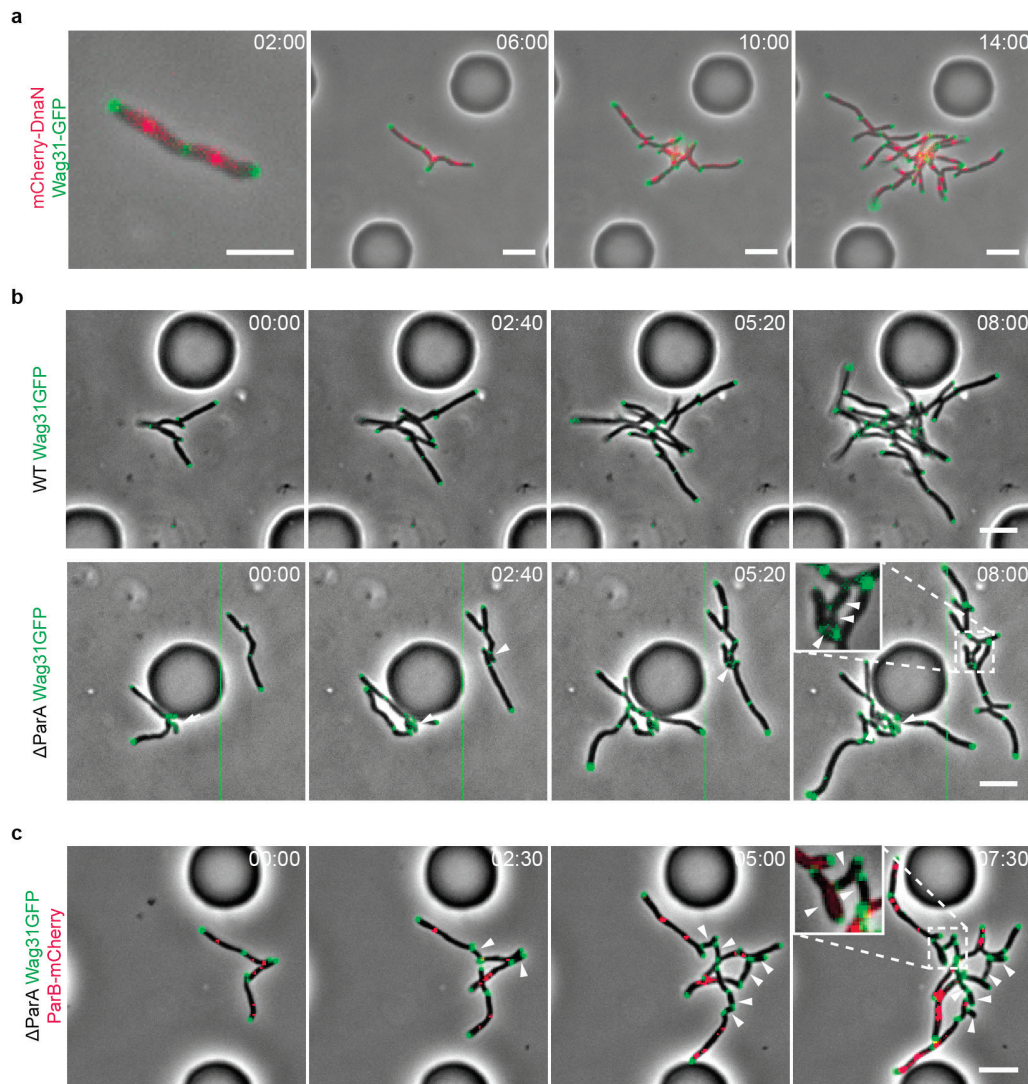


Figure 2.7: Proof-of-concept screen for mutations affecting morphological and subcellular markers. Representative merged fluorescence and phase-contrast images of **(a)** *M. smegmatis* expressing mCherry-DnaN and Wag31GFP in a microchamber, **(b)** *M. smegmatis* establishing a microcolony in a microchamber. The wild-type and Δ parA strains both express Wag31-GFP. Close-up of anucleate cells at 08:00. **(c)** Representative fluorescence and phase-contrast images of the Δ parA strain establishing a colony in a microchamber. The Δ parA strain expresses ParB-mCherry and Wag31-GFP. Time is indicated as hh:mm. White arrows indicate anucleate cells. Scale bars represent 5 μ m.

As a proof-of-concept screen, wild-type and Δ parA strains of *M. smegmatis*, both expressing the subcellular marker Wag31-GFP, were grown in 96-well plates, randomly arrayed onto an epoxy-coated glass slide as described previously, and

imaged by time-lapse microscopy. Mutants lacking $\Delta parA$ can be distinguished from wild-type cells by the accumulation of small anucleate cells that stop growing and dividing due to the absence of DNA. Wag31-GFP was used to mark the cytoplasmic compartmentalization of the nascent daughter cells and, combined with temporal tracking, allowed recognition of anucleate non-dividing cells (Figure 2.7b, white arrows). As an additional marker, ParB-mCherry foci should only be observed in cells with *parS* sequences for binding, and thus should be absent from anucleate cells (Figure 2.7c). A total of 384 microchambers were screened by time-lapse microscopy with a temporal resolution of 20 minutes; of these, 364 microchambers were randomly seeded with the wild-type strain and 20 with the $\Delta parA$ strain. A blinded screen identified 95% of the microchambers spotted with $\Delta parA$ cells, demonstrating that the platform can be used to screen for mutants using cellular and subcellular markers. The ability to screen for mutants using subcellular markers (like mCherry-DnaN, ParB-mCherry, Wag31-GFP) will greatly expand the range of potential applications for the new HCS/HTS screening platform.

To recapitulate, using the microfluidic screening platform I successfully imaged several subcellular markers, including DnaN, Wag31, and ParB, and I was able to perform a mock genetic screen based on prokaryote cellular morphology and subcellular markers.

2.6.3 Proof of concept screen to identify phenotypes emerging in fluctuating environment: bacterial persistence

In the previous section, I validated the capability of the new microfluidic screening platform to image single prokaryotic cells with subcellular resolution. Two cell cycle markers, DnaN and Wag31, were imaged to identify mutants with altered cell cycle behavior in a mock screen. This first proof-of-concept screen was performed in regular growth medium, as it did not require any complex medium profile. However, with its built-in micromechanical valves, the microfluidic screening platform enables elaborate environmental perturbations for more complex screenings. Some phenotypes, such as bacterial persistence, require switching repeatedly between

different medium sources. Using the microfluidic screening platform, I performed a second proof-of-concept screen on different bacterial persistence phenotypes to show the ability of the method to identify phenotypes that emerge only in dynamically changing environments.

2.6.3.1 Isoniazid

Isoniazid (INH) is an antibiotic of choice to study persistence. Discovered in 1952, it has since become a frontline anti-tuberculosis drug. Historically, it has been used for treating both active and latent tuberculosis. Most importantly, INH is bactericidal antibiotic with rapid killing activity – yet, paradoxically, it has poor sterilizing activity due to high rates of persistence. INH is a pro-drug that is activated by the bacterial catalase-peroxidase (KatG) after cellular entry by passive diffusion (Bardou *et al.*, 1998) to generate an INH-NAD adduct (Timmins *et al.*, 2006). The INH-NAD adduct inhibits the enzyme InhA, a 2-*trans*-enoyl-acyl carrier protein reductase responsible for the biosynthesis of mycolic acids, a major and essential component of the mycobacterial cell wall (Figure 2.8).

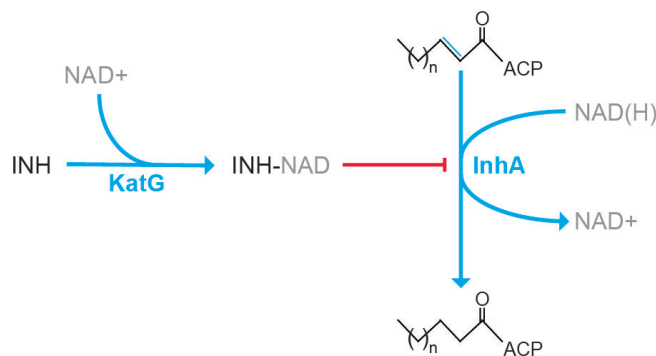


Figure 2.8: Mechanism of action of isoniazid. INH hampers mycolic acid biosynthesis through inhibition of the InhA enzyme.

2.6.3.2 Screening for altered persistence

The second screening was therefore performed in a dynamically changing environment to identify phenotypes emerging in complex medium profiles, i.e. switching between regular medium and INH-containing medium. Wang and co-workers reported that deletion of the *MSMEG_1946* gene, encoding NADH pyrophosphatase (NudC) in *M. smegmatis*, resulted in increased sensitivity to isoniazid (INH). NudC was found to degrade the KatG-activated form of INH, an INH-NAD adduct (Wang *et al.*, 2011) that inactivates the InhA enzyme responsible for mycolic acid biosynthesis, an essential component of the mycobacterial cell wall. Mutant cells lacking *nudC* are killed more efficiently by INH as compared to wild-type cells.

As a proof-of-concept screen for “persistence mutants”, wild-type *M. smegmatis* and a mutant strain with the *nudC* gene disrupted by insertion of a transposon (Tn::*nudC*), both expressing cytosolic DsRed, were grown in 96-well plates, randomly arrayed onto an epoxy-coated glass slide as described previously (Section 2.6), and imaged by time-lapse microscopy on phase and red-fluorescence channels with a 60X objective which covers an area of approximately 70% of the microchamber’s total area. The experiment was divided in three phases. First, cells were initially grown for 24 hours in drug-free growth medium (7H9) to establish a microcolony. The study of persistence requires large microcolonies comprising thousands of individual cells, as the persistence rate is very low: approximately 10^{-2} for wild-type cells and 10^{-4} for *nudC* mutant cells. Second, the medium source was switched to INH-containing medium at ten-fold the minimum inhibitory concentration (MIC) for 48 hours. Third, the medium was switched back to regular growth medium in order to identify which microcolonies resumed growth (Figure 2.9). Disruption of the *nudC* gene resulted in increased susceptibility to INH and hence decreased survival to antibiotic exposure. No difference was noticeable between the wild-type and the *nudC* mutant during the first two phases, i.e. initial growth and antibiotic exposure. During the regrowth phase, the *nudC* mutant microcolonies failed to recover and resume growth upon antibiotic removal whereas wild-type colonies did.

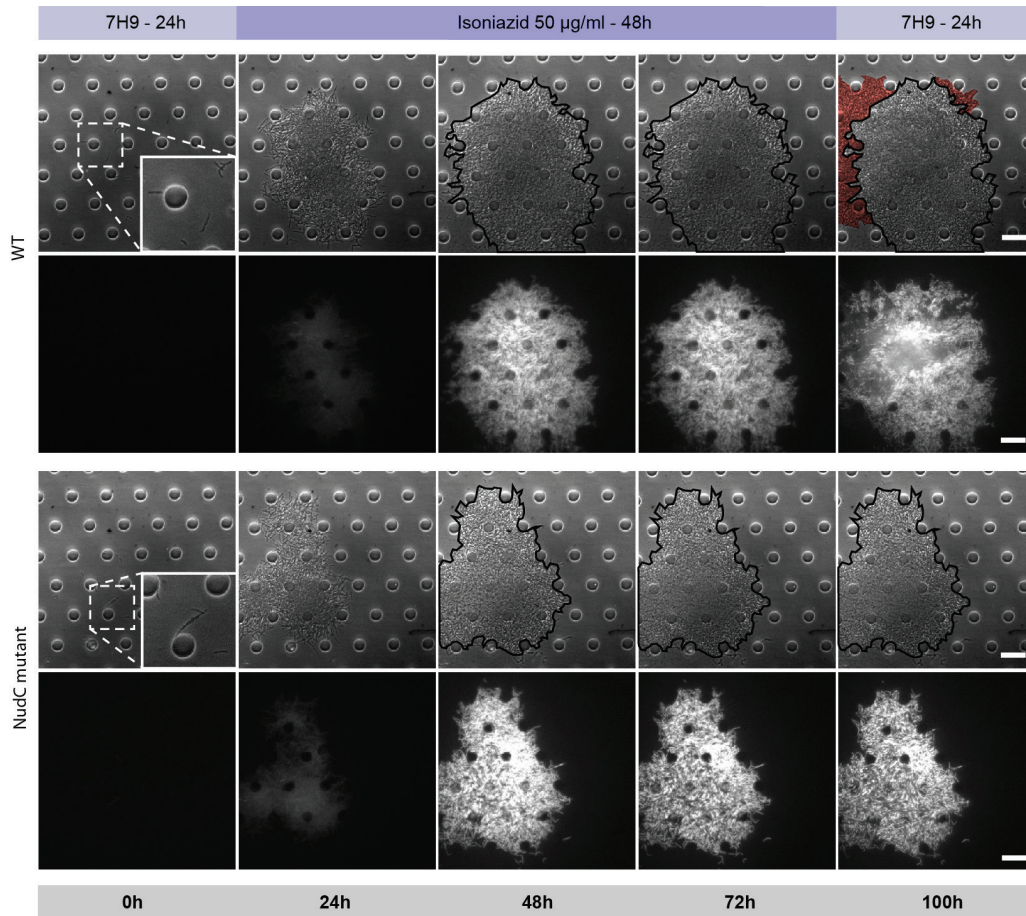


Figure 2.9: Proof-of-concept screen for bacterial persistence mutants. Representative red fluorescence and phase-contrast images from time-lapse series of wild-type and Tn::*nudC* microcolonies. Both strains expressed cytosolic DsRed. Black outlines show colony size at 48 hours; red coloring indicates bacterial growth after INH removal. Scale bars indicate 20 µm.

A total of 328 random microchambers were screened by time-lapse microscopy with a temporal resolution of 2 hours; of these, 312 microchambers were seeded with the wild-type strain and 16 with the Tn::*nudC* strain. Each microchamber was manually analyzed and, according to its phenotype, was assigned to one of the three following groups: wild-type phenotype (WT group), strongly decreased persistence (group I), or mildly decreased persistence (group II). A blinded screen successfully identified 15 of the 16 microchambers spotted with Tn::*nudC*, which clearly did not

resume growth upon INH removal; of these, 14 were annotated as “strongly decreased persistence” and only 1 was annotated as “mildly decreased persistence”. In addition, 14 wild-type microcolonies were falsely identified as potential Tn::*nudC* cells (Figure 2.10); of these, only 2 were annotated as “strongly decreased persistence” and 12 were annotated as “mildly decreased persistence”. Two types of selection could be envisaged for the actual screening: either a *strict selection* that would take into account only the candidates displaying a strong phenotype (group I), or a *broad selection* where both strong and weak phenotypes (groups I and II) would be selected for further analysis. In the mock screen described above, a strict selection would identify 14/16 Tn::*nudC* mutant spots (true positives) and only 2 wild-type spots (false positives) (Figure 2.10). A broad selection would increase the number of false positives (wild-type) to 14 while adding only 1 additional true positive (Tn::*nudC* mutant). In this context, then, I believe that a strict screen is more efficient.

Furthermore, no difference was observed between wild-type and Tn::*nudC* strains in the red fluorescence channel during antibiotic exposure (Figure 2.9). Cytosolic DsRed was used as an indicator of cell lysis; remarkably, although survival and regrowth of the Tn::*nudC* strain was strongly impaired, this strain did not show increased lysis compared to wild-type. These observations underscore that conventional screening methods using cellular fluorescence as a proxy for survival would not be capable of identifying this particular class of mutants.

In conclusion, using the dynamic control over the environment enabled by the microfluidic screening platform’s build-in micromechanical valves, we were able to identify phenotypes appearing only in a dynamically changing microenvironment. In a “classic” persistence screen, bacteria are typically grown in microwell plate and overall fluorescence is measured over time (Campen *et al.*, 2015). However, this technique wouldn’t allow the identification of *M. smegmatis* mutants like *nudC*, as the fluorescence of this strain during INH exposure remained comparable to the wild-type control. The critical parameter to identify this mutant was the regrowth during the third phase, which would not be easy to achieve in a 96-well plate format. The ability of the platform to switch repeatedly between different medium sources

clearly demonstrates the power of this technique to identify unexpected behaviors, such as the paradoxical phenotype displayed by the *M. smegmatis nudC* mutant (increased death not accompanied by any corresponding increase in cell lysis).

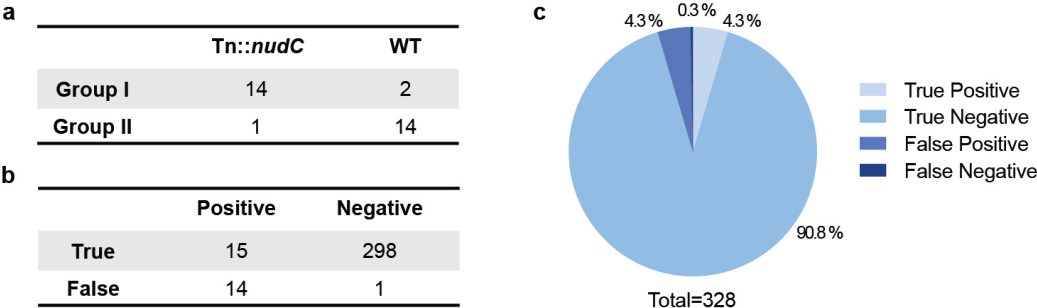


Figure 2.10: Outcome of the proof-of-concept screen for bacterial persistence mutants. (a) Table summarizing candidates identified in group I with strongly impaired persistence and group II with weakly impaired persistence. (b) Table summarizing true positives, true negatives, false positives, and false negatives. (c) Pie chart of true positives (correctly identified as Tn::*nudC* mutants); true negatives (correctly identified as wild-type); false positives (wild-type identified as Tn::*nudC* mutants); false negatives (Tn::*nudC* mutants identified as wild-type).

2.7 Conclusion and outlook

To address the lack of tools available for HCS/HTS screening of prokaryotic cells, I developed a versatile microfluidic screening platform allowing morphological and even subcellular screenings in prokaryotic cells. The platform fulfilled several criteria to carry out screenings with bacteria, which were:

- I. Single-cell resolution of prokaryotic cells,
- II. A Precise control over the growth environment,
- III. Imaging of thousands of mutant strains in parallel,

The platform displays 1,152 microchambers of 1.4 μm height on a footprint smaller than 4 cm^2 . With its build-in micromechanical valves, the flow medium can easily be switched repeatedly between two different sources, thus enabling complex medium profiles. In the device, medium exchange between microchambers and flow

channels occurs only by diffusion; thus, the time to reach 95% concentration of the new medium after a switch is approximately 14 minutes, which might be too slow for some applications. On the other hand, the time delay between microchambers located near the inlet area versus microchambers located near the outlet area was negligible (< 25seconds).

Using the new platform, two subcellular cell-cycle markers, mCherry-DnaN and Wag31-GFP, were imaged and used to perform a mock screen based on prokaryote cellular morphology and subcellular markers in a static environment, and a mutant with defective chromosome segregation and cell division ($\Delta parA$) was successfully identified in a blinded screen. Furthermore, the platform also permits more intricate screening protocols requiring a complex medium profile to identify mutations phenotypes that emerge only in fluctuating environments, such as bacterial persistence. Here again, I successfully identified a mutant (Tn::*nudC*) displaying impaired persistence in a blinded proof-of-concept screen.

In conclusion, the microfluidic screening platform has the potential to provide novel insights in numerous areas of microbiology through quantitative single-cell studies and HCS/HTS screens. The proof-of-concept screens presented in this chapter were performed with mycobacteria; however, the platform could be readily adapted for the analysis of various types of prokaryotes, such as *M. tuberculosis*, *E. coli*, *Bacillus subtilis*, etc. In addition, built-in micromechanical valves and division of the device into three independent sections with independent plumbing further increases its versatility. Here, I developed a new microfabricated tool for microbiological studies, which can be used to address many biological questions ranging from the behavior of microcolonies to the perturbation of subcellular functions/objects.

3 The microfluidic platform enables large-scale screening to identify genes involved in bacterial persistence

The focus of this chapter is the screening of two *M. smegmatis* mutant libraries by time-lapse microscopy using the high-throughput microfluidic screening platform in order to identify mutants with altered rates of persistence. The screenings are described in the following sections.

3.1 Screening a cytosolic DsRed-expressing *M. smegmatis* mutant library

3.1.1 The DsRed-expressing *M. smegmatis* mutant library

A first screen for “persistence mutants” was performing using a DsRed-expressing *M. smegmatis* mutant library generated by random transposon mutagenesis (thanks to Dr. M. Elitas and Dr N. Dhar). Briefly, a strain of *M. smegmatis* mc²155 (wild-type) expressing DsRed from a strong constitutive promoter on a plasmid carrying a hygromycin resistance marker and integrated at the chromosomal *attB* phage attachment site was mutagenized using the fMycoMarT7 transposon donor

phagemid carrying a kanamycin resistance marker. See “Materials and Methods” for more information about generation of the transposon mutant library. Master plates of the mutant library were stored in 96-well plates at -80°C in 12% glycerol with 50 µg/ml hygromycin and 15 µg/ml kanamycin to select for the DsRed-expressing plasmid and the transposon, respectively.

3.1.2 Experimental procedure of the genetic persistence screen

Cells were inoculated from the original 96-well master plates into 96-well plates with V-shaped micro-wells and grown overnight in 7H9 medium without antibiotics. Plates were centrifuged prior to spotting; the V-shaped micro-wells improved sedimentation of the cells.

Mutants were spotted on an epoxy-coated coverslip using a microarrayer robot as described previously in section 2.5. The spotting process for a full array of 1,152 mutant strains (24 x 48) takes about 100 minutes. After spotting, the microfluidic device was immediately aligned on top of the spotted coverslip and bonded at 37°C for 30 minutes. The microfluidic screening platform was prepared fresh on the day of the experiment to ensure good bonding with the epoxy-coated coverslip.

The control layer valves were primed with water. The flow layer was primed with regular growth medium (7H9) to perfuse the microchannels and microchambers. Once both layers were primed, the 1,152 microchambers were imaged at two-hour time intervals for 96 hours (4 days). The experiment was divided into three phases: first, the cells were grown for 24 hours in antibiotic-free 7H9 medium; second, the flow was switched to 7H9 medium containing isoniazid (INH) at 50 µg/ml (10-fold the MIC) for 48 hours; third, the flow was switched back to antibiotic-free 7H9 medium and cell growth was allowed to recover for 24 hours.

3.1.3 Primary screen – DsRed-expressing *M. smegmatis* mutant library

A total of 1,106 *M. smegmatis* mutants expressing DsRed were analyzed in the microfluidic screening platform to identify mutants with altered (increased or decreased) rates of persistence, defined here as survival and regrowth after prolonged exposure to INH. All 1,106 mutants were imaged on a single device and four independent experiments were done to achieve high coverage and to test for the reproducibility of the results. Each of the 4,608 movies generated was annotated manually.

As mentioned previously, the experiment was divided into three phases. We used the growth characteristics of wild-type *M. smegmatis* as a reference to identify mutants with abnormal growth phenotypes (Figure 3.1). Wild-type *M. smegmatis* microcolonies formed in the first phase of growth. Upon switching the flow to medium containing INH, wild-type microcolonies continued to grow for some time until the microcolonies reached a stable size (between 36-72 hours into the experiment). At 72 hours, antibiotic was removed from the medium and wild-type microcolonies rapidly resumed growth. A mutant was considered to be a candidate “persistence mutant” if it exhibited the same phenotype in more than 50% of the time-lapse movies. The mutants were categorized as displaying a persistence phenotype similar to wild-type (the vast majority of mutants fell into this category, as expected), an increased rate of persistence, or a decreased rate of persistence.

Typically, mutants with a low-persistence phenotype arrested growth and formed stable microcolonies during INH exposure, but failed to regrow upon INH removal. As an example, a mutant with a transposon insertion in the *MSMEG_0031* gene is a representative low-persistence mutant that does not regrow after INH washout (Figure 3.1). In contrast, high-persistence mutants rapidly expanded upon INH removal, and some even exhibited increased growth during INH exposure; an example is a mutant with a transposon insertion in the *MSMEG_5268* gene (Figure 3.1).

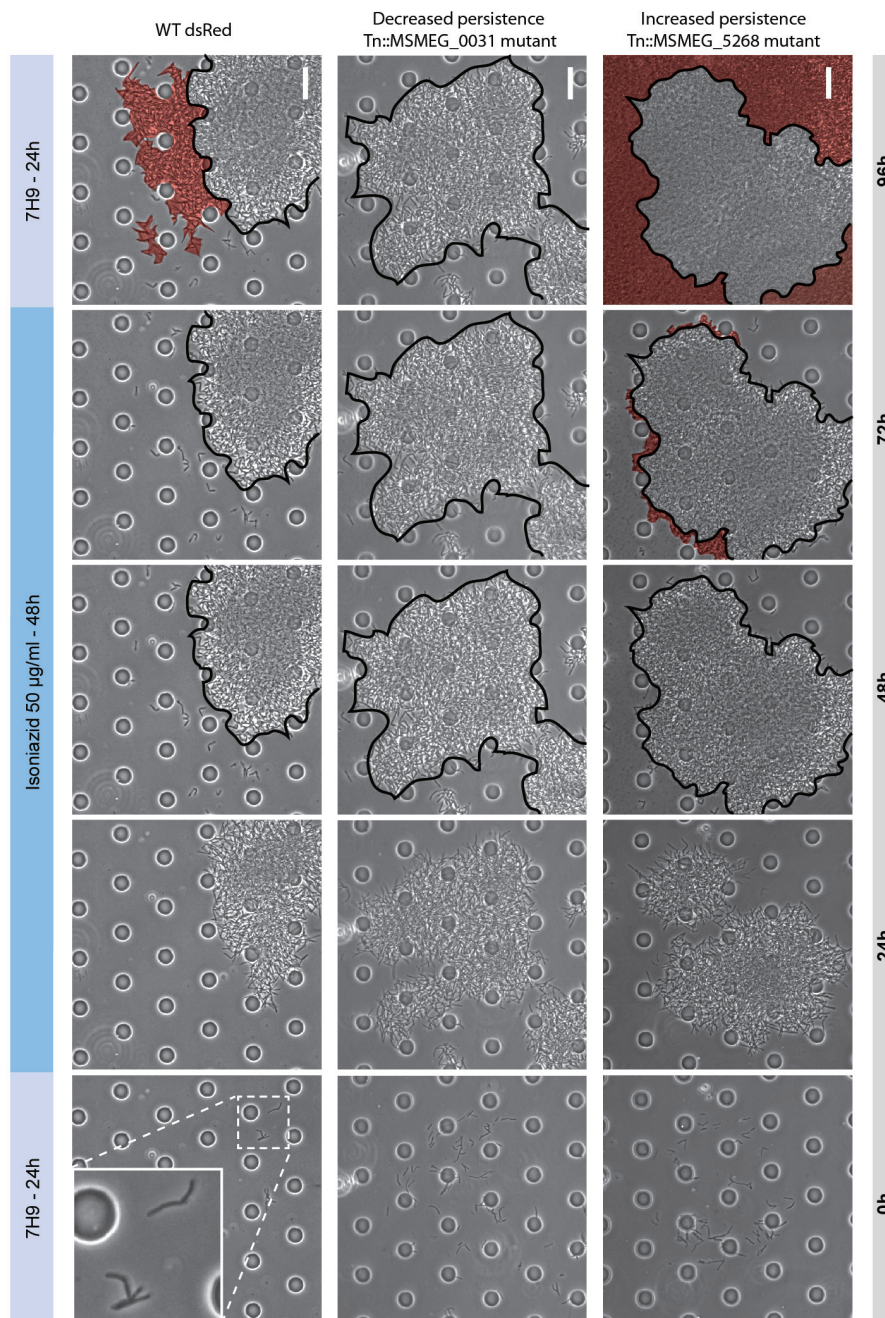


Figure 3.1: The screening process and representative mutants with altered persistence rates. Representative *M. smegmatis* mutants that exhibited altered rates of persistence. The Tn::MSMEG_0031 mutant exhibited a lower rate of persistence than wild-type. The Tn::MSMEG_5268 mutant exhibited a higher rate of persistence than wild-type. Scale bars indicate 20 µm. Black outlines show microcolony size at 48 hours. Red shading indicates bacterial growth during INH exposure and after INH removal.

Some time-lapse movies were removed from analysis due to the microcolony size, as the number of persister within a microcolony depends on the colony size. For example, a very small microcolony might fail to regrow upon antibiotic removal purely for statistical reason: the fewer cells the smaller the chance to have one or more persister cells in the microcolony. In these situations it would not be possible to distinguish a low-persistence phenotype from a wild-type persistence phenotype. Conversely, analyzing very large microcolonies is challenging since regrowth may occur out of the field of view, and access of the antibiotic might be hindered in a very large microcolony, thereby biasing the phenotype.

Initially 1,140 mutant strains were investigated. Of these, 34 strains were not represented by any high-quality time-lapse movie, thus reducing the actual size of the library screened to 1,106 mutants (Figure 3.2a). More than 80% of the mutant library was covered by 2-4 high-quality movies. Of these, mutants that exhibited a consistent phenotype in ≥ 2 of the time-lapse movies were selected as candidate “persistence mutants”. For example, any mutant represented by 4 high-quality movies was selected if it exhibited a consistent phenotype in 2, 3, or 4 movies. Similarly, any mutant represented by 3 high-quality movies available was selected only if the phenotype was seen in 2 or 3 movies. Finally, mutants represented by only 2 high-quality movies available were selected for further analysis only if the phenotype was consistent in both movies (Figure 3.2b). With these criteria we identified 81 candidates in the primary screen, 28 of which showed a low-persistence phenotype, and 53 of which showed a high-persistence phenotype. In the primary screen we chose to apply a fairly broad selection in order to capture all potentially persistent mutants.

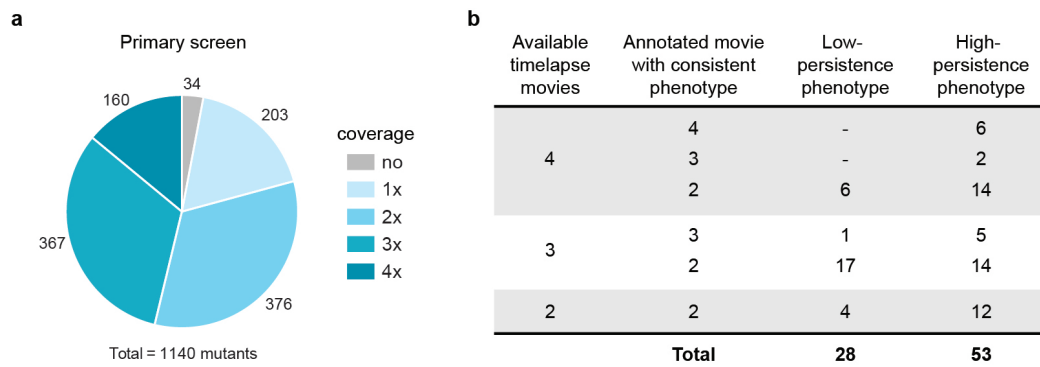


Figure 3.2: Ds-Red-expressing *M. smegmatis* mutant library primary screen coverage and selection criteria for mutants with altered rates of persistence. (a) High-quality time-lapse movie coverage for primary screening. 1,140 mutants were screened initially with a maximal coverage of 4 time-lapse movies per mutant. (b) *M. smegmatis* candidates displaying an altered rate of persistence; a cutoff of 50% was imposed for selection.

To these 81 mutants, 8 candidates, which were previously identified with an altered rate of persistence by Dr Elitas, were added for the secondary screening to confirm their behavior. These candidates included 7 mutants with potentially increased persistence and only one mutant with decreased persistence. In summary, the 89 candidates included 60 candidates with increased persistence and 29 mutants with decreased persistence phenotype.

3.1.4 Secondary screen – DsRed-expressing *M. smegmatis* mutant library

The 89 candidates were rescreened in a secondary screen using the same microfluidic platform to eliminate potential false positives. In the secondary screen each mutant was spotted up to 12 times per device, drastically increasing the number of technical repeats available per mutant. The secondary screening was repeated twice, therefore a coverage of 24 time-lapse movies were available per candidate, and more than 10 time-lapse movies were available for 56 of the 89 mutants (63%) (Figure 3.3a).

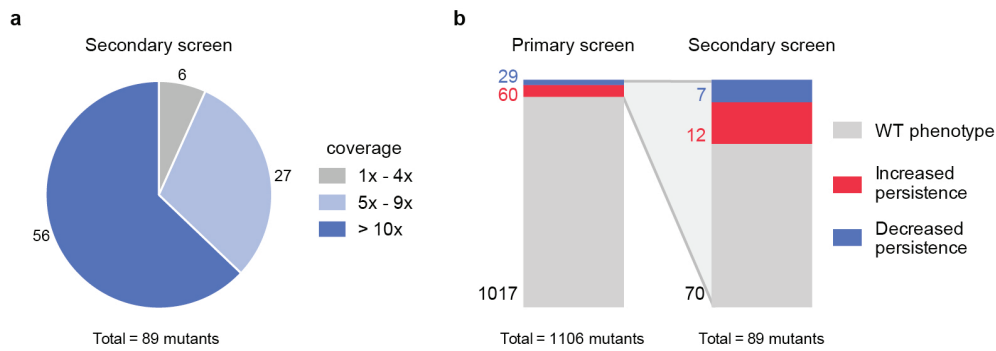


Figure 3.3: Secondary screen coverage and outcome. (a) High quality time-lapse movie coverage for secondary screening, with a maximal coverage of 24 time-lapse movies per mutant. **(b)** 1,106 mutants were analyzed in a primary screen (n = 4 independent experiments), and 89 candidates from this screening were assessed in a secondary screen (n = 2 independent experiments), from which 19 were confirmed.

The criterion of selection of high-persistence mutants was the same as for primary screen, i.e. a cutoff of 50% of the time-lapse movies. Regarding low-persistence mutants, the criterion of selection was broadened since, as aforesaid, small micro-colonies might mask a low-persistence mutant. To not miss any potential candidate, we decided to use a cutoff of 40%. Using those criteria, 19 out of 89 candidates were confirmed in the secondary screen, of which 7 displayed lower persistence and 12 displayed increased persistence (Figure 3.3b).

The transposon insertion site for each of these mutants was located and the disrupted gene was identified and listed in Table 3.1 and Table 3.2 for mutants displaying increased and decreased persistence phenotype respectively.

Mutated gene	Annotated gene function
<i>MSMEG_5783</i>	Pseudogene, acetyltransferase (mshD)
<i>MSMEG_3620</i>	Conserved hypothetical protein
<i>MSMEG_6416</i>	Phosphoglycerate mutase
<i>MSMEG_2570</i>	Xanthine/uracil permease
<i>MSMEG_5030</i>	Conserved hypothetical protein
<i>MSMEG_4124</i>	Conserved hypothetical protein
<i>MSMEG_2576</i>	Deoxyribodipyrimidine photo-lyase

<i>MSMEG_6284</i>	Cyclopropane-fatty-acyl-phospholipid synthase
<i>MSMEG_5268</i>	Hypothetical protein
<i>MSMEG_2281</i>	Conserved hypothetical protein
<i>MSMEG_0777</i>	F420-dependent glucose-6-phosphate dehydrogenase
<i>MSMEG_1974</i>	Propane monooxygenase coupling protein

Table 3.1: DsRed-expressing mutants displaying increased persistence phenotype.

Mutated gene	Annotated gene function
<i>MSMEG_0031</i>	Penicillin binding protein
<i>MSMEG_1946</i>	NAD(P) pyrophosphatase, NudC
<i>MSMEG_0034-35</i>	Intergenic region
<i>MSMEG_0034</i>	FHA domain protein
<i>MSMEG_4121</i>	GntR-family protein transcriptional regulator
<i>MSMEG_4301</i>	Acyl-CoA synthase
<i>MSMEG_3902-03</i>	Intergenic region

Table 3.2: DsRed-expressing mutants displaying decreased persistence phenotype.

Increased-persistence phenotypes displayed distinctive dynamics leading to enhanced survival to antibiotic treatment. More specifically, during antibiotic exposure some mutants were able to actively divide and grow at the colony-level, a trait shared by the whole population, or at foci-level, owing to some offspring. Other mutants exhibited a dynamic similar to wild-type during antibiotic exposure, however, upon antibiotic removal, they exhibited a much higher recovery compared to that of the wild-type, once again at the colony- or foci-level. These different dynamics are summarized in the table below (Table 3.3).

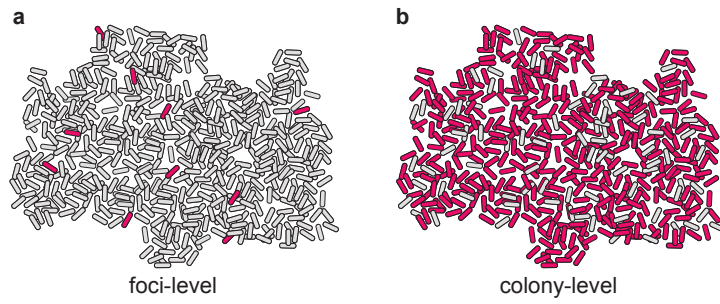


Figure 3.4: schematic of two distinct dynamics for enhanced survival to antibiotic exposure.

During antibiotic exposure some mutants were able to actively divide and grow **(a)** at foci-level, owing to some offspring (indicated as red cells), or **(b)** at the colony-level, a trait shared by the whole population. Other mutants exhibited a much higher recovery compared to that of the wild-type, once again at the colony- or foci-level.

Mutated gene	1. Growth observed during antibiotic exposure		2. Growth observed during recovery phase	
	a. Foci	b. Colony	a. Foci	b. Colony
<i>MSMEG_5783</i>	10.0 %	10.0 %	70.0 %	10.0 %
<i>MSMEG_3620</i>	-	90.9 %	9.1 %	-
<i>MSMEG_6416</i>	-	72.7 %	18.2 %	9.1 %
<i>MSMEG_2570</i>	-	100.0 %	-	-
<i>MSMEG_5030</i>	-	76.9 %	23.1 %	-
<i>MSMEG_4124</i>	-	100.0 %	-	-
<i>MSMEG_2576</i>	-	79.0 %	21.0 %	-
<i>MSMEG_6284</i>	-	28.6 %	42.8 %	28.6 %
<i>MSMEG_5268</i>	14.3 %	14.3 %	57.1 %	14.3 %
<i>MSMEG_2281</i>	-	58.9 %	41.1 %	-
<i>MSMEG_0777</i>	21.4 %	-	78.6 %	-
<i>MSMEG_1974</i>	7.1 %	14.3 %	64.3 %	14.3 %

Table 3.3: Mutants with increased persistence exhibiting distinctive dynamics leading to enhance survival during antibiotic exposure. Each time-lapse was manually annotated and sorted in one of the four following categories: active division observed during antibiotic at (1.a) foci- or (1.b) colony-level, superior growth observed during recovery phase at (2.a) foci- or (2.b) colony-level compared to that of the wild-type. Values are normalized to the total number of time-lapse movies

available for each mutant and are represented as percentages. In bold is the preferred dynamic of enhanced persistence for each mutant.

Two main dynamics of survival were observed throughout the collections of mutants. First, through active division during antibiotic exposure at the whole colony level or, second, through enhanced recovery upon antibiotic removal at foci-level (i.e. not a commonly-shared feature throughout the clonal population) compared to that of the wild-type. Enhanced survival through active division at foci-level or recovery of the whole colony upon antibiotic removal were rarely observed.

3.1.5 Batch culture analysis and candidate mutant validation

The 19 mutants identified and validated in our screen were validated by standard batch-culture experiments, including kill curve and minimum inhibitory concentration (MIC) assays.

Wild-type *M. smegmatis* kill curves in batch cultures show biphasic kinetics: in the first phase INH rapidly kills the majority of the bacterial population, followed by a lower killing rate in the second phase due to the presence of persister cells. Increased or decreased persister mutants deviated markedly from the wild-type curve (Figure 3.3). High-persistence mutants clearly clustered above the wild-type control during the persistence phase of the kill curves; conversely, low-persistence mutants clustered below the wild-type kill curve.

A “fractional survival ratio” (FSR) for these mutants was calculated as the ratio of mutant to wild-type cells present at 48 hours, where mutants with a ≥ 3 -fold increased or decreased FSR_{WT} were considered to be true positives. Kill curves and FSR_{WT} confirmed the phenotypes of 14 out of 19 candidates: 10 with increased survival and 4 with decreased survival (Table 3.4).

The *MSMEG_5783* gene was identified by BLAST (NCBI) as a pseudogene (*mshD*) of a mycothiol synthase (acetyltransferase) gene due to a nucleotide insertion leading to a frameshift from the 249th amino acid, the intact protein being constituted of 296

amino acids. Yet, disruption of *MSMEG_5783* was previously reported as resulting in INH resistance (Rawat *et al.*, 2007) and disruption of this gene was similarly identified here as conferring a high-persistence phenotype. Thus, we hypothesize that the gene does in fact encode a functional product.

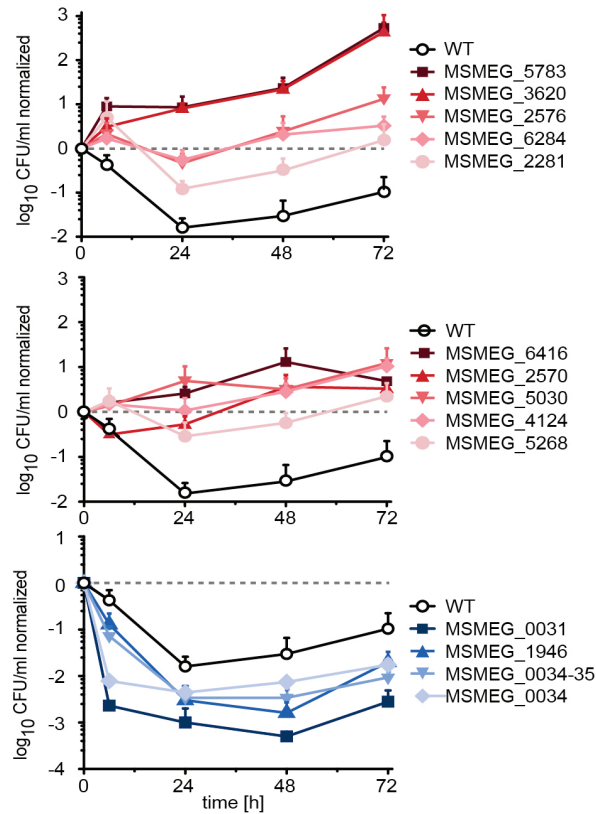


Figure 3.5: Kill curves of mutants with altered persistence. Kill curves of mutants exhibiting high-persistence (red) or low-persistence (blue) phenotypes compared to the wild-type control (black). Points on the kill curves represent means and error bars represent the standard deviation of the means ($n \geq 3$ independent experiments).

All high-persistence mutants exhibited higher survival than wild-type at 6 hours of INH exposure, except for mutant Tn::*MSMEG_2570*; growth of this mutant was initially inhibited by INH, but it rapidly recovered and grew continuously from 24 hours onwards. Likewise, four other mutants (Tn::*MSMEG_2576*, Tn::*MSMEG_6284*, Tn::*MSMEG_2281*, and Tn::*MSMEG_5268*) exhibited decreased numbers of colony-forming units (CFU) until 24 hours but recovered from 48 hours onwards.

Furthermore, five mutants (Tn::MSMEG_5783, Tn::MSMEG_3620, Tn::MSMEG_6416, Tn::MSMEG_5030, and Tn::MSMEG_4124) divided continuously during INH exposure, demonstrated by increasing CFU/ml, initially at a very high rate (Figure 3.5). Four of these mutants (Tn::MSMEG_3620, Tn::MSMEG_6416, Tn::MSMEG_5030, and Tn::MSMEG_4124) were identified as actively dividing during the microfluidic screen, a behavior that was confirmed in batch-culture experiments.

Interestingly, three of the four low-persistence mutants had transposon insertions in the same operon or just upstream of the operon (Tn::MSMEG_0031, Tn::MSMEG_0034, and Tn::MSMEG_0034-35), indicating that this operon may be crucially important for allowing cells to persist during antibiotic exposure. Two mutants with impaired persistence, Tn::MSMEG_0031 and Tn::MSMEG_0034, succumbed to rapid killing initially within the first 6 hours of antibiotic exposure, which then slowed and reached a plateau lower than that in the wild-type strain.

To ascertain that our high-persistence mutants have *bona fide* persistence phenotypes and not antibiotic resistance phenotypes, we measured the INH minimum inhibitory concentration (MIC) for each mutant. A MIC comparable to wild-type suggests that the observed persistence to INH is not due to decreased antibiotic sensitivity or the expression of a resistance mechanism.

Overall, MICs of high-persistence mutants were similar to or slightly higher than wild-type ($< 2 \times \text{MIC}_{\text{WT}}$) except for four mutants: Tn::MSMEG_5783, Tn::MSMEG_3620, Tn::MSMEG_6416, and Tn::MSMEG_5030, which exhibited a ≥ 2 -fold increase in their MICs (Table 3.4). Note that the microfluidic screen described above was performed at concentrations much higher than the MICs of these mutants, specifically at $[\text{INH}] = 50 \mu\text{g/ml}$. These mutants, except for Tn::MSMEG_4124, were observed to divide continuously during antibiotic exposure in the microfluidic screen. Yet, Tn::MSMEG_4124, which also divided continuously in the presence of INH, displays an MIC comparable to the wild-type MIC. Interestingly, the Tn::MSMEG_5783 mutant exhibited a FSR of ~ 790 and although its MIC was >2 -fold the wild-type MIC it wasn't as high as one could expect for a strain that was previously reported in the literature as being INH-resistant ([Rawat, 2007](#)).

Finally, the MICs of the low-persistence mutants were all slightly below the wild-type MIC, with the exception of mutant Tn::MSMEG_1946, which exhibit almost a 2-fold increase in antibiotic sensitivity.

Mutated gene	Fractional Survival Ratio at 48h	Minimum inhibitory concentration [µg/ml]	Annotated gene function
MSMEG_5783	790.1 ± 562.5	8.9 ± 3.1	Acetyltransferase, GNAT family
MSMEG_3620	736.6 ± 404.8	18.8 ± 6.2	Conserved hypothetical protein
MSMEG_6416	438 ± 435.6	10.1 ± 1.0	Phosphoglycerate mutase
MSMEG_2570	122.9 ± 101.3	4.6 ± 0.6	Xanthine/uracil permease
MSMEG_5030	107.4 ± 82.4	7.6 ± 2.3	Conserved hypothetical protein
MSMEG_4124	93.8 ± 50.8	4.9 ± 0.3	Conserved hypothetical protein
MSMEG_2576	82.2 ± 97.9	5.9 ± 1.0	Deoxyribodipyrimidine photo-lyase
MSMEG_6284	69.7 ± 57.9	5.4 ± 0.2	Cyclopropane-fatty-acyl-phospholipid synthase
MSMEG_5268	19.3 ± 8.6	4.8 ± 0.3	Hypothetical protein
MSMEG_2281	10.7 ± 9.2	4.0 ± 1.2	Conserved hypothetical protein
wild type	1 ± 1.2	3.4 ± 0.9	—
MSMEG_0031	0.018 ± 0.002	2.5 ± 0.0	Penicillin binding protein
MSMEG_1946	0.054 ± 0.038	1.9 ± 0.6	NAD(P) pyrophosphatase
MSMEG_0034-35	0.116 ± 0.115	2.6 ± 0.1	Intergenic region
MSMEG_0034	0.250 ± 0.014	2.6 ± 0.1	FHA domain protein

Table 3.4: Fractional survival ratios (FSR) and minimum inhibitory concentrations (MIC). Summary table of candidates validated by conventional batch experiments with INH. The corresponding mutated genes, FSR at 48 hours compared to the wild-type control, and INH MIC are listed.

3.2 Screening the mCherry-DnaN Wag31-GFP expressing *M. smegmatis* mutant library

Although performed on a small (pilot) scale, the screen of the DsRed-expressing *M. smegmatis* mutant library already implicated several interesting genes in bacterial persistence. However it would be of particular interest to screen a *M. smegmatis* mutant library with fluorescent cell-cycle markers to gain insight regarding the

dynamics of persister replication and division during INH exposure. In chapter 2, we demonstrated the ability of the microfluidic screening platform to image two cell cycle markers: mCherry-DnaN, a marker of the DNA replisome, and Wag31-GFP, a marker of the division septum. We therefore performed a second pilot screen with a mutant library carrying both markers. This cell-cycle reporter strain could be used not only to identify mutants with abnormal cell-cycle phenotypes during the screening, but also for quantitative follow-up studies of candidate mutants with altered persistence rates. However, the identification and characterization of mutants with abnormal cell cycle phenotypes are beyond the scope of this thesis.

3.2.1 The mCherry-DnaN Wag31-GFP *M. smegmatis* mutant library

The second screen for persistence mutants was performed using a mCherry-DnaN Wag31-GFP-expressing *M. smegmatis* mutant library. First, a plasmid carrying the marker Wag31-GFP was integrated at the chromosomal *attB* site in a strain expressing a clean knock-in of the mCherry-DnaN reporter gene at the *dnaN* locus (Santi *et al*, 2013). The mutant library was generated by random transposon insertion as previously described in section 3.1.1.

3.2.2 Experimental procedure of the genetic persistence screen

The experimental procedure was similar to the one for the screening of the DsRed-expressing mutant library (section 3.1.2). The only difference was in the spotting procedure: instead of spotting 1,152 unique mutants on one device, 576 mutants were spotted in technical duplicates. This would reduce the spotting time to 60 minutes and thereby enhance bacterial survival during the spotting procedure.

As previously, the screening experiment was divided into three phases: first, mycobacteria were grown for 24 hours in antibiotic-free 7H9 medium; second, the flow was switched to 7H9 medium containing INH at 50 µg/ml (10-fold the MIC) for 48 hours; third, the flow was switched back to antibiotic-free 7H9 medium and cells

were allowed to recover and resume growth for 24 hours. The experiment was repeated twice, generating a maximum of four movies per mutant. Each of the 2,304 movies was analyzed manually.

3.2.3 Primary screen - mCherry-DnaN Wag-GFP-expressing *M. smegmatis* mutant library

A total of 570 *M. smegmatis* mutants expressing mCherry-DnaN and Wag31-GFP were analyzed, alongside 6 wild-type strains for comparative purposes, in the microfluidic screening platform to identify mutants with altered persistence rates. All mutants were imaged on a single device in duplicate, repeated in two independent experiments to achieve high coverage and to test for the reproducibility of the results.

As previously, we used the growth characteristics of wild-type *M. smegmatis* as a reference to identify mutants with abnormal growth phenotypes (Figure 3.1). Initially 570 mutants were investigated, yet 30 strains were not covered by any high-quality time-lapse movies, thus reducing the size of the library screened to 540 mutants (Figure 3.6a). 80% of the mutant library was covered at least in duplicates, reaching a maximum of 4 movies. Mutants with ≥ 2 high-quality time-lapse movies displaying a consistent phenotype in ≥ 2 of the movies were selected as candidates with altered persistence rates. We identified 76 candidates in the primary screen, 29 of which showed a low-persistence phenotype and 47 of which showed a high-persistence phenotype (Figure 3.6b). In the primary screen we chose to apply a fairly broad selection in order to capture all potential persistence mutants

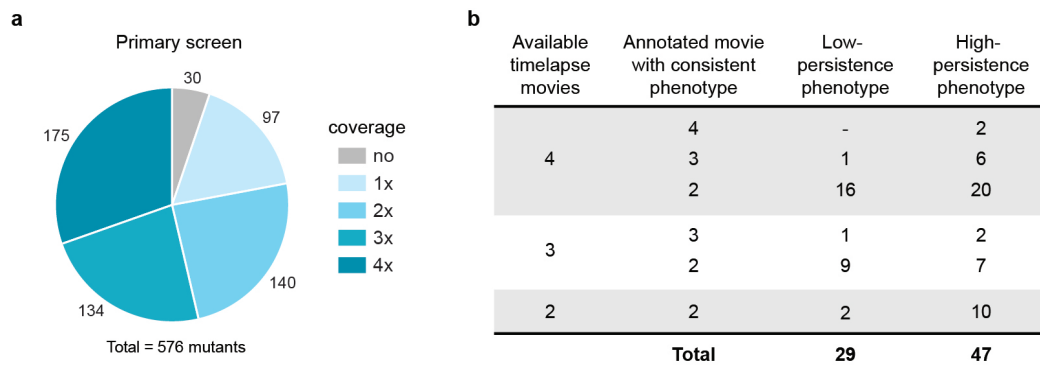


Figure 3.6: Primary screen coverage of mCherry-DnaN Wag31-GFP-expressing *M. smegmatis* mutant library and selection criteria for mutants with altered persistence rates. (a) High-quality time-lapse movie coverage for primary screening. 570 mutants were spotted, alongside 6 wild-type strains for comparative purposes, and screened with a maximum coverage of 4 time-lapse movies per bacterial strain. **(b)** *M. smegmatis* candidates consistently displaying an altered rate of persistence. A cutoff of 50% was imposed for selection.

3.2.4 Secondary screen – mCherry-DnaN Wag-GFP-expressing *M. smegmatis* mutant library

The 76 candidates were rescreened in a secondary screen using the same microfluidic platform to eliminate potential false positives. In the secondary screen each mutant was spotted up to 12 times per device to increase the number of technical repeats available per mutant. The secondary screening was repeated twice; thus, a coverage of up to 24 time-lapse movies per candidate was achieved.

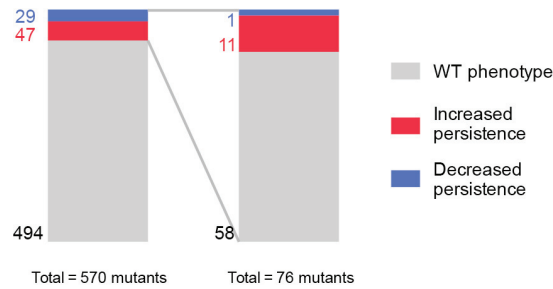


Figure 3.7: Secondary screen coverage and outcome. 570 mutants were analyzed in a primary screen (n = 2 independent experiments) and 76 candidates from the primary screen were assessed in a secondary screen (n = 2 independent experiments), of which 12 mutants bred true.

The criterion for selection of high-persistence mutants was the same as for the primary screen and the DsRed-expressing *M. smegmatis* mutant library screen, i.e. a cutoff of 50% of the time-lapse movies. Regarding low-persistence mutants, the criterion of selection was broadened since, as aforesaid, small microcolonies might mask a low-persistence mutant. In order not to miss any potential candidates, we decided to use a cutoff of 40%. Using those criteria, 12 out of 76 candidates were confirmed in the secondary screen, of which 1 mutant displayed a low-persistence phenotype and 11 mutants displayed a high-persistence phenotype (Figure 3.7).

The transposon insertion site for each of these mutants was located, the disrupted gene was identified and listed Table 3.5 for mutants displaying increased and decreased persistence phenotype respectively. The mutants are ranked according to how consistently the phenotype was observed. Up to 24 time-lapse movies could be available.

Time-lapse movies with consistent altered persistence	Mutated gene	Annotated gene function
95 % increased	<i>MSMEG_0208</i>	Ribonuclease
92 % increased	<i>MSMEG_6264</i>	Putative oxidoreductase
90 % increased	<i>MSMEG_1019</i>	Ribonucleoside-diphosphate reductase, α subunit
88 % increased	<i>MSMEG_6135-6</i>	Intergenic region
88 % increased	<i>MSMEG_5665</i> & <i>MSMEG_5666</i>	Hypothetical proteins & Hypothetical conserved proteins
80 % increased	<i>MSMEG_5167</i>	Major facilitator superfamily protein MFS_1

80 % increased	<i>MSMEG_0166</i>	GntR-family protein transcriptional regulator
75 % increased	<i>MSMEG_5159</i>	DNA-binding response regulator, putative
69 % increased	<i>MSMEG_5345</i>	Glycosyl hydrolases family protein 16
67 % increased	<i>MSMEG_1105</i>	No annotated function
67 % increased	<i>MSMEG_4107</i>	Phosphoglycerate mutase, putative
43 % decreased	<i>MSMEG_6815</i>	Secreted protein

Table 3.5: mCherry-DnaN Wag-GFP-expressing mutants displaying increased and decreased persistence phenotype.

Note that the transposon inserted once in an intergenic region between *MSMEG_6135* and *MSMEG_6136*, which are annotated as hypothetical protein and membrane protein TerC family protein respectively. In another mutant the transposon inserted in a region with two overlapping genes: *MSMEG_5665* and *MSMEG_5666*, encoding for hypotheticals proteins. Consequently, in this mutant, two genes are mutated simultaneously.

3.3 Discussion and outlook

The work described in this chapter aimed to demonstrate the potential of the HCS/HTS microfluidic screening platform to identify mutants displaying phenotypes that emerge only in dynamically changing environments, focusing on the specific example of bacterial persistence under fluctuating antibiotic pressure. The microfluidic screening platform was applied to two distinct mutant libraries in order to identify genes implicated in persistence during antibiotic exposure.

Although it might seem counter-intuitive to perform a genetic screen to identify genes involved in persistence, since it is a transient phenotypic state rather than a stable (heritable) genotypic state, we believe that this phenotype (persistence) nonetheless has a genetic basis. As previously described, a clonal bacterial population displays numerous phenotypes with different molecular compositions; some offspring may be better suited to survive environmental impacts such as

antibiotic treatment. Here, we seek to understand what are the genes that play a critical role in bacterial persistence, as, for example, a higher copy number of a certain protein at the moment of antibiotic exposure could promote the survival of some rare individuals. Mutants identified in both screens with altered rates of persistence highlight genes that are somehow involved, directly or indirectly, in persistence.

A first pilot screen of a DsRed-expressing *M. smegmatis* mutant library identified 19 candidates with altered persistence rates, of which 14 displayed increased persistence while 7 displayed decreased persistence. Conventional batch assays (kill curves) confirmed the phenotype of 14 out of 19 candidates: 10 with increased survival and 4 with decreased survival (Table 3.4). In a conventional batch-culture killing assay, mutants displaying 3-fold increased or decreased FSR, compared to the wild-type control, were considered to be true positives. The number of validated phenotypes depended on the chosen threshold for the FSR at 48 hours, as most of the 19 candidates displayed survival ratios in the direction expected, that is increased FSR for high-persistence mutants and decreased FSR for low-persistence mutants. In the following paragraphs, we will focus on the different genes identified whose disruption leads to increased or decreased persistence.

Interestingly, the disruption of *MSMEG_5783* was previously reported as inducing resistance to INH (Rawat, 2007). In the work presented here, a Tn::*MSMEG_5783* mutant exhibited an exceptionally high fractional survival after 48 hours of antibiotic exposure (FSR = 790), although its MIC was barely twice that of the wild-type. Similarly, it was reported that deletion of *MSMEG_1946* resulted in increased sensitivity to INH-mediated killing; in the work presented here, the FSR of a Tn::*MSMEG_1946* mutant was two orders of magnitude lower than wild-type yet the MIC was less than 2-fold lower compared to wild-type. We conclude, albeit tentatively, that a slight shift in MIC might result in major phenotypes regarding persistence. Furthermore, no clear binary state of FSR and MIC ratios were observed: the correlation between the two was not consistent (Figure 3.8a). Instead, a rather gradual change in sensitivity was observed such that the distinction between persistence mutants and resistance mutants depends upon the chosen

threshold MIC (grey dashed line, Figure 3.8b). The MIC of the mutants identified in the DsRed-expressing *M. smegmatis* mutant library screen were plotted against the FSR and seemed to support the model proposed in Figure 3.8b, with a linear fit R^2 of 0.72.

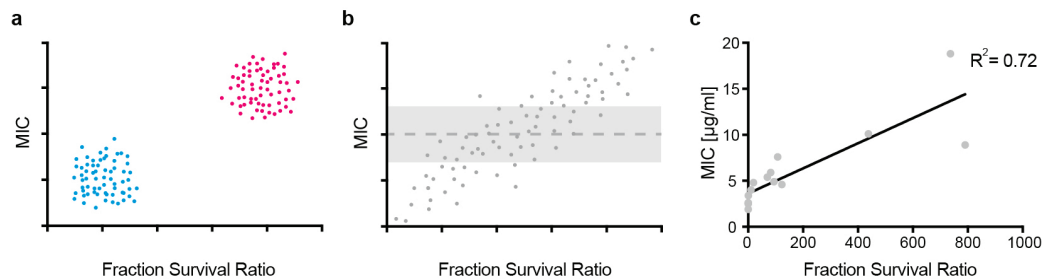


Figure 3.8: MIC versus FSR diagram. (a) Binary state model where resistant mutants (red) display a high MIC and a high FSR compared to non-resistant strains (blue). **(b)** The antibiotic sensitivity (MIC) and FSR gradually increase in parallel; the grey area indicates a potential threshold beyond which a mutant would be classified as “resistant”, but this threshold is not clearly defined. **(c)** MIC plotted against FSR for each mutant identified during the screen of the DsRed-expressing *M. smegmatis* mutant library. Linear fitting, $R^2=0.72$.

The distinction between persisters and resisters isn’t as simple as an MIC value. Furthermore, cross-talk between persistence and resistance mechanisms has been reported by De Groote and colleagues (De Groote *et al.*, 2011). More specifically, fosfomycin-resistant *Pseudomonas aeruginosa* conferred either by upregulation of *fosA*, through enzymatic modification of the antibiotic, or mutation in *glpT*, a transmembrane transporter of fosfomycin, resulted in decreased persistence to ofloxacin. These results demonstrate that mechanisms of persistence and resistance might be more tangled than first suggested.

The microscopy-based screening enabled the observation of different dynamics of survival of the collection of mutants with increased persistence (Table 3.3). Interestingly, except for Tn::MSMEG_5783 mutant, enhanced survival through active division at the population level during antibiotic exposure gave rise to the highest FSR at 48h, while mutants displaying increased persistence through enhanced recovery gave rise to mid-low FSR (Table 3.3) (Table 3.4). Additionally, no clear

relation between active division during antibiotic treatment and high MIC was observed.

A Tn::*MSMEG_0777* mutant was identified as a high-persistence mutant in the persistence mutant screen. The *MSMEG_0777* gene encodes a putative F420-dependent glucose-6-phosphate dehydrogenase; the homologous gene (*rv0407*) in *M. tuberculosis* is responsible for the activation of a class of antitubercular drugs bearing a nitroimidazopyran nucleus, such as PA-824 derivatives currently in clinical trials. Furthermore, mutations in *rv0407* cause resistance in both *M. tuberculosis* and *Mycobacterium bovis* (Stover *et al.*, 2000). The PA-824 compound shares some similar features with INH: first, PA-824 is a pro-drug that requires activation upon cellular entry albeit by a different mechanism that requires the F420-dependent glucose-6-phosphate dehydrogenase; second, similarly to INH, PA-824 inhibits cell wall biosynthesis but at a later stage. Interestingly, the disruption of *MSMEG_0777* by random insertion of the transposon in *M. smegmatis* resulted in a mildly increased persistence phenotype during INH exposure; its FSR at 48 hours was 2.3 ± 0.5 (data not shown).

MSMEG_2570 encodes for a putative xanthine/uracil permease involved in the passive transport of some specific small molecules across the membrane. Disruption of *MSMEG_2570* led to a high-persistence phenotype. As xanthine is structurally analogous to adenine, the core molecule of NADH, which is required for INH activation (section 2.6.1), we hypothesize that decreased levels of xanthine could potentially lead to decreased NADH levels and, thus, reduced activation of INH. Indeed, hypoxanthine, a derivative of xanthine, is obtained through deamination of adenine, which is a major component of NADH. Interestingly, a xanthine/uracil permease, *sp0287*, was found to be upregulated by fluoroquinolones in *Streptococcus pneumonia* (Marrer *et al.*, 2006).

Disruption of *MSMEG_2576*, encoding a putative deoxyribodipyrimidine photo-lyase, also led to an increased-persistence phenotype. Photo-lyases have been shown to respond to DNA damages and act in DNA repair (Richa *et al.*, 2015). It would be interesting to further investigate whether this phenotype is INH-specific or whether the increased phenotype is also observed in a broad range of antibiotics, i.e. if it

induce a general mechanism of antibiotic tolerance, we previously described the activation of the SOS response to DNA damages induce increased persistence (Dörr *et al.*, 2009).

The screen also identified a transposon insertion in *MSMEG_1946*, encoding a putative NADH pyrophosphatase (NudC), as a mutation conferring a low-persistence phenotype. The identification of this mutant would not have been possible with conventional cell-based screening assays, which typically measure a proxy signal (e.g. fluorescence), averaged over all cells within a micro-well. Indeed, this mutant did not show increased lysis during antibiotic exposure compared to the wild-type control, i.e. no difference in cytosolic DsRed fluorescence. However, the low-persistence phenotype was revealed during the recovery phase, because the mutant failed to resume growth after antibiotic removal. This mutant highlights the necessity to dynamically control the microenvironment in order to identify unexpected persistence phenotypes, which would be complicated in a micro-well format.

A second pilot screen of a DnaN-mCherry Wag-GFP expressing *M. smegmatis* mutant library identified 12 candidates with altered rates of persistence, of which 11 displayed increased persistence while 1 displayed impaired persistence. We will discuss now some of the genes identified as having altered persistence in this second screen.

A particularly interesting mutant identified with an increased rate of persistence is Tn::*MSMEG_0166*. More specifically, *MSMEG_0166* encodes for RoxY, a repressor of *oxyS* (Daugherty *et al.*, 2011). OxyS in turn represses *ahpC*, which encodes for a peroxidase involved in cellular detoxification. *ahpC* expression was previously reported as a compensatory mechanism to KatG detoxification in *M. tuberculosis* isoniazid-resistant KatG mutants (Sherman *et al.*, 1996); however, the overexpression of *ahpC* is not directly related to INH resistance (Heym *et al.*, 1997). Since disruption of *MSMEG_0166* would ultimately lead to decreased expression levels of *ahpC*, one would expect an increased sensitivity to antibiotics. Yet we observed increased persistence. The mechanisms underlying this increased persistence remain to be determined, but could be uncovered in further

experiments. Lastly, the transposon was inserted at the 690th nucleotide in a total gene length of 729 nucleotides (Table 7.2), the DNA binding sequences is located within the first 300 base pairs, it is possible that Tn::MSMEG_0166 remained somewhat functional.

The mutant Tn::MSMEG_5167 was identified as a candidate with increased persistence which could be associated with the efflux of INH. Indeed, MSMEG_5167 encodes for a major facilitator superfamily (MFS) transporter. MFS facilitates the transport of substrates across the membrane and numerous MFS transporters have been reported as contributors to multi-drug resistance through drug efflux (Alegre *et al.*, 2016).

In the mutant Tn::MSMEG_5159 persistence was also increased. The transposon was inserted in a DNA-binding response regulator, which is part of a two-component signal transduction system. Several two-component systems were reportedly involved in *M. tuberculosis* establishment of persistence during infection, and mutation in these systems would lead to attenuation of the bacteria, such as, for instance, MprAB (He *et al.*, 2006) or SenX3-RegX3 (Tischler *et al.*, 2013). Additionally, Dörr and colleagues reported the role of WigK/WigR for *Vibrio cholera* survival to cell-wall-targeting antibiotics exposure *in vitro* and during infection (Dörr *et al.*, 2016). Two-component systems regulate numerous bacterial processes; depending on the pathways regulated, disruption of such a system could lead either to decreased or increased persistence, the latter being the case for MSMEG_5159 disruption.

The unique mutant of the combinatory DnaN-mCherry- and Wag-GFP-expressing *M. smegmatis* library displaying decreased persistence was Tn::MSMEG_6815. Its gene product is described as a secreted protein, however little has been reported in *M. smegmatis*. However, the inactivation of its homolog in *M. tuberculosis*, rv2525c, resulted in increased susceptibility to beta-lactams antibiotics, and during upon antibiotic exposure its expression was indeed upregulated along with genes involved in cell wall biosynthesis (Saint-Joanis *et al.*, 2006). Interestingly, INH inhibits cell wall biosynthesis similarly to beta-lactams antibiotics.

In conclusion, the genes identified using the high-throughput screening platform demonstrate the potential of microfluidic devices to address relevant microbiological questions. Indeed, these experiments provide new insights into the genes and pathways that are critical for antibiotic persistence in mycobacteria. In particular, genes positively contributing to persistence (i.e., mutants with decreased rates of persistence), such as the F420-dependent glucose-6-phosphate dehydrogenase, could potentially identify new targets for drug discovery. Drugs that effectively target and kill persister cells would have wide ranging medical application, including, but not limited to, shortening the duration of chemotherapy and curtail emergence of resistance.

4 Quantitative single-cell analysis of *Mycobacterium smegmatis* mutants with altered rates of persistence during antibiotic exposure

In the previous chapter, I identified several mutants displaying altered rates of persistence. I am now interested in understanding what are the dynamics underlying these altered persistence phenotypes. For that purpose, I will quantitatively investigate the cell division and death during antibiotic exposure of two representative mutants.

4.1 Microfluidic platform modifications for single cell studies

The microfluidic screening platform was modified for quantitative single cell analysis. In these experiments cells were flowed into the device, which was plasma-bonded to a glass slide rather than spotted onto an epoxy-coated coverslip as

previously described. Hence, the ceilings of the microchambers could be lowered from 1.4 μm to 0.8 μm to improve imaging. This reduction in ceiling height would not have been possible in the previous platform, since microchambers with ceilings lower than 1.4 μm collapsed due to the wet spots and capillarity forces.

4.2 Scoring cell lysis

In preliminary experiments conducted using this new microfluidic platform, bacterial lysis on exposure to antibiotics was not easily discernible by phase contrast imaging or on the epi-fluorescence channels. Most of the cells appeared intact but did not recover upon antibiotic removal. Hence, for the purpose of the study, SYTOX® Green (Thermofisher), a cell-impermeable nucleic acid stain which selectively stains cells with a damaged cell wall permeability barrier, was used to score cell death during antibiotic exposure.

To verify that the nucleic stain itself was not cytotoxic, the interdivision time of wild-type *M. smegmatis* expressing cytosolic DsRed grown in regular medium (7H9) was compared to that of cells grown in medium supplemented with 50 nM of SYTOX® Green (Figure 4.1). Each microcolonies growth was exponentially fitted ($N(t) = N_0 \cdot 2^{kt}$) to extrapolate microcolonies' doubling time. No significant difference regarding the doubling time was observed: the interdivision time of bacteria exposed to SYTOX® Green 7H9 was 167.3 ± 12.3 min versus 165.1 ± 14.7 min in regular medium (Figure 4.1 b). Furthermore, regrowth of surviving persisters after drug removal was similar with or without use of the nucleic acid stain. Therefore, a concentration of 50 nM SYTOX® Green was used for all subsequent experiments.

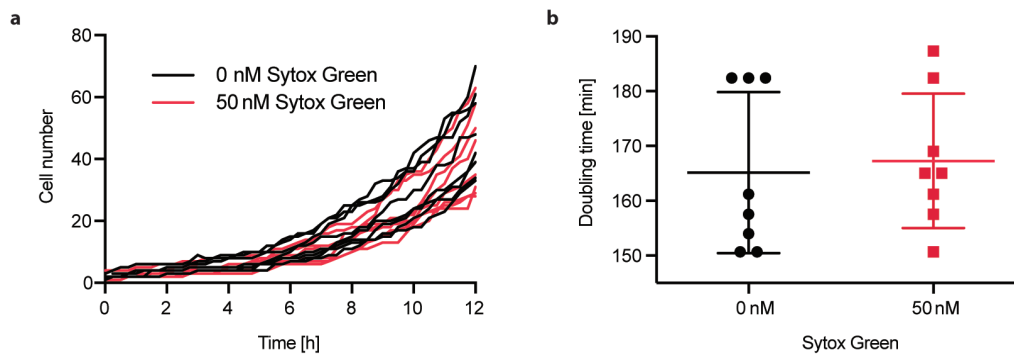


Figure 4.1: Influence of SYTOX® Green on wild-type *M. smegmatis* expressing DsRed. Cells grown in regular medium are shown in black, and cells grown in medium supplemented with 50 nm of SYTOX® Green are shown in red. (a) Single-colony traces representing the number of cells in the microcolony over time. (b) Averaged doubling time of each microcolony. Data represented are means or traces of 8 individual microcolonies in each experimental condition. The temporal resolution was of 15 min.

Figure 4.2 displays a representative time-lapse movie used for quantitative single-cell analysis of cell division and death dynamics during antibiotic exposure. *M. smegmatis* was first cultured in regular medium to establish a microcolony in a microchamber, at time 0h the medium is switched to medium containing INH for 48h. At 48h, the antibiotic is removed to enable cell recovery. SYTOX® was of a great help to identify intact bacteria with compromised cell wall (Figure 4.2).

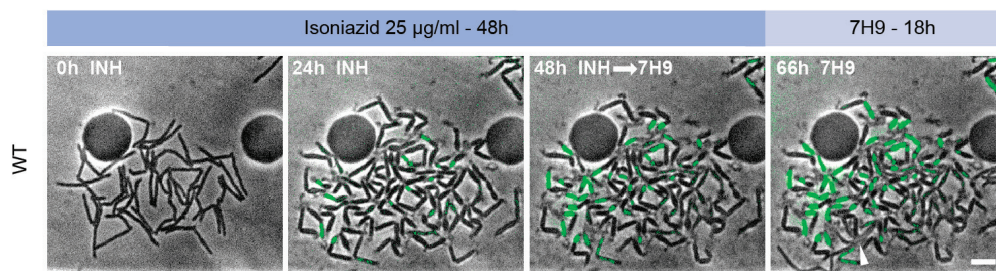


Figure 4.2: Representative time-lapse movie of single-cell analysis of cell divisions and cell deaths during antibiotic exposure. Representative merged fluorescence and phase channel time-lapse movie of a wild-type *M. smegmatis* colony exposed to INH for 48h. SYTOX® green stains bacteria with compromised cell wall. White arrow indicates cells resuming growth, and scale bar represents 5 µm.

4.3 Influence of the size of the microcolony on division and killing during antibiotic exposure

Another important aspect to consider for single cell analysis is the size, or the number of bacteria, in a microcolony as it might impact on division and killing events. Particularly, in the microfluidic screening platform the antibiotic diffuses from the main channel to the microchambers and reaches the bacterial microcolonies laterally. Therefore, it is conceivable that in case of a large-microcolony, cells located in the center of a chamber encounter less antibiotic than those at the edges. To address this issue, division and killing events of wild-type *M. smegmatis* exposed to INH for 48h were recorded in microcolonies of different sizes, ranging from 71 cells to 210 cells (Figure 4.3). The colony size corresponds to the number of bacterial cells forming the colony at the beginning of antibiotic exposure. To identify different possible patterns Eng. Katrin Schneider developed an analytical method to reveal differences in cell division and death in single-cell experiments: the number of events are normalized to the colony size and summed over time. Thus, when the number of events is plotted over time, slopes indicate event rates. In the current control experiment, no patterns related to the colony size were observed, either for division events or for death events. The slopes of normalized division events were uniform between the different bacterial colony sizes (Figure 4.3a), whereas normalized death event slopes exhibited more variability, but this variability was not related to variation in colony size (Figure 4.3b). Therefore, at least for microcolonies comprising less than 210 cells, no differences in terms of killing and division were observed. Additionally, persisters were found to arise regardless of their position in the microcolony.

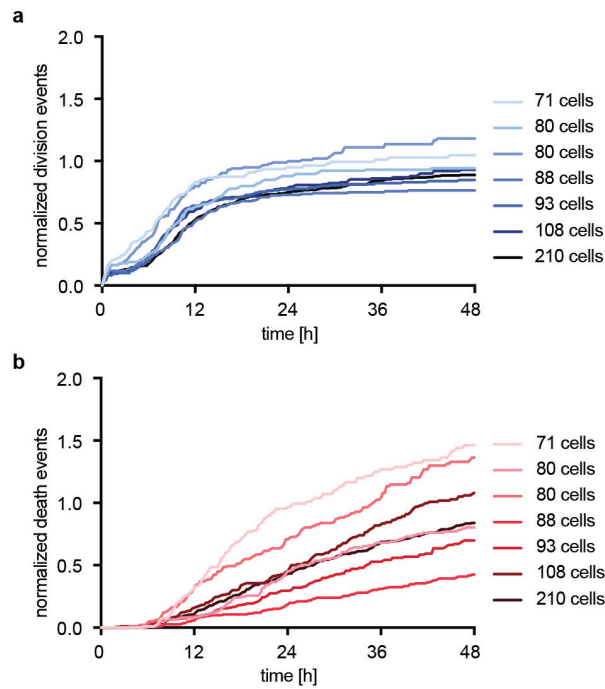


Figure 4.3: Division and death events in microcolonies of different sizes. (a) Division and **(b)** death events were normalized to colony size and summed over time for colonies ranging from 71 cells to 210 cells at time 0 which corresponds to the beginning of INH exposure.

4.4 Dynamics of cell division and cell death in *M. smegmatis* mutants displaying altered rates of persistence during and after antibiotic exposure

4.4.1 Experimental procedure for single-cell experiments

Cells were inoculated and cultured overnight in 10ml of 7H9 medium without antibiotic. Cells from exponential phase ($OD_{600\text{ nm}}$ 0.4 to 0.7), were centrifuged and re-suspended in 500 μ l of 7H9 without antibiotic.

The microfluidic screening platform with lowered ceilings (0.8 μ m) was micro-fabricated as previously described (Section 2.2). This chip was oxygen plasma-

bonded (10 seconds plasma) to a glass coverslip, and baked at 80°C for a couple of hours to strengthen the bonding.

The control valves were primed with sterile water before cells were introduced into the device from the purge inlet at 3 psi with the outlet valve closed; this process took approximately 10 minutes. As the platform has three independent subsets, the wild-type strain and the two selected mutants were loaded independently and imaged on one single device, repeated twice on separate devices (Figure 4.4). Once the cells were loaded, 7H9 medium with and without INH were primed. The purge inlet as the flow channels were purged at 5 psi to clear them of any potential cells that could grow and obstruct the flow. The concentration of INH used in these experiment was 25 µg/ml. Microchambers were imaged at 15 minute intervals for 100 hours on three channels: phase, red fluorescence and green fluorescence.

The experiment was divided into three phases. In the first phase of growth, *M. smegmatis* grew and formed small microcolonies. In the second phase, when microcolonies reached an approximate size of 40-200 individual cells, the medium was switched to INH-containing medium. After 48h of antibiotic exposure, INH was removed for the third and last phase in order to observe the cells' recovery.

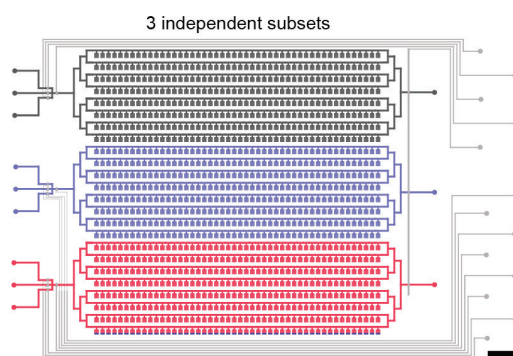


Figure 4.4: The microfluidic screening platform and its three independent subsets. The platform is divided in independent subsets: black, blue, and red. Each platform can carry up to three different bacterial strains. For quantitative single cell analysis, wild-type *M. smegmatis* alongside with Tn::*MSMEG_0034-35* and Tn::*MSMEG_6284* mutants were loaded into separate subsets of the same device and were monitored in parallel. Scale bar indicates 2 mm.

4.4.2 Selection of mutants with altered rate of persistence

Two DsRed-expressing *M. smegmatis* mutants with altered rates of persistence identified in the persistence screen (Section 3.1) were selected for in-depth analysis of their dynamics during antibiotic exposure at the single-cell level (Figure 4.5).

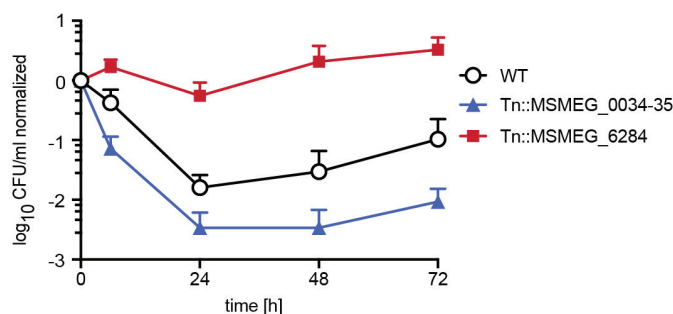


Figure 4.5: Kill curves for mutants with altered persistence. Mutants exhibiting increased (red) or decreased (blue) persistence compared to wild-type strain in batch experiment. Kill curve points represent means ($n \geq 3$ independent experiments). Error bars correspond to the standard deviation of the means.

The first mutant selected, Tn::*MSMEG_6284*, displayed increased persistence. *MSMEG_6284* encodes for a cyclopropane-fatty-acyl-phospholipid synthase (Table 3.4) involved in fatty acid and phospholipid metabolism and thus might be involved in cell wall synthesis. Tn::*MSMEG_6284* mutant exhibited high survival ratio after 48h of INH exposure, approximately 70 (Figure 4.5), while displaying only a mild increase in MIC compared to wild-type: MIC_{Tn::MSMEG_6284} was 5.4 μ g/ml compared to an MIC_{WT} of 3.4 μ g/ml (Table 4.1).

The second mutant selected from the screening was Tn::*MSMEG_0034-35*, which displayed decreased persistence. The transposon inserted in an intergenic region between *MSMEG_0034* and *MSMEG_0035* genes upstream of a highly conserved operon. Though the operon has been studied more extensively in *Mycobacterium tuberculosis* (*M. tuberculosis*) than in *M. smegmatis*, we do know that it encodes for genes involved in signal transduction and cell division. The operon boundaries aren't

very clear, Fernandez *et al.* reported that it spans from *MSMEG_0034* to *MSMEG_0029* (in case of *M. smegmatis*), or *rv0019c* to *rv0014c* (in case of *M. tuberculosis*) (Fernandez *et al.*, 2006). Yet, several operon prediction algorithms include *MSMEG_0035* in the same operon however with a lower confidence. Furthermore, its expression in *M. tuberculosis* was reported to be correlated, with the expression of the second gene of the conserved operon, corresponding to is *rv0018c* in *M. tuberculosis* and *MSMEG_0033* in *M. smegmatis* (Boshoff *et al.*, 2004). The transposon insertion location right upstream to the operon might perturb the expression of the downstream genes. Furthermore, the operon seems to play an important role in regulating persistence as 3 of the 4 mutants identified during the screen in chapter 3 as displaying impaired persistence had the transposon insertion within or upstream of the operon (Table 3.4). Tn::*MSMEG_0034-35* displayed an MIC comparable to wild-type (less than a two-fold decrease) while its survival was a tenth of that of the wild-type after 48h exposure to INH (Table 4.1).

Mutated gene	Fractional Survival Ratio at 48h	Minimum inhibitory concentration [µg/ml]	Annotated gene function
MSMEG_6284	69.7 ± 57.9	5.4 ± 0.2	Cyclopropane-fatty-acyl-phospholipid synthase
wild type	1 ± 1.2	3.4 ± 0.9	—
MSMEG_0034-35	0.116 ± 0.115	2.6 ± 0.1	Intergenic region

Table 4.1: Fractional survival ratio and minimum inhibitory concentration of selected mutants for single cell analysis. Tn::*MSMEG_6284* and Tn::*MSMEG_0034-35* candidates validated by conventional batch experiments. Columns give mutated genes, fractional survival ratios at 48h compared to wild-type strain during kill curve and minimum inhibitory concentration of INH. Data represent means and standard deviation of $n \geq 3$ independent experiments.

4.4.3 Dynamics of cell division and cell death during INH exposure

During antibiotic exposure, the constant number of cells during the persistence phase observed in kill curves performed in batch (Figure 4.5) hides a dynamic, balanced state of cell division and death, as demonstrated by Wakamoto and

colleagues (Wakamoto *et al.*, 2013). This dynamic state might have an important role in bacterial survival during antibiotic treatment, as increased division or decreased killing could possibly enhance survival for instance. In an attempt to understand the dynamics of persistence, killing and division within micro-colonies of the above-mentioned mutants exhibiting altered persistence, were monitored during antibiotic exposure and these were compared to the dynamics in wild-type *M. smegmatis*.

Quantitative single-cell results based on time-lapse fluorescence microscopy of wild-type *M. smegmatis*, mutant Tn::MSMEG_6284 and mutant Tn::MSMEG_0034-35 during 48 hours of antibiotic ([INH] = 25 µg/ml) exposure is presented in Figure 4.6. As previously described, division events are normalized to the colony size and summed over time (Figure 4.6a). In the first few frames, cells continued to divide before INH diffused throughout the whole microchambers (Section 2.6.1). Cell elongation is first arrested followed by *reductive* division, which is marked by a sharp decrease in mean cell size (Wakamoto *et al.*, 2013), typically owing to cell division without elongation. Cell division during antibiotic exposure was similar across the different strains studied, including wild-type mutant strains. Most of the division events occurred between 6 and 24 hours after the antibiotic switch. After approximately 18-24h, cell division generally reached a plateau. Single-cell analysis revealed similar division rates between the two mutants. More specifically, Tn::MSMEG_6284 mutant displayed a marginally greater division rate compared to wild-type cells, while the division rate of Tn::MSMEG_0034-35 mutant was delayed and slightly decreased. Thus, division rate is likely not the major factor behind their oppositely altered rates of persistence.

Cell death was also monitored during antibiotic exposure. Cell death was indicated by SYTOX® Green positive cells or by physical lysis of cells on the phase channel, with the former being much more common (Section 4.2). Death events were normalized to colony size and summed over time (Figure 4.6b). Death rates clearly exhibited more heterogeneity between the mutants than the division rates. After an initial lag phase, cells started to either lyse or to stain positive to SYTOX®. Tn::MSMEG_6284, an increased persistence phenotype, had a lag phase of ~6 hours

like the wild-type, and exhibited a death rate only slightly lower than the wild-type. Regarding Tn::MSMEG_0034-35 mutant, the initial lag phase was longer than wild-type and this strain, although this strain was initially characterized to have impaired persistence, it paradoxically experienced a much lower rate of cell death than both wild-type and Tn::MSMEG_6284. This behavior was consistently observed in two independent experiments.

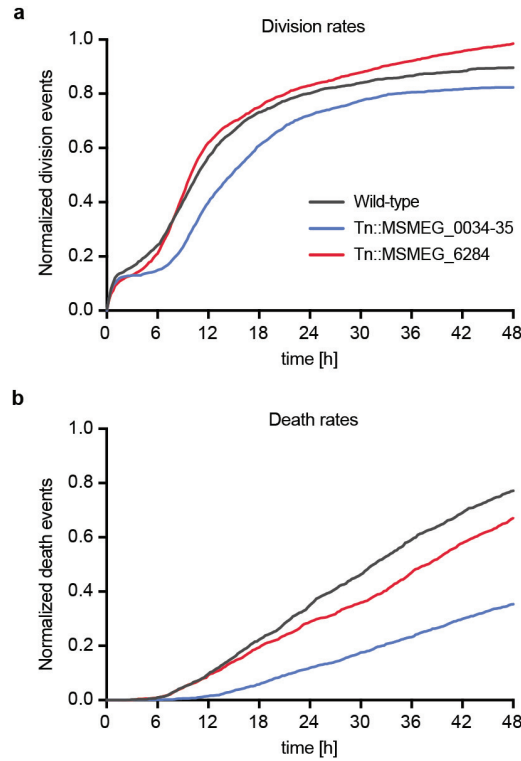


Figure 4.6: Quantitative single-cell analysis of cell division and killing during antibiotic exposure. (a) Division and (b) death events were normalized to colony size and summed over time. The division and death rates of wild-type *M. smegmatis* Tn::MSMEG_0034-35 and Tn::MSMEG_6284 are represented. Results are the mean of 2 independent experiments (n=2), where ≥ 7 independent micro-colonies were analyzed in each experiment. Time 0 correspond to INH switch ([INH] = 25 µg/ml).

Finally, the death rate for each strain was approximated by a linear fit between 12h and 48h of exposure to antibiotic treatment. The slopes of these linear fits and their standard deviations are reported in Table 4.2.

	Slope \pm SD	R ²
Wild-type	0.0193 \pm 0.0037	0.997
Tn::MSMEG_0034-35	0.0097 \pm 0.0022	0.991
Tn::MSMEG_6284	0.0171 \pm 0.0025	0.999

Table 4.2: Slopes of death rates slopes.

Details about the quantitative measurements taken during INH exposure in both independent experiments are reported in Table 4.3.

		Total number of			
		Cells at INH switch	Divisions during INH exposure	Lysis during INH exposure	SYTOX® green positive cells
Experiment 1	Wild-type	730	923	134	766
	Tn::MSMEG_0034-35	704	840	43	439
	Tn::MSMEG_6284	901	1087	116	898
Experiment 2	Wild-type	572	702	48	452
	Tn::MSMEG_0034-35	574	717	10	308
	Tn::MSMEG_6284	568	796	61	518

Table 4.3: Quantitative measurements of independent single-cell experiments. Summary of the total number of cells in the microcolony at INH switch, the number of divisions, and the number of lysed and SYTOX® positive cells during INH exposure in wild-type, Tn::MSMEG_0034-35 and Tn::MSMEG_6284 mutants.

4.4.4 Analysis of persister cells occurrence

After two days (48h) of antibiotic exposure, antibiotic was removed and cells were grown in regular medium to investigate recovery frequencies between the wild-type and the different mutants.

The number of persisters were normalized to the colony size and summed over time. Persister cells were counted from the start of elongation; hence only independent lineages of persistence were recorded and descendants of persister cells were not taken in account. In other words persister cells are cells that reactivate and resume growth.

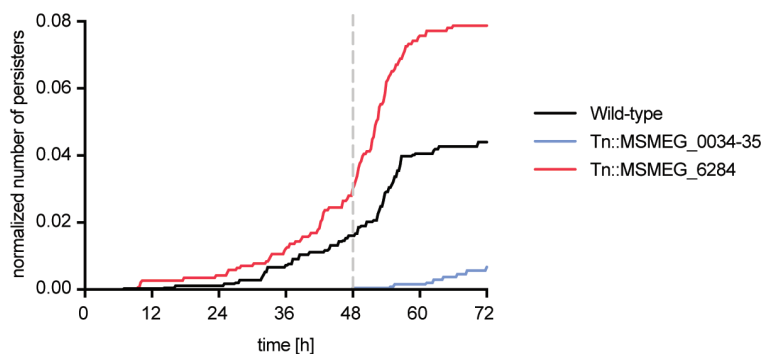


Figure 4.7: Independent lineage of persisters cells. The number of persister cells were normalized to the micro-colony size at each frame and summed over time. Persister cells of wild-type *M. smegmatis*, Tn::MSMEG_0034-35 and Tn::MSMEG_6284 are displayed. Results are the mean of two independent experiments (n=2) of ≥ 7 independent micro-colonies each. Time 0 corresponds to the INH switch ([INH]= 25 μ g/ml). The grey dashed line corresponds to INH removal at 48h.

With regards to Tn::MSMEG_6284, the mutant characterized by increased persistence phenotype, numerous persisters resumed growth upon antibiotic removal compared to the wild-type (Figure 4.7). Interestingly, many persister cells started elongating at a very slow rate during antibiotic exposure in both wild-type and Tn::MSMEG_6284 mutant. More specifically, the initial few Tn::MSMEG_6284 persister cells in each independent experiment began elongating between 10h and 24h after INH exposure respectively, while the initial wild-type persister cells began elongation between 16h and 25h after exposure. Antibiotic was removed at 48h, and in both wild-type and Tn::MSMEG_6284 mutant a rise in the number of persisters “awakening” was observed. This number plateaued at approximately 58h for both strains, that is, 10 hours after antibiotic removal. The frequency of Tn::MSMEG_6284 persister cells starting elongation during antibiotic exposure and upon antibiotic removal was much higher than that in the wild-type: 9.6 % versus 3.9 % respectively (Table 4.4). Even then, the frequency of Tn::MSMEG_6284 was most

likely underestimated due to cell crowding toward the end of the recovery phase. Independent microcolonies displayed very heterogeneous behavior regarding persistence; some were very active in terms of division and killing during INH exposure and give rise to numerous persisters while others displayed phenotypes comparable to the wild-type, with only a few cells recovering from antibiotic treatment.

	Persistence frequency
Wild-type	3.9 % \pm 3.5 %
MSMEG_0034-35	0.8 % \pm 0.3 %
MSMEG_6284	9.6 % \pm 0.1 %

Table 4.4: Summary of persistence frequency.

With regards to Tn::*MSMEG_0034-35*, characterized by decreased persistence, the dynamics of persistence differed. First, cells rarely resumed growth after antibiotic removal. Furthermore, unlike Tn::*MSMEG_6284* and wild-type persisters that began elongation during INH treatment, Tn::*MSMEG_0034-35* persisters did not begin elongation until much later. With one exception, persisters started elongating only after INH removal (Figure 4.7). In Tn::*MSMEG_0034-35* mutants, the frequency of persisters was particularly low at 0.8 %, compared to 3.9% for the wild-type (Table 4.4). Therefore, the results for both Tn::*MSMEG_6284* and Tn::*MSMEG_0034-35* were consistent with the results of the microfluidic screening and batch culture experiments.

In all three strains, numerous cells remained physically intact but failed to resume growth after antibiotic removal. To test whether these cells were truly intact, the fraction of SYTOX® Green-negative cells (intact) was quantified at the first frame after INH removal, in order to distinguish truly intact cells from those with compromised cell walls (Figure 4.8). In case of Tn::*MSMEG_6284* mutant, the fraction of intact SYTOX® Green-negative cells was comparable to wild-type, 53.2% \pm 10.7% versus 53.3% \pm 6.1% respectively. This fraction represents the cells that could potentially become persisters. Unexpectedly, the fraction of intact SYTOX® Green-

negative cells in the Tn::*MSMEG_0034-35* mutant was considerably higher at 72.1% \pm 4.7%. However these cells either failed to resume growth or did so at a much lower frequency compared to wild-type (Figure 4.8). The high number of intact, SYTOX® Green-negative Tn::*MSMEG_0034-35* cells is largely due to a lower death rate during antibiotic exposure compared to the wild-type and to Tn::*MSMEG_6284* mutant (Figure 4.6). Thus, even though a large number of Tn::*MSMEG_0034-35* cells remained physically intact and SYTOX® Green-negative perhaps due to a lower death rate during antibiotic exposure, most of these failed to recover after INH removal.

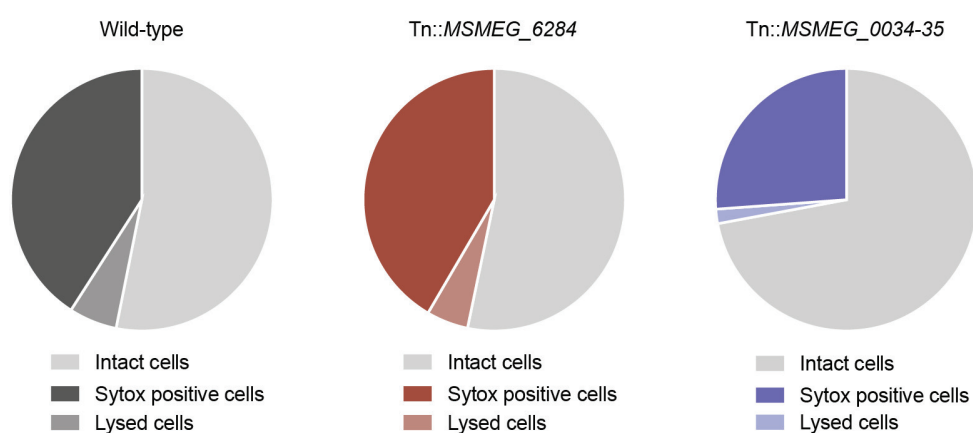


Figure 4.8: Fractions of physically intact cells upon antibiotic removal as indicated by SYTOX® Green negative. At the beginning of the recovery phase, the numbers of SYTOX® Green-positive and -negative physically intact cells were assessed. Wild-type and Tn::*MSMEG_6284* mutant displayed an average of 53.1% and 53.3% SYTOX® Green negative cells respectively, while 72.1% Tn::*MSMEG_0034-35* mutant cells were SYTOX® Green negative. Lysis was 5.9% for wild-type, 5.1% for Tn::*MSMEG_6284* and 1.8% for Tn::*MSMEG_0034-35*. Results are the mean of two independent experiments (n=2) of ≥ 7 independent micro-colonies each.

4.5 Discussion and outlook

In this chapter, I demonstrated the versatility of our HCS/HTS high-throughput microfluidic screening platform. Using the same design, by lowering the ceilings of

microchambers from 1.4µm to 0.8µm, the 2D microcolony growth of mycobacteria required for precise quantitative measurements was achieved. Thus, the microfluidic platform is useful not only for screening of 1152 genotypes in parallel, but also for conducting follow up studies on interesting mutants, at the single-cell resolution. In addition, the subdivision of the platform in three independent subsets enables the treatment of three different bacterial strains, subjected to the exact same experimental conditions (such as temperature, medium composition, medium pressure and flow rate, antibiotic concentrations, etc.), on the same device. This of course reduces inter-experimental variability while considerably reducing the time required for the analysis of three different strains.

The overall behavior of the two mutants with altered rates of persistence presented here was consistent with previous microfluidic screening and conventional batch experiments. However, more detailed measurements of cell divisions and deaths revealed interesting dynamics.

With regards to Tn::*MSMEG_0034-35* mutant, single-cell analysis revealed interesting and unexpected persistence kinetics. Cell division was similar to the wild-type, while death rate was, paradoxically, significantly lower than wild-type – even though that mutant was defective for persistence. Furthermore, at the beginning of the recovery phase, 72.1% ± 4.7% of the Tn::*MSMEG_0034-35* cells were intact and SYTOX® Green-negative, indicating that they could potentially resume growth, versus only 53.2% ± 10.7% for the wild-type cells. However, while wild-type cells were generally able to recover growth, mutant cells only rarely resumed growth. Although numerous Tn::*MSMEG_0034-35* cells remained physically intact and SYTOX® Green-negative, they were not able to recover which was consistent with what was previous observation via microfluidic screening.

With regards to Tn::*MSMEG_6284* mutant, the balance of cell division and death was very similar to the wild-type. However, the mutant displayed a tenuous advantage regarding division and a slightly reduced death rate, which, together, could account for the mechanism of increased persistence. Furthermore, the frequency of persister cells was also confirmed to be the higher than that in the wild-type strain.

Mycobacterial cell division is difficult to observe in phase-contrast images; therefore, some inaccuracies in cell division events reported here can be attributed to the absence of cell division markers in the mutant strains in these experiments. Cell division inaccuracies impact the estimates of total cell number and thereby on the estimates of cell division rate and death rate, which are both normalized to the total cell number. Santi *et al.* recently showed that the localization of a Wag-GFP fusion protein to the nascent division septum coincides with cytoplasmic compartmentalization (cytokinesis) of the nascent daughter cells (Santi *et al.* 2013). Single-cell analysis of mutants with altered rate of persistence from the mCherry-DnaN and Wag-GFP *M. smegmatis* mutant library would thus allow not only more precise measurements regarding cell division, but also the study of DNA replication dynamics during INH exposure through the DnaN cell-cycle marker.

5 Perspectives and outlook

5.1 Results overview

This thesis we reported the development of a novel, versatile, high-throughput microfluidic screening platform designed to interrogate bacterial libraries at single-cell resolution by time-lapse microscopy. Originally designed for eukaryotic cells, the device had to be completely re-engineered for prokaryotic cells. This HCS/HTS microfluidic platform enabled the screening of thousands of different bacterial genotypes in an area less than 4cm². Importantly, the platform's integrated micromechanical valves facilitate switches between different medium sources and allow precise control over the cellular microenvironment.

The platform even goes beyond single-cell resolution, enabling subcellular screening in prokaryotic cells. We successfully imaged two subcellular cell-cycle markers, mCherry-DnaN and Wag-GFP, in *M. smegmatis* for over 18h with a temporal resolution of 20min. A *M. smegmatis* expressing Wag-GFP, a marker for the septum, was used to perform a mock screen based on prokaryote subcellular morphology, during which a mutant with altered cell division was successfully identified. We also demonstrated the ability of the platform in identifying phenotypes emerging in dynamically controlled environments, such as persistence. In a proof-of-concept screening where a *M. smegmatis* mutant with impaired persistence was randomly

spotted among wild-type spots, the mutant was identified correctly with a success rate of 94% (section 2.6.3).

The platform was then applied to two *M. smegmatis* mutant libraries to identify genes involved in bacterial persistence, which requires repeated switches of the environment between regular growth medium and medium containing antibiotic. As previously described, the mechanisms behind persistence remain elusive, identifying the genes implicated could indicate potential targets for drug development, leading to the eradication of persister cells which are a major cause of recurrent infections and antibiotic treatment failure. A total of 1710 mutants were investigated using the HCS/HTS microfluidic screening platform, of which 31 mutants were identified as having altered rates of persistence compared to wild-type. The first screening was performed using a DsRed-expressing *M. smegmatis* mutant library composed of 1140 candidates and identified 19 mutants with altered rates of persistence, of which 12 exhibited increased persistence and 7 had decreased persistence. The second screening, in a background of *M. smegmatis* expressing mCherry-DnaN Wag-GFP, of a mutant library comprising 570 candidates, identified 12 mutants with altered rates of persistence, including 11 had increased persistence and 1 showed impaired persistence. Some particularly interesting genes were found to be implicated with persistence, such as *MSMEG_1946*, the NADH pyrophosphatase, responsible for the degradation of the active form of INH (INH-NAD), which could not have been identified in a conventional micro-well plate format screening assay. Also implicated was *MSMEG_0777*, the F420-dependent glucose-6-phosphate dehydrogenase, that was reported as a particularly promising target for a novel class of antitubercular drugs (Stover *et al.*, 2000). Surprisingly, *MSMEG_0777* mutant displayed slight increased persistence to INH, suggesting that the combination of these class of antitubercular drugs with INH might be problematic as the effectiveness could be decreased. However, the list of genes identified through the screenings may serve as candidate for new drug targets for mycobacterial infections such as tuberculosis.

Finally, in an attempt to understand the underlying dynamics of persistence, mutants with altered persistence were analyzed further, with their rates of and cell

divisions and deaths quantitatively measured during antibiotic treatment using the same microfluidic screening platform. Even though the division and death dynamics of the mutant with increased persistence resembled those of the wild-type, the mutant with impaired persistence paradoxically displayed the highest proportion of physically intact cells, but did fail to resume growth upon antibiotic removal.

Through these experiments, we demonstrated the highly versatile potential of the high-throughput microfluidic screening platform for prokaryote-imaging by time-lapse microscopy. First, we demonstrated the ability to screen at the cellular and subcellular levels of prokaryotic cells. Second, the on-chip micromechanical valves enabled screening of phenotypes that emerge only when exposed to complex medium profiles (i.e. persistence). Third, the subdivision of the platform into 3 independent subsets allowed parallel imaging of 3 different bacterial strains – or 3 different conditions – with quantitative single-cell measurements, thus considerably reducing experimental variation, but more importantly reducing experimental time by a factor of 3. In slow growing bacteria such as *Mycobacterium tuberculosis* (interdivision time of 24h approximately) this could be extremely valuable.

5.2 Limitations

Though the HCS/HTS high-throughput microfluidic screening platform described herein proved to be a powerful tool for microbiological studies, it nevertheless faced few hurdles and limitations, among which time resolution, the inability to use pathogenic strains, cell crowding, and the lack of an automated analysis tool were particularly problematic.

An important factor to consider when performing high-throughput screening by time-lapse microscopy is time resolution. The time required to complete the image acquisition of one round (1152 microchambers) on three different fluorescent channels is approximately 75 minutes. Our screenings were all performed with *M. smegmatis*, a relatively slow-growing bacterium (interdivision time 2.5-3 hours at 37°C). However, monitoring faster growing bacterial species such as *E. coli*

(interdivision time of 20 min at 37°C) could be problematic. If a high temporal resolution is required, several solutions can be considered. First, the screen could be performed at a lower temperature in order to slow bacterial growth rate. Second, reducing the image acquisition to two channels would decrease the time required for one round by two fold. Furthermore, we would like to mention also that new microscopes enable faster rounds of image acquisition through improved focus systems, which is the most important limiting factor. However, there is of course a trade-off between the number of microchambers to image and time resolution, and depending on the screening, these parameters should be chosen carefully.

The HCS/HTS microfluidic screening platform has been engineered for prokaryotic screening at single cell level, one limitation of this technique is the restricted use of non-pathogenic bacterial strains. Here, we focused on the non-pathogenic *M. smegmatis*, but the platform is indeed amenable for many different types of prokaryotes, ranging from the fast-growing *E. coli* to the highly pathogenic *M. tuberculosis*. That being said, several parameters should be carefully considered when using pathogenic prokaryotes. First, though several rounds of optimization of the microfluidic screening platform enabled high experimental success rates, the bonding between the PDMS device and epoxy coated glass does remain fragile with an elevated the risk of delamination. Second, the method of screening presented here requires the use of a micro-arrayer robot to address each genotype to a specific microchambers, the introduction of such robots in a biosafety level-3 room, for instance, imposes safety concerns.

The third drawback of the current method is the lack of automated image analysis, which in turn greatly limits quantitative analysis. In particular, mycobacterial cell division is difficult to observe, and, to date, no software is available for fully automated analysis of mycobacterial division. A few software packages do offer semi-automated analysis, such as BactImAs ([Maglica et al., 2014](#)) and BisQuit ([Mariani et al., in preparation](#)), but these are currently not amenable for large-scale screenings since they both require constant manual editing.

Finally, the last limitation of the method involves cell crowding. In mycobacterial strains, establishing large microcolonies, as is required to study persistence for

instance, dramatically decreases single-cell imaging quality. Mycobacteria are highly hydrophobic and tend to grow in three dimensions; hence, above a certain size, microcolonies form multilayers. These multilayered growth were not observed with other bacterial strains such as the *E.coli*, and seems to be mycobacteria-specific hurdle. Furthermore, other challenges result from cell-crowding: for instance, the generation of large microcolonies drives cells out the microchambers and, once in the flow channel, cells are be washed away towards the outlet. Thus, flow channels can be clogged by bacteria adhering to the glass and establishing new microcolonies. This problem could be solved by adding a valve in order to hermetically seal the microchambers and sequentially flush lysis buffer and regular medium.

To conclude, each of these limitations should be considered prior to any screening and solutions carefully examined. We believe that the the lack of automated image analysis method is the most pressing challenge and must be addressed in order to advance large-scale screening.

5.3 Outlook

We previously mentioned the absence of high-content screening tools for prokaryotes. This high-throughput microfluidic screening platform is the first of its kind and opens news doors for bacterial studies. Image-based screenings could provide insight into very diverse biological processes of prokaryotes, such as gene expression, cellular response to drugs, gene network circuits, inter-cellular communications, gene knockout phenotypes, etc. We here focused mostly on *M. smegmatis*, but the introduced high-throughput microfluidic screening platform does enable the interrogation of mutant libraries of numerous bacterial strains by time-lapse microscopy, without requiring any re-engineering. This presents a very valuable toolbox for microbiologists.

In the present screening, we identified genes implicated in bacterial persistence. To further this line of inquiry, it would be of interest to characterize each mutant in depth using the same platform, as performed for a few representative mutants in

chapter 4. In addition to cell division and death dynamics during antibiotic exposure, building reporter strains for the identified genes on a wild-type background would provide insight about how gene expression is related to cell survival to antibiotic for instance.

To conclude, through this novel high-throughput microfluidic screening platform, we have provided a highly versatile new research tool for microbiologists, offering quantitative single-cell information previously not accessible for prokaryotes to address a plethora of biological questions.

6 Materials and Methods

6.1 Bacterial strains and culture conditions

Mycobacterium smegmatis (*M. smegmatis*) mc²155 and derivative strains were grown in Middlebrook 7H9 medium (Difco) supplemented with 0.5% albumin, 0.2% glucose, 0.085% NaCl, 0.5% glycerol, and 0.05% Tween-80. Aliquots were stored in 15% glycerol at –80°C and thawed at room temperature before use; individual aliquots were used once and discarded.

To facilitate microscopic observation, an *M. smegmatis* strain expressing a cytosolic dsRed was constructed, by cloning dsRed downstream a strong constitutive promoter, carried on a single-copy plasmid integrated at the chromosomal attB site; the plasmid also carries a hygromycin resistance marker. For the study of the cell cycle markers, i.e. DnaN and Wag, an *M. smegmatis* strain expressing a mCherry-DnaN fusion protein was provided by Dr Santi. The strain was constructed using a method for two-step homologous recombination with the plasmid pIS225, which was inserted into the chromosome of wild-type *M. smegmatis* ([Santi *et al.*, 2013](#)). Wag-GFP was inserted at the attB site in the mCherry-DnaN expressing strain.

6.2 Kill curves in batch culture

Mycobacterial cells were grown to mid-log phase (OD_{600} of 0.4-0.6) and diluted to OD_{600} of 0.05 in fresh 7H9 medium. Then INH was added at a concentration of 50 μ g/ml at time 0. At 0, 6, 24, 48, and 72 hours after drug addition, survival was assessed by withdrawing aliquots of the cultures, plating serial dilutions on LB agar and scoring colonies after 3-4 days at 37°C.

6.3 Minimum inhibitory concentration assays

Mycobacterial cells were grown to mid-log phase (OD_{600} of 0.2-0.5) and diluted to OD_{600} of 0.001 in fresh 7H9 medium. MIC assays were run in Costar 96-well transparent flat-bottom plates. Then, 2-fold serial dilutions of INH ranging from 80 μ g/ml to 0.078 μ g/ml was prepared with 2 ml of cultures those were aliquoted into 15 ml test tubes. As a control, one well of culture was left drug-free and one well was fresh 7H9 medium as a blank. Well plates were incubated at 37 °C for 24 hours, resazurin was then added and incubated for 18 more hours. Reduction of resazurin was assessed by measuring fluorescence using a TECAN plate reader, at an excitation wavelength of 560nm and emission wavelength of 590 nm. When the measurements were done, the absorbance of the blank was subtracted from readouts from each of the wells. MIC was defined using a Lambert and Pearson's nonlinear regression method for determining MIC.(Lambert et al. Susceptibility testing: accurate and reproducible minimum inhibitory concentration (MIC) and non-inhibitory concentration (NIC) values. J Appl Microbiol (2000) vol. 88 (5) pp. 784-90)

6.4 Mutagenesis and generation of a *M. smegmatis* mutant library

For the pilot screen, a library of 1152 *M. smegmatis* mutants expressing cytosolic dsRed was generated by random mutagenesis using a retrotransposon. The

fMycoMarT7 transposon donor phagemid, which carries a selectable marker for kanamycin resistance, was used to mutagenize a strain of *M. smegmatis* mc²155 expressing DsRed. Cells were grown at 37°C to late-log phase (OD₆₀₀ 1.0) in 7H9 medium, washed twice with MP buffer (50 mM Tris, pH 7.5, 150 mM NaCl, 10 mM MgSO₄, 2 mM CaCl₂), and resuspended in 1/10th original volume in MP buffer. 10¹⁰ PFU (plaqueforming units) of phage per ml of original culture were added for 3 hours at 37°C. Infected cells were plated on LB agar plus 50 µg/ml hygromycin and 25 µg/ml kanamycin. After 3 days, well-isolated colonies were individually picked with sterile toothpicks into 96-well microtiter plates containing 7H9 plus 50 µg/ml hygromycin and 25 µg/ml kanamycin. Plates were incubated at 37°C for 5 days. Original 96-well master plates were stored at -80°C in 15% glycerol while the copy plates were inoculated, grown in 7H9 media, and then used for spotting. The exact same procedure was used for generating the mutant library of *M. smegmatis* expressing DnaN-mCherry Wag-GFP.

6.5 Microfluidic device and fabrication

The design of the chip was designed by L-edit (Tanner EDA) and is composed of two functional layers: a flow layer and a control layer. Both molds were fabricated in the clean room facility of the micronanotechnology (CMI, EPFL, Switzerland). The control layer consists of channels and microvalves controlling the flow inputs and outputs, this layer has a height of 12µm. The control layer consists of flow channel of a height of 12µm and a microchamber of a height of 1.4µm. Each of these structures requires writing of chrome masks. Due to PDMS shrinkage, control and flow layer molds were scaled up to 100.5% and 101.5% respectively to fit the spotting pitch of the array.

The microfluidic chip molds were fabricated with standard photolithography methods. A chrome mask coated with AZ1518 (Nanofilm, Westlake Village CA) was written on a DWL200 (Heidelberg Instruments Mikrotechnik GmbH Germany) with a 10 mm head. Masks were developed with AZ351 (MicroChemicals GmbH, Germany) in a DV10 robot (Suess MicroTec AG, Germany), etched in perchloric bath

for 90 s and stripped with Technistrip P1316 for 10 min. These masks were used to pattern photoresist-coated wafers on a MJB4 mask aligner (Suess Microtec AG) of power 20 mW/cm². Two different molds were produced: a flow wafer and a control wafer. The flow layer mold was fabricated as follow: first, microchambers were patterned on the wafer, once microchambers were exposed and developed microchannels were consecutively patterned on top. Microchambers of height 1.4µm were made of AZ nLof spun at 3500 rpm for 40s on a SSE SB20 coater followed by 1 min soft bake 110°C, then using appropriate mask the wafer was exposed for 3.7 s on a MJB4 mask aligner (Suess Microtec AG), power 20 mW/cm². A post-exposure bake of 1 min at 110°C was required prior development in MF-CD-26 developer for 20-30 s. A hardbake of 8 min at 175°C was performed to harden the photoresist. The microchannels were made of AZ9260 (MicroChemicals GmbH) as they required a rounded cross section in order to ensure hermetic closing of valves. The wafer was coated with AZ9260 on a SSE SB20 coater at a speed of 1000 rpm for 50s, followed by a soft bake of 6min at 114°C. The wafer was exposed 42 s and directly developed for 7-10min with AZ400 developer in two successive baths; AZ400 was diluted with distilled water at a ratio 1:3. A final baking step at 175°C for 8min was required to anneal the photoresist (Table 6.1). A slightly different recipe was used for producing microchambers of lower height (0.8µm), the photoresist AZ nLof was diluted with 3:1 ratio PGMEA:nLof and spun at 3250 rpm on a SSE SB20 coater followed by 1 min soft bake 110°C, the exposure time using the MJB4 Mask aligner was decreased to 2.4s, all the other steps for development and for the microchannels remained the same as described (Table 6.2).

The control layer mold was made of a single layer of SU8 GM1070 (Gerseltec, Switzerland). SU8 was coated on a Sawatec LSM250 spin coater (Sawatec AG, Switzerland) at 5500 rpm for 40s. A soft bake of 5min at 130°C was required. The exposure dose was 200 mJ, after post-exposure bake the control layer mold was develop in 2 consecutive PGMEA baths. A final hard bake was done at 110°C for 15min (Table 6.3).

Structure and resist	Steps	Technical details		
Microchambers AZ nLof	Spin coating	3500 rpm	40 s	SSE SB20 coater
	Soft bake	110°C	1 min	SSE SB20 coater
	Exposure	20 mW/cm ²	3.7s	MJB4 mask aligner
	Poste-exposure bake	110°C	1 min	SSE SB20 coater
	Development	MF-CD-26	20-30s	Wet bench
	Hard bake	175°C	8 min	Ceram hotplate
Microchannels AZ9260	Spin coating	1000 rpm	50 s	SSE SB20 coater
	Soft bake	114°	6 min	SSE SB20 coater
	Exposure	20 mW/cm ²	42 s	MJB4 mask aligner
	Development	AZ 400 1:3	7-10min	Wet bench
	Hard bake	175°C	8 min	Ceram hotplate

Table 6.1. Summary of flow layer mold fabrication with microchambers of height 1.4µm

Structure and resist	Steps	Technical details		
Microchambers	Spin coating	3250 rpm	40 s	SSE SB20 coater
	Soft bake	110°C	1 min	SSE SB20 coater

AZ nLof diluted nLof:PGMEA 3:1	Exposure	20 mW/cm ²	2.4s	MJB4 mask aligner
	Poste-exposure bake	110°C	1 min	SSE SB20 coater
	Development	MF-CD-26	20-30s	Wet bench
	Hard bake	175°C	8 min	Ceram hotplate

Table 6.2. Summary of fabrication of microchambers of height 0.8 µm.

Structure	Steps	Technical details		
Micromechanical valves SU8 GM1070	Spin coating	5500 rpm	40 s	Sawatec LSM 250
	Soft bake	130°C	5 min	Sawatec LSM 250
	Exposure	10 s	20 mW/cm ²	MJB4 mask aligner
	Poste-exposure bake	90°C	40 min	Sawatec LSM 250
	Development	PGMEA	2x2min	Wet bench
	Hard bake	110°C	15 min	Sawatec LSM 250

Table 6.3. Summary of control layer mold fabrication

The microfluidic device consisted of two layers of polydimethylsiloxane (PDMS, Sylgard 184, Dow Corning Corp., Middland, MI): the flow layer and the control layer. PDMS was mixed in a ratio 1:20 and 1:5, elastomer to curing agent, for the flow and control layer

respectively. The 1:20 mixture was poured on the flow layer wafer and spun at 2000 rpm for 35 s with a P6700 spin coater (Specialty coating systems Inc., Indianapolis, IN). 1:5 PDMS was poured on the control layer wafer and degassed for 10min in a dessicator. Both molds were baked at 80°C for 30min. Holes for control layers were punched with a manual hole-puncher (Schmidt Technology Corp, Cranberry Twp., PA), using a steal punch with an outside diameter of 0.024 in (Ref. # CR0320245N21R4, Technical innovations Inc., Angleton, TX). Control layer was then aligned manually on flow layer and both layers were bonded at 80°C for 90min. Finally, each device was cut and peeled off the mold, holes were punched in the flow layer.

6.6 Cell preparation and spotting procedure

Transposon induced mutant libraries were grown in 7H9 medium with Kanamycin (15µg/ml) and Hygromycin (50µg/ml) in 96 well plates. These plates were kept as a master plate (back up) frozen at -80°C in 10% Glycerol. For each experiment, we replicated of 1152 *M. smegmatis* mutants into 96-well V-shape plates (Nunc Ref. #249662, Fisher scientific, Switzerland) and incubated overnight at 37°C in Middlebrook 7H9 medium (Difco) supplemented with 0.5% albumin, 0.2% glucose, 0.085% NaCl, 0.5% glycerol, and 0.05% Tween-80. Cells were spun down by centrifugation at 1250 rpm for 1min. Each mutant was spotted on an epoxysilane coated glass coverslip (ref. #25x60-1-c50-25, thermo fisher scientific specialty glass, portsmouth, nh) using a DNA micro-arrayer (Qarray2, Genetix, UK), and four arraying pins, resulting in an array of 1152 (24x48) spots of column and row pitch of 375µm and 750µm respectively. To prevent desiccation of cell spots during spotting humidity was set to 60%. A PDMS chip was aligned on top of the spotted cells by eye and each mutant was addressed to a specific microchamber. PDMS and coverslip were bonded at 37°C for 60 min before priming the microfluidic chip.

6.7 Chip priming and medium switch

Control valves were connected to the device with metal pins (0.3 mm ID, 0.65 mm OD) pressurized via water filled tygon tubing (0.02 in ID, 0.06 in OD). Valves were primed at 5 psi, pressure was then increased to 18 psi to ensure hermetic closing of underlying flow channels. As soon as the control lines were primed, the flow layer was primed with 7H9 medium at 1.5 psi, the outlet valves were closed when medium reached it in order to out-gas the remaining air in the device through PDMS. Outlet let valves were opened as soon as the chip was fully primed with medium.

M. smegmatis mutants were cultured in microfluidic device for 24h in 7H9 medium at 37°C to establish microcolonies. The flow medium was then switched on-chip to 7H9 medium containing 50µg/ml INH for 48h, then cells were again exposed to 7H9 medium for 24h to assess survival. Medium switching was performed by opening and closing on-chip micromechanical valves. Throughout the time course, 1152 microchambers were imaged on phase contrast and fluorescence channels at 2-hours intervals.

6.8 Time-lapse movies acquisition – persistence screen

Live imaging of dsRed *M. smegmatis* was performed during 96h at a time-lapse of 2h by a fully automated epi-fluorescence microscopy (Nikon Eclipse Ti-E, Nikon Instruments Inc., Melville, NY) equipped with an oil immersion 60X objective (NA 1.4, Nikon ref.#MRD31602). The microscope was enclosed in an incubation chamber maintained at 37°C. Bacteria were imaged both on phase contrast and fluorescence channel using a LED system (470nm) at 50% intensity combined with a TexasRed filter (Ref. #F36-504, AHF Analysentechnik AG, Germany). Autofocus was performed with Perfect Focus System (PFS, Nikon instruments Inc.). Images were acquired with on a back-illuminated EMCCD camera (Ixon DU-888, Andor Technology, UK). Acquisition time was set to 200ms for the fluorescent channel with an EM-gain of 100, and an analog gain of 2.4. We used an in-house Visual Basic

program to control the microscope, its peripherals, the EMCCF Camera and the valves.

6.9 *M. smegmatis* mutant candidates selection

Time-lapse movie were analyzed manually, primary screening of 1152 mutants was performed four times (n=4), and secondary screening was performed twice (n=2). Very large and very small micro-colonies were removed from analysis. Mutants with two to four movies available were analyzed and potential mutants with altered persistence were selected for secondary screening when exhibiting the same phenotype in over 50% of the movies. A secondary screening was performed with the candidate mutants. As mutant with decreased persistence are more difficult to discriminate/detect/identify due to their nature a less stringent selection procedure was performed to confirm their phenotype during secondary screening. Mutants were annotated as high persisters if exhibiting the same phenotype in over 50% of the movies in each independent screening experiment, while candidates were annotated as decreased persistence when exhibiting the same phenotype in over 50% of the movies when experiments were pooled together and including small micro-colonies.

6.10 Identification of fMycoMarT7 transposon insertion sites

Genomic DNA was extracted from 5 -10 ml cultures at OD600 ~0.8 using lysozyme treatment, proteinase K digestion, Cetrimide (hexadecyltrimethyl-ammonium bromide (CTAB)) saline, and chloroform extraction (Sonnenberg, 1998). Genomic DNA where digested with BamHI restriction enzyme (New England Biolabs). The digested DNA fragments were circularized using a T4 DNA ligase (rapid DNA ligation kit, Thermo Fisher) and electroporated into competent PIR1 Escherichia coli. Kanamycin-resistant colonies were selected, and plasmid DNA was isolated (QIAprep Spin Miniprep Kit, QIAGEN) and sent to sequence using the primer

cttctgagcgggactctgggg (Microsynth), which hybridizes near one end of the fMycoMarT7 transposon.

6.11 Electrocompetent cells preparation and electroporation

For *PIR1 E. coli*, a competent cell culture was grown from 1ml vial of glycerol frozen stock in 50 ml 7H9 medium in a 250 mL glass flask with metal cap, shaking at 37°C to an OD₆₀₀ of ~ 0.8. Cells were kept on ice for 30 minutes, spun down at 4,000 rpm, 20 min, thrice washed with ice cold 10 % glycerol, and resuspended in 1/1, 1/2, 1/50 vol 10 % ice cold glycerol respectively. 45 µl was aliquoted into a cuvette (2 mm-gap), circular self-ligated gDNA was added, and pulsed at 2.5 kV, 1000 Ohms, 25 uF. Electroporations were recovered in 1.5 mL SOC medium for 1-1.5 hours, in 15 mL polypropylene tube shaking at 37 deg, before centrifuging and plating onto Kanamycin LB plates.

6.12 Flowing bacterial cells in the microfluidic screening platform for time-lapse microscopy

For the in-depth single cells studies on mutant with altered rate of persistence, the platform was produced as described previously with microchambers of height 0.8µm and bonded to glass coverslip by oxygen plasma. Mycobacterial cells were grown to exponential phase (OD₆₀₀ 0 of 0.4-0.6) in 8ml of 7H9 complete medium, spun down 10min at 3500 rpm and resuspended in 450 µl of 7H9. Cells were then flowed in the PDMS device from the purge inlet at 3psi with the outlet valve closed in order to build pressure in the device. Once the platform was primed, 7H9 regular medium and medium containing INH (25 µg/ml) were primed. Both media were supplemented with 50nm of SYTOX® Green (Thermofisher).

Live imaging of dsRed *M. smegmatis* was performed during 100h at a time-lapse of 15min by a fully automated epi-fluorescence microscopy (Nikon Eclipse Ti-E, Nikon

Instruments Inc., Melville, NY) equipped with an oil immersion 100X objective. The microscope was enclosed in an incubation chamber maintained at 37°C. Bacteria were imaged both on phase contrast and fluorescence channel using a LED system at 50% intensity combined with a TRITC filter (Ref. #F36-503, AHF Analysentechnik AG, Germany). Autofocus was performed with Perfect Focus System (PFS, Nikon instruments Inc.). Images were acquired with on a back-illuminated EMCCD camera (Ixon DU-888, Andor Technology, UK). Acquisition time was set to 150ms for both fluorescent channels. We used an in-house Visual Basic program to control the microscope, its peripherals, the EMCCF Camera and the valves.

7 Appendices

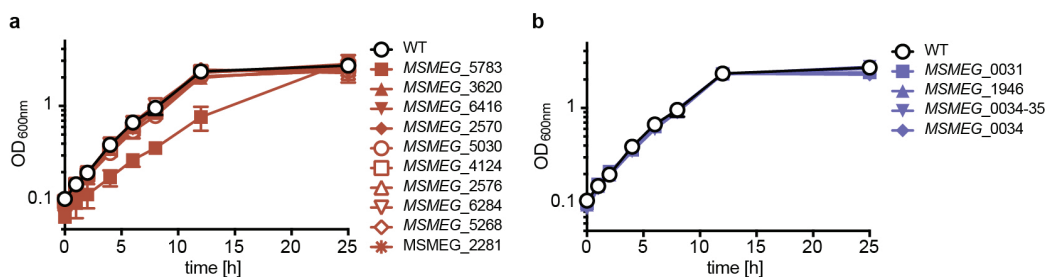


Figure 7.1: Growth of DsRed-expressing *M. smegmatis* mutants with altered rates of persistence. Growth of mutants displaying (a) increased and (b) decreased persistence. Results are the mean \pm standard deviation of 2 independent experiments.

<i>M. smegmatis</i> CP0000480.1	<i>M. tuberculosis</i> h37r	Gene length	Transposon insertion site	Annotated function
MSMEG_5783	No homolog	889 bp	796 bp	Pseudogene, acetyltransferase (mshD)
MSMEG_3620	rv1855c	930 bp	482 bp	Conserved hypothetical protein
MSMEG_6416	rv3837c	687 bp	375 bp	Phosphoglycerate mutase
MSMEG_2570	No homolog	1422 bp	-	Xanthine/uracil permease
MSMEG_5030	rv1261c	450 bp	239 bp	Conserved hypothetical protein
MSMEG_4124	No homolog	1188 bp	1180 bp	Conserved hypothetical protein
MSMEG_2576	No homolog	1359 bp	96 bp	Deoxyribodipyrimidine photo-lyase

<i>MSMEG_6284</i>	rv3720	1314 bp	525 bp	Cyclopropane-fatty-acyl-phospholipid synthase
<i>MSMEG_5268</i>	rv1078	1134 bp	-	Hypothetical protein
<i>MSMEG_2281</i>	No homolog	549 bp	451 bp	Conserved hypothetical protein
<i>MSMEG_0777</i>	rv0407	1014 bp	405 bp	F420-dependent glucose-6-phosphate dehydrogenase
<i>MSMEG_1974</i>	No homolog	345 bp	131 bp	Propane monooxygenase coupling protein
<i>MSMEG_0031</i>	rv0016c	1476 bp	1130 bp	Penicillin binding protein
<i>MSMEG_1946</i>	rv3199c	936 bp	258 bp	NAD(P) pyrophosphatase, NudC
<i>MSMEG_0034-35</i>	rv0019c-20c	135 bp	66 bp	Insertion 66 bp upstream of <i>MSMEG_0034</i> gene, intergenic region is 135bp
<i>MSMEG_0034</i>	rv0019c	96 bp	468 bp	FHA domain protein
<i>MSMEG_4121</i>	No homolog	741 bp	31 bp	GntR-family protein transcriptional regulator
<i>MSMEG_4301</i>	No homolog	1785 bp	548 bp	Acyl-CoA synthase
<i>MSMEG_3902-03</i>	rv2115c	0 bp	135 bp	Insertion 0 bp upfront <i>MSMEG_3902</i>

Table 7.1: Transposon insertion sites in DsRed-expressing *M. smegmatis* mutants with altered rates of persistence. Summary table of mutated gene in *M. smegmatis*, its homolog in *M. tuberculosis*, mutated gene length, transposon insertion site within the gene, and annotated function.

<i>M. smegmatis</i> CP0000480.1	<i>M. tuberculosis</i> h37r	Gene length	Transposon insertion site	Annotated function
<i>MSMEG_0208</i>	No homolog	378 bp	233 bp	Ribonuclease

<i>MSMEG_6264</i>	No homolog	1188 bp	1161 bp	Putative oxidoreductase
<i>MSMEG_1019</i>	<i>rv3051c</i>	2121 bp	966 bp	Ribonucleoside-diphosphate reductase, α subunit
<i>MSMEG_6135-36</i>	<i>rv2723c</i>	101 bp	23 bp	Intergenic region (101 bp), transposon insertion 23 bp upstream of <i>MSMEG_6135</i>
<i>MSMEG_5665 & MSMEG_5666</i>	<i>rv0898c</i>	348 bp & 249 bp	61 bp & 239 bp	Insertion in nucleotide position 61 of <i>MSMEG_5665</i> and 239 of <i>MSMEG_5666</i>
<i>MSMEG_5167</i>	No homolog	1206 bp	7 bp	Major facilitator superfamily protein MFS_1
<i>MSMEG_0166</i>	No homolog	729 bp	690 bp	GntR-family protein transcriptional regulator, putative
<i>MSMEG_5159</i>	No homolog	786 bp	308 bp	DNA-binding response regulator AV1H7
<i>MSMEG_5345</i>	No homolog	801 bp	318 bp	Glycosyl hydrolases family protein
<i>MSMEG_1105</i>	-	1147 bp	666 bp	No annotated function
<i>MSMEG_4107</i>	No homolog	687 bp	395 bp	Phosphoglycerate mutase, putative
<i>MSMEG_6815</i>	<i>rv2525c</i>	786 bp	437 bp	Secreted protein

Table 7.2: Transposon insertion sites in DnaN-mCherry- and Wag-GFP-expressing *M. smegmatis* mutants with altered rates of persistence. Summary table of mutated gene in *M. smegmatis*, its homolog in *M. tuberculosis*, mutated gene length, transposon insertion site within the gene, and annotated function.

8 Bibliography

- Ackermann, M. (2015). A functional perspective on phenotypic heterogeneity in microorganisms. *Nat Rev Micro* 13, 497–508.
- Ahrberg, C.D., Manz, A., and chung, B.G. (2016). Polymerase chain reaction in microfluidic devices. *Lab Chip* 16, 3866–3884.
- Amato, S.M., Fazen, C.H., Henry, T.C., Mok, W.W.K., Orman, M.A., Sandvik, E.L., Volzing, K.G., Brynildsen, M.P. (2014). The role of metabolism in bacterial persistence. *Frontiers in Microbiology* 5.
- Anderson, G.G. (2003). Intracellular Bacterial Biofilm-Like Pods in Urinary Tract Infections. *Science* 301, 105–107.
- Araci, I.E., and Quake, S.R. (2012). Microfluidic very large scale integration (mVLSI) with integrated micromechanical valves. *Lab on a Chip* 12, 2803–2806.
- Balaban, N.Q., Merrin, J., Chait, R., Kowalik, L., and Leibler, S. (2004). Bacterial Persistence as a Phenotypic Switch. *Science*.
- Balagaddé, F.K., You, L., Hansen, C.L., Arnold, F.H., and Quake, S.R. (2005). Long-term monitoring of bacteria undergoing programmed population control in a microchemostat. *Science* 309, 137–140.
- Bardou, F., Raynaud, C., Ramos, C., Laneelle, M.A., and Lanrelle, G. (1998). Mechanism of isoniazid uptake in *Mycobacterium tuberculosis*. *Microbiology* 144, 2539–2544.
- Bennett, M.R., and Hasty, J. (2009). Microfluidic devices for measuring gene network dynamics in single cells. *Nat Rev Genet* 10, 628–638.
- Bigger, J.W. (1944). Treatment of staphylococcal infections with penicillin by intermittent sterilisation. *The Lancet* 244, 497–500.
- Boshoff, H.I.M., Myers, T.G., Copp, B.R., McNeil, M.R., Wilson, M.A., and Barry, C.E. (2004). The Transcriptional Responses of *Mycobacterium tuberculosis* to Inhibitors

- of Metabolism: NOVEL INSIGHTS INTO DRUG MECHANISMS OF ACTION. *Journal of Biological Chemistry* 279, 40174–40184.
- Boutros, M., Heigwer, F., and Laufer, C. (2015). Microscopy-Based High-Content Screening. *Cell* 163, 1314–1325.
- Brouzes, E., Medkova, M., Savenelli, N., Marran, D., Twardowski, M., Hutchison, J.B., Rothberg, J.M., Link, D.R., Perrimon, N., and Samuels, M.L. (2009). Droplet microfluidic technology for single-cell high-throughput screening. *Proceedings of the National Academy of Sciences* 106, 14195–14200.
- Campen, R.L., Ackerley, D.F., Cook, G.M., and O'Toole, R.F. (2015). Development of a *Mycobacterium smegmatis* transposon mutant array for characterising the mechanism of action of tuberculosis drugs: Findings with isoniazid and its structural analogues. *Tuberculosis* 95, 432–439.
- Cheong, R., Paliwal, S., and Levchenko, A. (2010). High content screening in microfluidic devices. *Expert Opinion on Drug Discovery* 5, 715.
- Chia, N.-Y., Chan, Y.-S., Feng, B., Lu, X., Orlov, Y.L., Moreau, D., Kumar, P., Yang, L., Jiang, J., Lau, M.-S., et al. (2010). A genome-wide RNAi screen reveals determinants of human embryonic stem cell identity. *Nature* 468, 316–320.
- Chong, Y.T., Koh, J.L.Y., Friesen, H., Kaluarachchi Duffy, S., Cox, M.J., Moses, A., Moffat, J., Boone, C., and Andrews, B.J. (2015). Yeast Proteome Dynamics from Single Cell Imaging and Automated Analysis. *Cell* 161, 1413–1424.
- Christophe, T., Ewann, F., Jeon, H.K., Cechetto, J., and Brodin, P. (2010) High-content imaging of *Mycobacterium tuberculosis*-infected macrophages: an *in vitro* model for tuberculosis drug discovery, *Future Medicinal Chemistry* 2, 1283-1293.
- Danino, T., Mondragón-Palomino, O., Tsimring, L., and Hasty, J. (2010). A synchronized quorum of genetic clocks. *Nature* 463, 326–330.
- Daugherty, A., Powers, K.M., Standley, M.S., Kim, C.S., and Purdy, G.E. (2011). *Mycobacterium smegmatis* RoxY Is a Repressor of oxyS and Contributes to Resistance to Oxidative Stress and Bactericidal Ubiquitin-Derived Peptides. *Journal of Bacteriology* 193, 6824–6833.
- Dénervaud, N., Becker, J., Delgado-Gonzalo, R., Damay, P., Rajkumar, A.S., Unser, M., Shore, D., Naef, F., and Maerkl, S.J. (2013). A chemostat array enables the spatio-temporal analysis of the yeast proteome. *Proceedings of the National Academy of Sciences* 110, 15842–15847.
- Dhar, N., and McKinney, J.D. (2007). Microbial phenotypic heterogeneity and antibiotic tolerance. *Current Opinion in Microbiology* 10, 30–38.
- Dörr, T., Lewis, K., and Vulić, M. (2009). SOS Response Induces Persistence to Fluoroquinolones in *Escherichia coli*. *PLOS Genetics* 5, e1000760.
- Du, G., Fang, Q., and Toonder, den, J.M.J. (2016). Microfluidics for cell-based high throughput screening platforms-A review. *Anal. Chim. Acta* 903, 36–50.
- Dutta, N.K., and Karakousis, P.C. (2014). Latent Tuberculosis Infection: Myths, Models, and Molecular Mechanisms. *Microbiol. Mol. Biol. Rev.* 78, 343–371.

- Elowitz, M.B. (2002). Stochastic Gene Expression in a Single Cell. *Science* 297, 1183–1186.
- Elvira, K.S., i Solvas, X.C., Wootton, R.C.R., and deMello, A.J. (2013). The past, present and potential for microfluidic reactor technology in chemical synthesis. *Nature Chem* 5, 905–915.
- Fauvart, M., De Groote, V.N., and Michiels, J. (2011). Role of persister cells in chronic infections: clinical relevance and perspectives on anti-persister therapies. *J. Med. Microbiol.* 60, 699–709.
- Fernandez, P., Saint-Joanis, B., Barilone, N., Jackson, M., Gicquel, B., Cole, S.T., and Alzari, P.M. (2006). The Ser/Thr Protein Kinase PknB Is Essential for Sustaining Mycobacterial Growth. *Journal of bacteriology*. 188, 7778-7784.
- Gefen, O., and Balaban, N.Q. (2009). The importance of being persistent: heterogeneity of bacterial populations under antibiotic stress. *FEMS Microbiology Reviews* 33, 704–717.
- Gerdes, K., and Maisonneuve, E. (2012). Bacterial Persistence and Toxin-Antitoxin Loci. *Annu. Rev. Microbiol.* 66, 103–123.
- Germain, E., Castro-Roa, D., Zenkin, N., and Gerdes, K. (2013). Molecular Mechanism of Bacterial Persistence by HipA. *Molecular Cell* 52, 248-254.
- Gomez, J.E., and McKinney, J.D. (2004). M. tuberculosis persistence, latency, and drug tolerance. *Tuberculosis (Edinb)* 84, 29–44.
- Groisman, A., and Quake, S. (2004). A Microfluidic Rectifier: Anisotropic Flow Resistance at Low Reynolds Numbers. *Phys. Rev. Lett.* 92, 094501.
- De Groote, V.N., Fauvart, M., Kint, C.I., Verstraeten, N., Jans, A., Cornelis, P., Michiels, J. (2011). *Pseudomonas aeruginosa* fosfomycin resistance mechanisms affect non-inherited fluoroquinolone tolerance. *J Med Microbiol* 60, 329-336.
- Guo, M.T., Rotem, A., Heyman, J.A., and Weitz, D.A. (2012). Droplet microfluidics for high-throughput biological assays. *Lab Chip* 12, 2146–2155.
- Hannan, T.J., Totsika, M., Mansfield, K.J., Moore, K.H., Schembri, M.A., and Hultgren, S.J. (2012). Host–pathogen checkpoints and population bottlenecks in persistent and intracellular uropathogenic *Escherichia coli* bladder infection. *FEMS Microbiology Reviews* 36, 616–648.
- Harms, A., Maisonneuve, E., and Gerdes, K. (2016). Mechanisms of bacterial persistence during stress and antibiotic exposure. *Science* 354, 4268.
- He, H., Hovey, R., Kane, J., and Singh, V. (2006). MprAB is a stress-responsive two-component system that directly regulates expression of sigma factors SigB and SigE in *Mycobacterium tuberculosis*. *Journal of Bacteriology* 188, 2134-2143.
- Heym, B., Stavropoulos, E., Honoré, N., Domenech, P., Saint-Joanis, B., Wilson, T.M., Collins, D.M., Colston, M.J., and Cole, S.T. (1997). Effects of overexpression of the alkyl hydroperoxide reductase AhpC on the virulence and isoniazid resistance of *Mycobacterium tuberculosis*. *Infection and Immunity*, 1395-1401.

- Hobby, G.L., Meyer, K., and Chaffee, E. (1942). Observations on the Mechanism of Action of Penicillin. *Proceedings of the Society for Experimental Biology and Medicine*, 281-285.
- Honarnejad, K., Daschner, A., Giese, A., Zall, A., Schmidt, B., Szybinska, A., Kuznicki, J., and Herms, J. (2013). Development and Implementation of a High-Throughput Compound Screening Assay for Targeting Disrupted ER Calcium Homeostasis in Alzheimer's Disease. *PLoS ONE* 8, e80645.
- Huh, W.-K., Falvo, J.V., Gerke, L.C., Carroll, A.S., Howson, R.W., Weissman, J.S., and O'Shea, E.K. (2003). Global analysis of protein localization in budding yeast. *Nature* 425, 686–691.
- Jakiela, S., Kaminski, T.S., Cybulski, O., Weibel, D.B., and Garstecki, P. (2013). Bacterial growth and adaptation in microdroplet chemostats. *Angew. Chem. Int. Ed. Engl.* 52, 8908–8911.
- Jiang, L., Boitard, L., Broyer, P., Chaire, A.-C., Bourne-Branchu, P., Mahé, P., Tournoud, M., Franceschi, C., Zambardi, G., Baudry, J., et al. (2016). Digital antimicrobial susceptibility testing using the MilliDrop technology. *Eur. J. Clin. Microbiol. Infect. Dis.* 35, 415–422.
- Jo, M.C., Liu, W., Gu, L., Dang, W., and Qin, L. (2015). High-throughput analysis of yeast replicative aging using a microfluidic system. *Proceedings of the National Academy of Sciences* 112, 9364–9369.
- Alegre, A.O., Paul, S., Labarbuta, P., and Law, C.J. (2016). Insight into determinants of substrate binding and transport in a multidrug efflux protein. *Sci. Rep.* 6, 22833.
- Kaminski, T.S., Scheler, O., and Garstecki, P. (2016). Droplet microfluidics for microbiology: techniques, applications and challenges. *Lab Chip* 16, 2168–2187.
- Kang, L., chung, B.G., Langer, R., and Khademhosseini, A. (2008). Microfluidics for drug discovery and development: From target selection to product lifecycle management. *13*, 1–13.
- Keren, I., Kaldalu, N., Spoering, A., Wang, Y., and Lewis, K. (2004). Persister cells and tolerance to antimicrobials. *FEMS Microbiology Letters* 230, 13–18.
- LaFleur, M.D., Qi, Q., and Lewis, K. (2009). Patients with Long-Term Oral Carriage Harbor High-Persister Mutants of *Candida albicans*. *Antimicrob. Agents Chemother.* 54, 39–44.
- Levin, B.R., and Rozen, D.E. (2006). Non-inherited antibiotic resistance. *Nat Rev Micro* 4, 556–562.
- Lewis, K. (2007). Persister cells, dormancy and infectious disease. *Nat Rev Micro* 5, 48–56.
- Long, Z., Nugent, E., Javer, A., Cicuta, P., and Sclavi, B. (2013). Microfluidic chemostat for measuring single cell dynamics in bacteria. *Lab on a Chip* 13, 947–954.
- Maerkl, S.J. (2009). Integration column: Microfluidic high-throughput screening. *Integr. Biol.* 1, 19.

- Maisonneuve, E., Shakespeare, L.J., Jørgensen, M.G., and Gerdes, K. (2011). Bacterial persistence by RNA endonucleases. *Proceedings of the National Academy of Sciences* 108, 13206-11.
- Maisonneuve, E., Gerdes, K. (2014). Molecular mechanisms underlying bacterial persisters. *Cell* 157, 539-548.
- Marrer, E., Schad, K., Satoh, A.T., Page, M.G.P., Johnson, M.M., Piddock, L.J.V. (2006). Involvement of the Putative ATP-Dependent Efflux Proteins PatA and PatB in Fluoroquinolone Resistance of a Multidrug-Resistant Mutant of *Streptococcus pneumoniae*. *Antimicrob Agents Chemother* 50, 685-693.
- Mattiazzi Usaj, M., Styles, E.B., Verster, A.J., Friesen, H., Boone, C., and Andrews, B.J. (2016). High-Content Screening for Quantitative Cell Biology. *Trends in Cell Biology* 26, 598-611.
- Mekterović, I., Mekterović, D., and Maglica, Ž. (2014). BactImAS: a platform for processing and analysis of bacterial time-lapse microscopy movies. *BMC Bioinformatics* 15, 251.
- Melin, J., and Quake, S.R. (2007). Microfluidic Large-Scale Integration: The Evolution of Design Rules for Biological Automation. *Annu Rev Biophys Biomol Struct.* 36, 213-231.
- Miller, O.J., Harrak, El, A., Mangeat, T., Baret, J.-C., Frenz, L., Debs, El, B., Mayot, E., Samuels, M.L., Rooney, E.K., Dieu, P., et al. (2012). High-resolution dose-response screening using droplet-based microfluidics. *Proceedings of the National Academy of Sciences* 109, 378-383.
- Moyed, H.S., and Bertrand, K.P. (1983). *hipA*, a newly recognized gene of *Escherichia coli* K-12 that affects frequency of persistence after inhibition of murein synthesis. *Journal of Bacteriology* 155, 768-775.
- Navarro, G., Cheng, A.T., Peach, K.C., Bray, W.M., Bernan, V.S., Yildiz, F.H., and Lington, R.G. (2014). Image-Based 384-Well High-Throughput Screening Method for the Discovery of Skyclammycins A to C as Biofilm Inhibitors and Inducers of Biofilm Detachment in *Pseudomonas aeruginosa*. *Antimicrob. Agents Chemother.* 58, 1092-1099.
- Neumann, B., Walter, T., Hériché, J.-K., Bulkescher, J., Erfle, H., Conrad, C., Rogers, P., Poser, I., Held, M., Liebel, U., et al. (2010). Phenotypic profiling of the human genome by time-lapse microscopy reveals cell division genes. *Nature* 464, 721-727.
- Niederholtmeyer, H., Sun, Z.Z., Hori, Y., Yeung, E., Verpoorte, A., Murray, R.M., and Maerkl, S.J. (2015). Rapid cell-free forward engineering of novel genetic ring oscillators. *Elife* 4, e09771.
- Nieland, T.J.F., Logan, D.J., Saulnier, J., Lam, D., Johnson, C., Root, D.E., Carpenter, A.E., and Sabatini, B.L. (2014). High Content Image Analysis Identifies Novel Regulators of Synaptogenesis in a High-Throughput RNAi Screen of Primary Neurons. *PLoS ONE* 9, e91744.
- Okumus, B., Landgraf, D., Lai, G.C., Bakhsi, S., Arias-Castro, J.C., Yildiz, S., Huh, D., Fernandez-Lopez, R., Peterson, C.N., Toprak, E., et al. (2016). Mechanical slowing-

down of cytoplasmic diffusion allows in vivo counting of proteins in individual cells. *Nat Comms* 7, 11641.

Orman, M.A., and Brynildsen, M.P. (2013). Dormancy Is Not Necessary or Sufficient for Bacterial Persistence. *Antimicrob. Agents Chemother.* 57, 3230–3239.

Piraino, F., Volpetti, F., Watson, C., and Maerkl, S.J. (2016). A Digital–Analog Microfluidic Platform for Patient-Centric Multiplexed Biomarker Diagnostics of Ultralow Volume Samples. *ACS Nano* 10, 1699–1710.

Pu, Y., Zhao, Z., Li, Y., Zou, J., Ma, Q., Zhao, Y., Ke, Y., Zhu, Y., Chen, H., Baker, M.A.B., et al. (2016). Enhanced Efflux Activity Facilitates Drug Tolerance in Dormant Bacterial Cells. *Molecular Cell* 62, 284–294.

Rawat, M., Johnson, C., Cadiz, V., and Av-Gay, Y. (2007). Comparative analysis of mutants in the mycothiol biosynthesis pathway in *Mycobacterium smegmatis*. *Biochem. Biophys. Res. Commun.* 363, 71–76.

Richa, Sinha, R.P., and Häder, D.P. (5AD). Physiological Aspects of UV-Excitation of DNA - Springer. *Top Curr Chem* 356, 203–248.

Saint-Joanis, B., Demangel, C., Jackson, M., Brodin, P., Marsollier, L., Boshoff, H., and Cole, S.T. (2006). Inactivation of Rv2525c, a Substrate of the Twin Arginine Translocation (Tat) System of *Mycobacterium tuberculosis*, Increases Lactam Susceptibility and Virulence. *Journal of Bacteriology* 188, 6669–6679.

Santi, I., and McKinney, J.D. (2015). Chromosome Organization and Replisome Dynamics in *Mycobacterium smegmatis*. *mBio* 6, e01999–14.

Santi, I., Dhar, N., Bousbaine, D., Wakamoto, Y., and McKinney, J.D. (2013). Single-cell dynamics of the chromosome replication and cell division cycles in mycobacteria. *Nat Comms* 4.

Sherman, D.R., Mdluli, K., Hickey, M.J., Arain, T.M., Morris, S.L., Barry, C.E., and Stover, C.K. (1996). Compensatory *ahpC* gene expression in isoniazid-resistant *Mycobacterium tuberculosis*. *Science* 272, 1641–1643.

Shim, J.-U., Olguin, L.F., Whyte, G., Scott, D., Babbie, A., Abell, C., Huck, W.T.S., and Hollfelder, F. (2009). Simultaneous determination of gene expression and enzymatic activity in individual bacterial cells in microdroplet compartments. *J. Am. Chem. Soc.* 131, 15251–15256.

Sönnichsen, B., Koski, L.B., Walsh, A., Marschall, P., Neumann, B., Brehm, M., Alleaume, A.M., Artelt, J., Bettencourt, P., Cassin, E., et al. (2005). Full-genome RNAi profiling of early embryogenesis in *Caenorhabditis elegans*. *Nature* 434, 462–469.

Squires, T., and Quake, S. (2005). Microfluidics: Fluid physics at the nanoliter scale. *Rev. Mod. Phys.* 77, 977–1026.

Stover, C.K., Warrener, P., VanDevanter, D.R., and Sherman, D.R. (2000). A small-molecule nitroimidazopyran drug candidate for the treatment of tuberculosis. *Nature* 405, 962–966.

Taniguchi, Y., Choi, P.J., Li, G.W., Chen, H., Babu, M., Hearn, J., Emili, A., and Xie, X.S. (2010). Quantifying *E. coli* Proteome and Transcriptome with Single-Molecule Sensitivity in Single Cells. *Science* 329, 533–538.

- Thorsen, T., Maerkl, S.J., and Quake, S.R. (2002). Microfluidic large-scale integration. *Science* 298, 580–584.
- Timmins, G.S., and Deretic, V. (2006) Mechanisms of action of isoniazid. *Molecular Microbiology* 62, 1220–1227.
- Tischler, A.D., Leistikow, R.L., Kirksey, M.A., Voskuil, M.I., and McKinney, J.D. (2012). *Mycobacterium tuberculosis* Requires Phosphate-Responsive Gene Regulation To Resist Host Immunity. *Infection and Immunity* 81, 317–328.
- Unger, M.A., Chou, H.P., Thorsen, T., Scherer, A., and Quake, S.R. (2000). Monolithic microfabricated valves and pumps by multilayer soft lithography. *Science* 288, 113–116.
- Van den Bergh, B., Fauvart, M., Michiels, J., (2017). Formation, physiology, ecology, evolution and clinical importance of bacterial persisters. *FEMS Microbiology Reviews*.
- Velve-Casquillas, G., Le Berre, M., Piel, M., and Tran, P.T. (2010). Microfluidic tools for cell biological research. *Nano Today* 5, 28–47.
- Vizeacoumar, F.J., van Dyk, N., S Vizeacoumar, F., Cheung, V., Li, J., Sydorsky, Y., Case, N., Li, Z., Datti, A., Nislow, C., et al. (2010). Integrating high-throughput genetic interaction mapping and high-content screening to explore yeast spindle morphogenesis. *J. Cell Biol.* 188, 69–81.
- Wakamoto, Y., Dhar, N., Chait, R., Schneider, K., Signorino-Gelo, F., Leibler, S., and McKinney, J.D. (2013). Dynamic Persistence of Antibiotic-Stressed *Mycobacteria*. *Science* 339, 91–95.
- Wang, P., Robert, L., Pelletier, J., Dang, W.L., and Taddei, F. (2010). Robust Growth of *Escherichia coli*. *Current Biology* 20, 1099–1103.
- Wang, X.D., Gu, J., Wang, T., Bi, L.J., Zhang, Z.P., Cui, Z.Q., Wei, H.P., Deng, J.Y., and Zhang, X.E. (2011). Comparative analysis of mycobacterial NADH pyrophosphatase isoforms reveals a novel mechanism for isoniazid and ethionamide inactivation. *Molecular Microbiology* 82, 1375–1391.
- Whitesides, G.M. (2006). The origins and the future of microfluidics. *Nature* 442, 368–373.
- Xia, Y., and Whitesides, G.M. (1998). SOFT LITHOGRAPHY. *Annu. Rev. Mater. Sci.* 28, 153–184.
- Yawata, Y., Nguyen, J., Stocker, R., and Rusconi, R. (2016). Microfluidic Studies of Biofilm Formation in Dynamic Environments. *Journal of Bacteriology* 198, 2589–2595.
- Ye, N., Qin, J., Shi, W., Liu, X., and Lin, B. (2007). Cell-based high content screening using an integrated microfluidic device. *Lab Chip* 7, 1696.
- Zanella, F., Lorens, J.B., and Link, W. (2010). High content screening: seeing is believing. *Trends Biotechnol.* 28, 237–245.

9 Curriculum vitae

Amanda Verpoorte

Address	Av. William-Fraisse 6, 1006 Lausanne, Switzerland
Telephone	079 257 41 00
Email	amanda.verpoorte@gmail.com
Nationality	Swiss
Date of Birth	June 24 th , 1988

Academic Record

2012 – present	<p>PhD in Bioengineering, Laboratory of Microbiology and Microsystems, Global Health Institute, Prof. John D. McKinney, Swiss Federal Institute of Technology (EPFL), Lausanne.</p> <p><u>Thesis advisors:</u> Prof. John D. McKinney, Prof. Sebastian J. Maerkl.</p> <p>My PhD thesis combines biology with a high level of technology and microengineering to study mycobacteria physiology, dynamics and persistence to antibiotic treatment. Focus on development of a novel microfluidic screening platform.</p>
2009 – 2011	<p>MSc in Bioengineering awarded by the Swiss Federal Institute of Technology (EPFL), Lausanne, Grade: 5.60/6. Mention of Excellence.</p> <p>2009 – 2010 / EPFL, Lausanne</p> <p>2010 – 2011 / Imperial College London, United Kingdom</p> <p><u>Master Project:</u> <i>Investigation of Integrin Expression in human Mesenchymal Stem Cells during Chondrogenesis in Different Culture Systems</i>, Project co-supervised by Prof. M. Stevens (Imperial College London) and by Prof. J. Hubbell (EPFL).</p>
2006 – 2009	<p>BSc in Life Science and Technologies, EPFL, Lausanne, Grade: 5.13/6.</p> <p><u>Bachelor Project:</u> <i>Tumor Targeting of Small Molecule Drugs</i>, Project supervised by Prof. J. Hubbell (EPFL).</p>

Scientific Background & Skills

Technical skills	<ul style="list-style-type: none"> ▪ Microfabrication & Microfluidics: soft-lithography, molding, multi-layered PDMS chip fabrication, plasma, surface chemistry, live-cell imaging in microfluidic devices. ▪ Microscopy: long-term time-lapse microscopy with live-cells. ▪ Cell handling: chondrocytes, mesenchymal stem cells, 3T3 fibroblasts, <i>Mycobacterium smegmatis</i>, <i>Escherichia coli</i>. ▪ Biology: stem cell differentiation, kill curves, minimum concentration assays. ▪ Cloning: transposon mutagenesis, knock-in, PCR and standard molecular biology techniques.
Informatics & computing	Illustrator, Photoshop, MS Office, Prism, L-edit, ImageJ, Matlab.

Conference Contribution & Publications

Poster presentations	Global Health Institute retreat , Arolla, Switzerland. June 2016 CMI Annual Review Meeting , Lausanne, Switzerland. May 2015 Microfluidics , Heidelberg, Germany. July 2014 SystemsX , Lausanne, Switzerland. Oct. 2014 CMI Annual Review Meeting , Lausanne, Switzerland. May 2013
Oral presentation	Selected speaker for Global Health Institute retreat , Arolla, Switzerland. June 2016
Publications	<p>A microfluidic screening platform enables high-throughput single-cell screening to identify genes involved in bacterial persistence, Verpoorte A, Elitas M, Dhar N, Maerkl SJ, McKinney JD. <i>Manuscript in preparation</i>.</p> <p>Rapid cell-free forward engineering of novel genetic ring oscillators, Niederholtmeyer H, Sun ZZ, Hori Y, Yeung E, Verpoorte A, Murray TM, Maerkl SJ, <i>eLife</i>. 2015; 4.</p> <p>The Changing Integrin Expression and a Role for Integrin $\beta 8$ in the Chondrogenic Differentiation of Mesenchymal Stem Cells, LaPointe VLS, Verpoorte A, Stevens MM, <i>PLoS One</i>, 2013; 8(11).</p>

Teaching Assistant

Autumn 2013	Microbiology, third year Life Sciences Bachelor students. Supervision of exercises on microbial membranes, metabolism, motility, differentiation and individuality.
-------------	---

2013- 2015	Advanced Bioengineering Methods Laboratory, first year Life Science Master students. Supervision of the microfabrication in the clear room and operation of a microfluidic chip for the time-lapse microscopy of bacteria.
------------	---

Extracurricular Experience

April 2016 – present	Committee Member of the Consulting Society EPFL Organization of networking events with consulting firms, internal workshops and the first EPFL Business Game in October 2016.
2009 – 2010	Member of the EPFL Photo Club Committee - Treasurer and members supervisor Organising cultural events and activities around photography, such as exhibitions, workshops and courses.
Dec. 2007 – Oct. 2008	Publication and Design Officer for Forum EPFL One of the largest European recruiting events with 180 companies and 6000 students attending. Budget: CHF 800'000. My responsibilities: prepare and negotiate the production of all documents related to EPFL Forum's activities with publishers.

Languages

French	Fluent.
English	Fluent.
Italian	Good oral and written skills, intensive class at <i>Torre Di Babele</i> school, Rome, Level C1, Sept. 2015.

Personal Interests

Travel photography, horse riding, skiing, running, love to travel and experience different cultures – trip around the world for 7 months: September 2011 - April 2012.